MODULATION OF INTEGRIN ACTIVITY FOR DIAGNOSTIC AND THERAPEUTIC APPLICATIONS

Mariarosaria De Simone

Dottorato in Scienze Biotecnologiche –XXIII ciclo
Indirizzo Biotecnologie Industriali e Molecolari
Università di Napoli Federico II

Dottorato in Scienze Biotecnologiche – XXIIIciclo
Indirizzo Biotecnologie Industriali e Molecolari
Università di Napoli Federico II

MODULATION OF INTEGRIN ACTIVITY FOR DIAGNOSTIC AND THERAPEUTIC APPLICATIONS

Mariarosaria De Simone

Dottoranda: Mariarosaria De Simone

Relatore: Prof. Ettore Benedetti

Correlatore: Dr. Laura Zaccaro

Coordinatore: Prof. Giovanni Sannia

Alle persone più importanti della mia vita:

Ai miei genitori, Lino e Michela, per aver reso possibile, con il loro costante sostegno, la realizzazione di questo importante obiettivo.

A mia sorella, Raffaella, per essere stata un'inesauribile fonte di ottimismo ed allegria anche nei momenti più difficili.

Al mio fidanzato, Felice, per essermi sempre stato vicino, anche quando eravamo distanti ed aver contribuito a rendere perfetta questa tesi e molto altro!!!

INDEX

ABBREVIATIONS

BOC	Butossicarbonyl
DCM	Dicloromethan
DIPEA	Diisopropilethylammina
DMEM	Dulbecco's Modified Eagle Medium
DMF	Dimethylformammide
ECs	Endothelial cells
EDT	Ethanedithiol
ERK	Extracellular Signal-Regulated Protein kinase
ESI-MS	Electrospray Ionization-Mass Spectrometry
FAK Kinase	Focal Adhesion kinase
FBS	Precolostral bovine Serum
Fmoc	9-Fluorenilmetossicarbonyl
FTIR	Fourier Transform Infrared Spectroscopy
HATU	2-(1H-9-Azobenzotriazole-1-yl)-1,1,3,3,-tetramethyluronium
HBTU	2-(1H-Benzotriazole-1-ile)-1,1,3,3-tetramethyluronium esafluoro phosphate
HEPES	(4 (2-hydroxyethyl) - acido 1-piperazineethanesulfonic)
hFN	Human Fibronectin
HOBt	Hydroxybenzotriazole
MAPKinase	Mitogen-Activated Protein Kinase
LC-MS	Liquid chromatography-mass spectrometry
MeIm	Mesitylene Imidazole
MeOH	Methanol
MSNT	1-(mesitylenesulfonyl)-3-nitro-1H-1,2,4-triazole
Mtt	methoxytritile
NMP	N-Methyl-2-pyrrolidone
NMR	Nuclear magnetic resonance spectroscopy
OAll	O-Allyl
OtBu	O-t-Butyl
Pbf	2,2,4,6,7-pentamethyl-2,3-dihydrobenzofuran-5-ylsulfonyl
PyBop	Benzotriazol-1-yl-oxytripyrrolidinophosphonium hexafluorophosphate
RP-HPLC	Reverse Phase High Performance Liquid Chromatography
SEM	Scanning Electron Microscopy
tBu	t-Butyl
TIS	Triisopropylsilane
TEM	Transmission electron microscope Spectroscopy
TFA	Trifluoroacetic acid
Trt	Trityl
Uv-Vis	Ultraviolet-Visible Spectroscopy
VEGF	Vascular Endothelial Growth factor
VSMC	Vascular Smooth Muscle Cells

SUMMARY

Over the past decade, the scientific research spent many efforts to develop therapeutic and diagnostic systems able to contact selectively the target cells and to minimize their diffusion in healthy organs. For this purpose the most diffuse approach was targeting the molecular markers overexpressed on the tissues of interest. In this contest, the integrin family of cell adhesion receptors was one of the most studied markers. (Tucker G.C., 2006).

In particular, among all integrins, αvβ3 receptor was particularly studied in the last decade. Physiologically, it mediates many different biological processes such as intracellular signalling, cell migration, proliferation, and survival through interactions with ECM proteins such as vitronectin, fibronectin and osteopontin. The receptor mediates cell adhesion to extracellular matrix by recognizing the conserved Arg-Gly-Asp sequence of several plasma and matrix proteins. It is strongly overexpressed in activated EC, melanoma, glioblastoma and prostate cancers and in granulation tissue, whereas is not detectable in quiescent blood vessels or in the dermis and epithelium of normal skin. Therefore it can be considered a tumour and activated endothelium marker.

In the last decade several αvβ3 ligands able to modulate the receptor activity were developed as drugs for therapy, as tracers for diagnosis and as ligands for targeted drug delivery systems.

Among these molecules, the pentapeptide c(RGDf[NMe]V), also known as Cilengitide, is the most active , αvβ3/αvβ5 antagonist reported in literature and is in phase III clinical trials as antiangiogenic drug for glioblastoma therapy (Dechantsreiter M.A., et al., 1999; Reardon D.A., 2008; Tabatabai G., et al., 2010).

However, even if all αvβ3 ligands reported in the literature have a good affinity for the receptor, they present a low selectivity and bind, even if with lower affinity, also other integrin receptors structurally homologues of αvβ3 such as αvβ5 integrin (Smith J.W., et al., 2003; Eskens F.A., et al., 2003). In contrast with αvβ3 that has a relatively limited cellular distribution αvβ5 is widely expressed by many malignant tumor cells.

Therefore, to target αvβ3-mediated processes for diagnostic or therapeutic purposes, the development of new compounds that can discriminate between αvβ3 and αvβ5 is required to minimize the side-effects and increase the therapeutic effectiveness.

In 2006 our research group designed and synthesized a novel and selective peptide antagonist, referred to as RGDechiHCit, to visualize αvβ3 receptor on tumour cell (Del Gatto A., et al., 2006). It is a chimeric peptide containing a cyclic RGD motif and two echistatin C-terminal moieties covalently linked by spacer sequence. Cell adhesion assays showed that RGDechiHCit selectively binds, αvβ3 integrin and does not cross-react with, αvβ5 and, αIIbβ3 integrins (Del Gatto A., et al., 2006). Furthermore, PET and SPECT imaging studies confirmed that the peptide selectively localizes on αvβ3 expressing tumor cells in xenograft animal model (Zannetti A., et al., 2009). In this experimental setting, the chimeric RGDechiHCit was not able to detect a signal originating from the newly formed intratumoral blood vessels. This may be due to incomplete neovascularization and, hence, low levels of αvβ3 expression or to the murine origin of the integrin on newly formed blood vessels because the rational design of the chimeric RGD peptide was based on the crystal structure of the extracellular region of human αvβ3. Therefore the main purpose of

the present PhD thesis was to evaluate in vitro and in *vivo* effects of RGDechiHCit on neovascularization.
In particular, we first assessed the *in vitro* peptide properties on bovine aortic ECs, VSMC and then *in vivo*, in Wistar Kyoto (WKY) rats and c57BL/6 mice, the ability of this cyclic peptide to inhibit angiogenesis in comparison with Cilengitide.
A major evidence that is brought up by our results is the peculiar selectivity of RGDechiHCit towards EC, as compared to c(RGDf[NMe]V). Indeed, RGDechiHCit fails to inhibit VSMC proliferation *in vitro*, opposite to c(RGDf[NMe]V). This feature could be due to the selectivity of such a novel compound towards , αvβ3, VSMCs indeed express αvβ3 only during embryogenesis (Eliceri B.P., et al., 1998; Illario M., et al., 2005), but express other integrins which may be blocked by c(RGDf[NMe]V). On the contrary, αvβ3 is expressed on ECs, thus conferring RGDechiHCit selectivity toward this cell type. It is only an indirect evidence, that needs further investigation in following experiments. Comparable results between the two antagonists were obtained on wound healing and Matrigel plugs invasion. Our data suggest that inhibition of the endothelial integrin system is sufficient to inhibit angiogenesis.
In conclusion the potential antiangionenic activity of the peptide opens new fields of application for the treatment of pathophysiological conditions associated to angiogenesis such as cancer, proliferative retinopathy and inflammatory disease.
In the nanotechnology field, gold nanoparticles (AuNPs) are playing a pivotal role in providing new types of targeted delivery systems to permit the selective entry of one or multiple drugs in the primary tumor, as well as at the site of metastasis and its microenvironment. AuNPs can be indeed used to deliver a cargo, such as an anticancer drugs, or a radionuclide to tumor sites as well they can be also employed in tumor phothermal therapy for their plasmon resonance properties (Melancon M., et al., 2009). In both cases the targeted drug approach is achieved by the exploitation of molecular markers over-expressed in cancerous tissues such as αvβ3 integrin.
Unfortunately, nanogold tend to aggregate in solution and so it is difficult to preserve them for long time. To solve this issue they can be functionalized with various organic ligands to create organic-inorganic hybrids with advanced functionality. It was recently reported the use of peptide sequences based on the GC repeats as stabilizing agents for the preparation of monolayer gold nanoparticles (Krpetić Z., 2009).
On the basis of this data, we designed and synthesized a new chimeric peptide (thereafter named RGD$(GC)_2$, displaying motifs for both targeting and capping functions. A RGD-containing peptide, derived from the Cilengitide, was chosen as a targeting ligand for, αvβ3 integrin receptor and a GC including peptide was selected in order to stabilize the gold nanoparticles. AuNPs functionalised with this peptide were prepared and characterized by Uv-Vis, ATR-IR, XRD, NMR techniques and TEM microscopy. Finally we tested the ability of the obtained nanosystems, named RGD$(GC)_2$AuNPs, to permeate the target cells membrane (U-87 MG, glioblastoma cells). In all these studies we used as negative control peptide named $(GC)_2$ corresponding to the capping motif obtaining the gold nanoparticles named $(GC)_2$AuNPs.
Our results encourage us to retain that this system could be a good starting point to develop selective gold nanodevices useful in the field of biotechnologies for therapeutic and diagnostic applications.

RIASSUNTO

Negli ultimi anni numerosi studi hanno dimostrato che molte delle patologie attualmente più diffuse sono caratterizzate dall' iperespressione di alcune molecole considerate come marcatori molecolari (Wehrle-Haller B., et al., 2003).
Per questo motivo, al fine di ottenere una maggiore specificità sia nella cura che nella diagnosi delle malattie, la ricerca, in particolare nel campo delle biotecnologie, ha avuto come principale obiettivo dei propri studi lo sviluppo di specifici sistemi bersaglio basati sul riconoscimento dei marcatori molecolari overespressi dalle cellule malate (Gordon C.T., 2006).
In quest'ambito, ha destato un grande interesse nella comunità scientifica una famiglia di recettori di adesione cellulare presente sulla superficie di vari tipi di cellule e coinvolta in importanti processi biologici: le integrine.
Le integrine sono glicoproteine eterodimeriche appartenenti alla famiglia dei recettori di adesione cellulare la cui principale funzione consiste nell'integrare e mettere in comunicazione l'esterno della cellula (ECM) con il suo l'interno (citoscheletro). Esse sono costituite da una subunità α ed una subunità β legate in modo non covalente che attraversano la membrana cellulare. Nei mammiferi sono attualmente noti almeno 24 eterodimeri diversi di integrina composti da 18 tipi di subunità α ed 10 tipi di subunità β. Una singola catena β può interagire con numerose catene α formando vari tipi di recettori che legano specifici ligandi dando il via a molteplici eventi cellulari (Hynes R.O. et al.,1996; Takada Y.et al., 2003). Difatti, in seguito all'interazione con determinate molecole dell' ECM, le integrine formano dei *cluster* molecolari ed attivano uno o più *pathway* di segnali intracellulari quali chinasi (serina/treonina chinasi e MAP chinasi), recettori per fattori di crescita, canali ionici e determinano il controllo dell'organizzazione del citoscheletro, necessari per la sopravvivenza, la proliferazione, il differenziamento e la migrazione cellulare (Eliceri B.P., et al.,1999).
In particolare, notevole attenzione è stata rivolta all' integrina αvβ3, overespressa sulla superficie delle cellule vascolari di molti tessuti tumorali e coinvolta in importanti processi biologici tra cui l'angiogenesi ossia, la formazione di nuovi vasi sanguigni a partire da capillari preesistenti (Liu Z., et al., 2008). Tale processo si verifica principalmente durante lo sviluppo embrionale mentre negli individui adulti avviene in caso di rimarginazione di ferite, ciclo mestruale e gravidanza ed è finemente regolato dall'equilibrio tra fattori pro-angiogenici ed anti-angiogenici. In presenza di particolari stimoli quali ipossia, stress cellulare, insorgenza di un tumore, tale equilibrio si altera ed i fattori pro-angiogenici, tra cui anche l'integrina αvβ3, prevalgono in maniera incontrollata dando luogo alla così detta "angiogenesi patologica", alla base della sopravvivenza e della metastasi della massa cancerosa.
Dato il rilevante ruolo biologico esercitato dall'integrina αvβ3, negli ultimi anni sono state sintetizzate numerose molecole capaci di modularne l'attività.
Fra i più noti ligandi di natura peptidica si considera il potente peptide ciclico Cilengitide, attualmente in Fase III di valutazione clinica per la terapia antiangiogenica del glioblastoma (Dechantsreiter M.A., et al., 1999; Reardon D.A., 2008; Tabatabai G., et al., 2010). Tuttavia, tale molecola presenta un limite: non è selettiva per l'integrina αvβ3, difatti lega, anche se con minore affinità, anche altre integrine strutturalmente omologhe ad essa quali αvβ5 ed α1β5.
Tra le varie molecole sviluppate, di recente, è stato realizzato un nuovo ligando selettivo per l'integrina αvβ3 denominato RGDechiHCit (Del Gatto A., et al., 2006).
Tale molecola è stata ottenuta legando covalentemente, mediante un opportuno *linker*, una porzione ciclica riconducibile alla sequenza del peptide Cilengitide ed una

porzione lineare derivata dai residui localizzati all'estremità C-terminale dell'Echistatina (un antagonista naturale della suddetta integrina). Saggi di adesione cellulare hanno dimostrato che tale peptide è capace di inibire l'adesione di cellule sovraesprimenti αvβ3 in modo altamente selettivo e con un'affinità di legame paragonabile alla Cilengitide. Inoltre, saggi in vivo hanno dimostrato che il peptide, opportunamente funzionalizzato è capace di visualizzare attraverso diverse tecniche di *imaging* molecolare quali SPETCT e PET (Zannetti A., et al., 2009). Nell'ambito di tali studi, il peptide RGDechiHCit non si è rivelato utile nella visualizzazione dei neovasi sanguigni intratumorali. Si è ipotizzato che ciò sia dovuto alla incompleta neovascolarizzazione e, di conseguenza, ai bassi livelli di espressione dell'integrina αvβ3, oppure al fatto che i neovasi siano di natura murina e il peptide sia stato, invece, progettato sulla base dell' integrina αvβ3 umana. Per tale ragione, uno dei principali obiettivi della presente tesi di dottorato è stato lo studio dell'attività antiangiogenica, sia in vivo che in vitro, del peptide RGDechiHCit sulle cellule vascolari.

A tal scopo, in collaborazione con i ricercatori del Dipartimento di Medicina Clinica, Scienze Cardiovascolari ed Immunologiche dell' Università degli studi di Napoli Federico II sono stati effettuati diversi esperimenti *in vitro* (saggi di adesione e proliferazione cellulare e studi dell'angiogenesi *in vitro* utilizzando preparazioni di Matrigel) su cellule vascolari endoteliali bovine (BAEC) e su cellule muscolari vascolari liscie (VSMC).

I saggi effettuati hanno dimostrato che il peptide RGDechiHCit è in grado di inibire l' l'angiogenesi. L'attività antagonista del peptide RGDechiHCit è stata confermata anche *in vivo* valutando l'effetto sulla cicatrizzazione delle ferite in modelli murini (*Wound healing*). In presenza del peptide in esame, infatti, il tempo di rimarginazione delle ferite praticate risulta maggiore rispetto alle ferite non trattate (Santulli G., et al., SUBMITTED) .

Sulla base dei buoni risultati ottenuti, possiamo quindi considerare RGDechiHCit un buon punto di partenza per lo sviluppo di molecole in grado di legare ed inibire selettivamente l'attività. Studi per migliorare la stabilità in siero del suddetto peptide ed identificarne la minima sequenza dotata di pari affinità e selettività per l'integrina αvβ3 sono attualmente in corso.

Di recente, la ricerca biotecnologica ha investito molte energie per sfruttare la capacità dei peptidi di riconoscere specifici recettori al fine di ottenere dei sistemi terapeutici selettivamente diretti sulle cellule overesprimenti i marcatori molecolari (Lim Y., et al., 2008) quali l'integrina αvβ3. In questo modo, una radiomolecola o un agente terapeutico è guidato dal peptide fino alla cellula *target* con una efficacia molto maggiore rispetto alle cellule normali. Negli ultimi anni, di conseguenza, si è verificato un notevole incremento dello sviluppo dei cosiddetti nano vettori (micelle, liposomi) ed aggregati di nano particelle d'oro (*nanogold*) che trovano utilità sia nel *drug delivery* che nel campo delle tecniche di *imaging* molecolare.

Pertanto, parallelamente, l'attività di ricerca è stata rivolta anche allo sviluppo di una nuova sequenza peptidica per la funzionalizzazione di nanoparticelle di oro allo scopo di sviluppare un sistema selettivo per il *targeting* dell'integrina αvβ3 con applicazioni sia in campo diagnostico che terapeutico.

Recentemente è stato riportato in letteratura che peptidi contenenti la sequenza GC sono capaci di stabilizzare le nanoparticelle di oro e di sfavorirne l'aggregazione in soluzione (Krpetić Z., 2009). L'aggregato ottenuto, può essere utilizzato sia come veicolo per il trasporto dei farmaci e di agenti traccianti che per la terapia fototermica grazie alle sue proprietà ottiche (Melancon M., et al., 2009).

Partendo da tali informazioni, è stato progettata una sequenza peptidica di tipo chimerico, RGD-$(GC)_2$, formata da una sequenza contente il motivo GC ripetuto due volte ed un peptide ciclico analogo della Cilengitide. Il peptide, è stato sintetizzato in fase solida utilizzando la chimica Fmoc ed amminoacidi opportunamente protetti.
Le nano particelle d'oro sono state preparate in un'unica reazione mediante riduzione dell'acido tetracloroaurico con boroidrato in presenza del peptide stabilizzante $_c$(RGDfE)AGCGGCG-NH_2 in collaborazione con il Dipartimento di Chimica Inorganica, Metallorganica ed Analitica "L. Malatesta" ed il Dipartimento di Biologia dell'Università di Milano. Istantaneamente si è formata una limpida soluzione rossa indice della formazione di nanoparticelle d'oro del diametro di circa 8.5 nm. Le particelle sono state purificate tramite dialisi. La funzionalizzazione e la dimensione delle nanoparticelle sono state verificate mediante UV-Vis, TEM, FTIR ed NMR. Inoltre, sono stati effettuati studi *in vitro*, su cellule di glioblastoma, per verificare la capacità delle nano particelle ottenute di penetrare nelle cellule bersaglio. Tutti gli studi effettuati, sono stati ripetuti usando il peptide aspecifico $(GC)_2$, da noi progettato e sintetizzato per disporre di un controllo negativo. Tale peptide, difatti, corrisponde alla molecola RGD-$(GC)_2$ priva del motivo RGD. I risultati ottenuti hanno rivelato un'alta efficienza di internalizzazione cellulare dopo soli 5 minuti di trattamento.
Ulteriori studi mirati alla comprensione del meccanismo di incorporazione delle nano particelle funzionalizzate sono tutt'ora in corso. Le numerose informazioni strutturali ricavate dallo studio delle nano particelle d'oro funzionalizzate, ottenute durante il presente lavoro di dottorato, aprono la strada alla progettazione e alla sintesi di nuovi e più efficaci sistemi diagnostici e terapeutici volti ad minimizzare gli effetti collaterali di agenti terapeutici e diagnostici.
Attualmente sono in allestimento esperimenti volti a chiarire il meccanismo con cui le nano particelle sono incorporate nelle cellule bersaglio e stabilire esattamente la quantità di molecole presenti sulla superficie di ciascun aggregato. In tal modo sarà possibile controllare il grado di funzionalizzazione del nanosistema ottenuto ed aumentarne l'efficienza.

1 INTRODUCTION

It is known that one of the primary goal of a successful pathology treatment and diagnosis is to target selectively the tissues of interest while minimizing the drug distribution in normal organs.
In cancer therapy the standard agents enter in normal tissues with indiscriminate cytotoxicity and do not preferentially accumulate at tumour sites. In same cases, the dose reaching the target organs may be also as little as 5% to 10% of the doses accumulating in normal tissues (de Bono J. S., et al., 2010). In this way, the pharmaceutical effect is decreased and the toxic effect to normal cells is increased.
In diagnostic field, the problems in the delivery of contrast agents are essentially the same as for therapeutic pharmaceuticals. Many tracers are indeed aspecifically captured from the normal tissues and they do not arrive in a sufficient quantity to the target organs failing the diagnosis of the pathology (Sugahara K.N., et al, 2009).
To solve these issues, in last decade, the scientific community spent many efforts to develop selective therapeutic and diagnostic systems.
Several approaches have been focused on improvement of the ability of anticancer drugs and contrast agents to avoid normal organs. One of the most effective strategies is the development of compounds able to target selectively markers overexpressed in tumour tissues.
Another strategy is to encapsulate drugs in particles (such as liposomes, micelles and nanovectors) that, opportunely functionalised with moiety able to recognize tumour markers, are able to selectively delivery the drug into cancer cells (targed drug delivery approach).
For both strategies, the integrins cell adhesion receptors represent appealing tumour markers to obtain selective compounds for therapeutic and diagnostic applications.

1.1 INTEGRINS

1.1.1 Structural informations

Integrins are a family of transmembrane receptors present on multiple types of cell surface that mediate cell–cell and cell–ECM (extracellular matrix) interactions.
On a structural point of view, they consist of α and β heterodimers which associate non-covalently in defined combinations. At least 24 distinct integrin heterodimers are formed by the combination of 18 α-subunits and 10 β-subunits both characterized by a large N-terminal extracellular domain, a transmembrane domain, and a short C-terminal intracellular tail. (Cox D., et al., 2010; Hynes R.O. et al.,1996; Takada Y., et al., 2003).

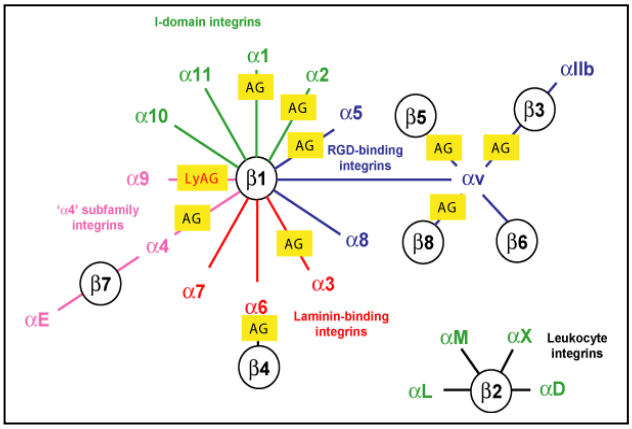

Fig. 1 Integrin family (Cox D., et al., 2010).

Outside the cell plasma membrane, α and β subunits form a binding pocket for ECM ligands (Takada Y., et al., 2007) that contain a specific structural element named I domain (also termed A-domain). In some integrins (e.g. α1β1 and α2β1), this peculiar site is inserted on the α chain toward the N-terminus. The receptors carrying this domain either bind to collagens, or act as cell-cell adhesion molecules (integrins of the β2 family) (Xiao T., et al., 2004). Those integrins that not presenting this inserted site in α chain, also have an I domain in their β subunit like αvβ3 and α5β1.
In both cases, the I domain contains the MIDAS (metal ion-dependent adhesion site), a ligand binding site permanently occupied by divalent cations and containing either a Ca^{++} or Mg^{++} ion. In addition there are two adjacent metal ion-binding sites that bind Ca^{++} named LIMBS (ligand-induced metal ion-binding site) and ADMIDAS (adjacent to metal ion-dependent adhesion site) respectively (Takagi J., et al., 2002). These regions interact with negatively charged residues in ligands. Indeed, the ligand aspartic acid-based sequences (e.g. RGD, LDV, KGD, RTD and KQAGD) bind to the majority of integrin ligands (Arnaout M.A., et al., 2002) (Figure 2).
In particular, the most diffused negative charged amino acid motif in the integrin-interaction site of ECM adhesive proteins (vitronectin, osteopontin, etc), is the amino acid sequence Arginine-Glycine-Aspartic acid ("RGD" in the one-letter amino acid code). So, different integrins bind ligands encompassing this amino acidic sequence (Humphries M.J., et al., 2003, Xiong J.P., et al., 2003).

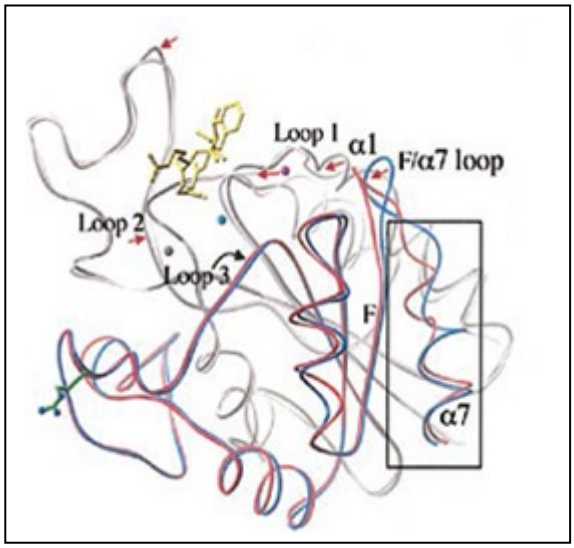

Fig. 2 The ligand binding site of αvβ3. Ligand is in yellow. The three metal ions present in the liganded form (LIMBS, MIDAS, and ADMIDAS) are shown in gray, cyan, and magenta, respectively (Xiong J.P., et al., 2003).

Nevertheless, even if different integrins recognise different proteins containing RGD sequences, the contest of the RGD sequence (flanking residues, three dimensional presentation and individual features of the integrin binding pockets) determines the specificity and the efficacy of interaction (Zaccaro L., et al., 2007).

1.1.2 Activation and biological role

Integrin extracellular domain binds directly components of the ECM and provides the traction necessary for cell motility. For this reason, integrins are usually classified as “adhesion molecules” but they are also important “signalling molecules”. Indeed, the integrin interactions with their ligands induce conformational changes in the extracellular domains leading to an increase in the affinity for ligands themselves as well as associations of integrins into clusters. This event, named “outside-in signaling” leads to the activation of different intracellular pathways like tyrosine and serine/threonine kinases activation, MAP kinases and other effectors proteins supporting the migration, proliferation and cellular differentiation (Legate K.R., 2009).

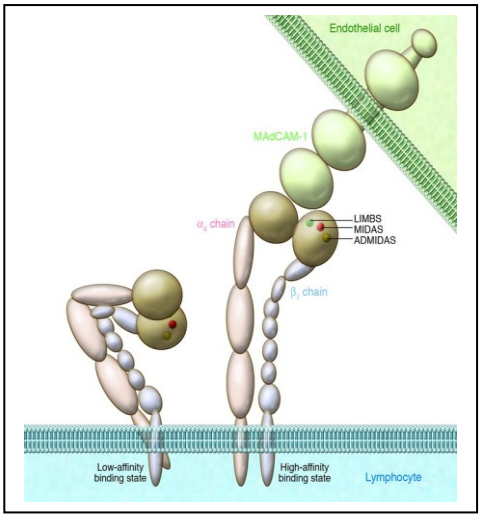

Fig. 3 Integrin outside-in signaling (Legate K. R., 2009).

Moreover, integrins modulate their activity also through another mechanism named “inside-out signalling”. In their resting state, integrins normally bind their ligands with low affinity; upon intracellular stimulation, a cellular signal induces a conformational change in the integrin cytoplasmic domain that propagates to the extracellular domain leading to a transformation of receptor from a low to a high affinity ligand binding state (Harburger D.S., et al., 2009).

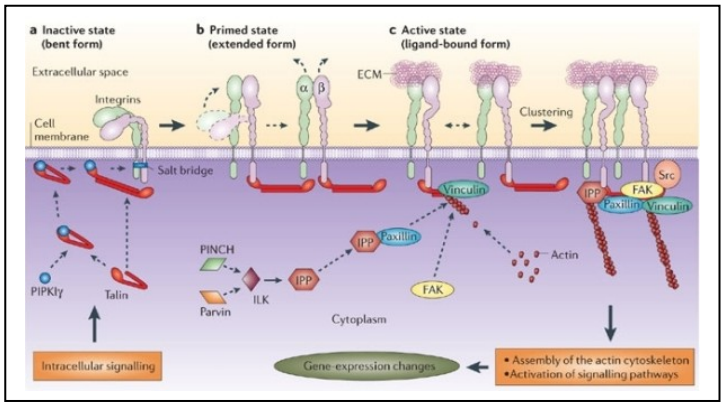

Fig. 4 Integrin inside-out signaling (Harburger D. S., et al., 2009).

1.1.3 Integrins and disease

Due to their crucial biological role, integrins are involved in a variety of different pathologies. One of the human disease caused by integrin defects is the Leucocyte Adhesion Deficiency type I (LAD-1), an autosomal recessive disorder of the immune system characterized by recurrent infections that are frequently life-threatening. It is caused by impaired extravasion of poli morpho nucleate cells and monocytes due to absence or mutation of β2-integrins (Anderson D.C., et al., 1987).
Another important pathology is the Glanzmann thrombasthenia. This is a disease caused by the failure of the platelet αIIβ3-integrin to make contacts with fibrinogen and fibrin, resulting in platelet dysfunction and prolonged bleeding time (Nair S., et al., 2002).
Moreover, integrins are implicated in epidermial disorders such as Epidermolysis bullosa, an autosomal recessive epidermal blister condition of the skin. It is due to the failure of the α6- or β4-integrin subunit to be expressed in functional heterodimer. This, induces disruption of the mechanical link between the basement membrane and the basal keratinocyte layer (Jonkmar M.F., 2002).
The integrins are also involved in many processes fundamental for the initiation, progression and metastasis of solid tumours and some of them are overexpressed on the cancer cells surface. Indeed, studies correlating integrin expression levels in human tumours with pathological outcomes, such as patient survival and metastasis, have identified several integrins that might have an important role in cancer progression. To date it is known that tumour cell expression of αvβ3, αvβ5, α5β1, α6β4, α4β1 and αvβ6 integrins is correlated with disease progression in different tumours (TABLE 1). The relevant environment of integrins in several pathologies has made them an interesting target for cancer therapy and diagnosis (Desgrosellier J.S., et al., 2010).

Tumour type	Integrins expressed	Associated phenotypes
Melanoma	αvβ3 and α5β1	Vertical growth phase [35,172–174] and lymph node metastasis[173,175]
Breast	α6β4 and αvβ3	Increased tumour size and grade[176], and decreased survival[177] (α6β4). Increased bone metastasis[36–38,64] (αvβ3)
Prostate	αvβ3	Increased bone metastasis[39]
Pancreatic	αvβ3	Lymph node metastasis[40]
Ovarian	α4β1 and αvβ3	Increased peritoneal metastasis[178] (α4β1) and tumour proliferation[179] (αvβ3)
Cervical	αvβ3 and αvβ6	Decreased patient survival[41,180]
Glioblastoma	αvβ3 and αvβ5	Both are expressed at the tumour–normal tissue margin and have a possible role in invasion[181]
Non-small-cell lung carcinoma	α5β1	Decreased survival in patients with lymph node-negative tumours[182]
Colon	αvβ6	Reduced patient survival[109]

TAB.1 Integrins involvement in cancer progression (Desgrosellier J.S., et al., 2010).

1.2 αvβ3 INTEGRIN

1.2.1 Structural informations

Integrin αvβ3 consists of a 125 kDa αv subunit and a 105 kDa β3 subunit. In 2001, crystal structure of the extracellular segment of integrin αvβ3 has been solved by X-Ray diffraction (Xiong J.P., et al 2001) (Figure 7). As was recently confirmed, the X-Ray structure shows that the heterodimeric molecule can exist in either an “extended” or "flexed" conformation (Xiong J.P., et al., 2009) (Figure 8).

Fig. 7 Integrin αvβ3 crystal structure (Xiong J.P., et al., 2001).

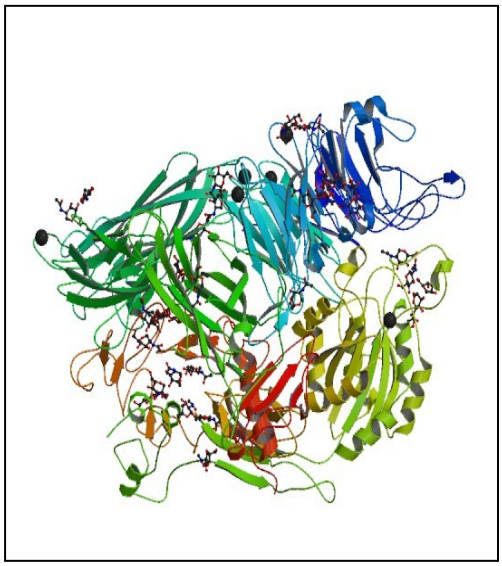

Fig. 8 Integrin αvβ3 ectodomain crystal structure (Xiong J.P., et al., 2009).

The available data indicate that the "flexed" or "bent" conformation represents the inactive form. The analysis of the crystallized conformer of αvβ3, resembles a large “head” on two “legs”. The head of the integrin, which is the minimal fragment that contains ligand-binding activity, comprises a β-propeller from the α subunit, an I domain from the β subunit (the β I domain) and an immunoglobulin “hybrid” domain below the β I domain. The α subunit leg of the integrin comprises three β sandwich domains, termed “thigh”, “calf1” and “calf2”. The β subunit leg contains a plexin-semaphorin-integrin domain (PSI), which is disordered in the structure, four EGF-like (Epidermial growth factor) repeats and a cystatin-like fold. The bend in the integrin is between thigh and calf1 in αv and at the conjuction of the hybrid domain, the two EGF repeats and the PSI domain (in β3) (Xiong J. P., et al., 2004).
In addition, in 2003, the crystal structure of αvβ3 in complex with an Arg-Gly-Asp ligand having sequence c(RGDf[NMeV]), the Cilengitide, a potent αvβ3 antagonist, actually in Phase III clinical trial for the glioblastoma treatment, was determined (Figure 9).

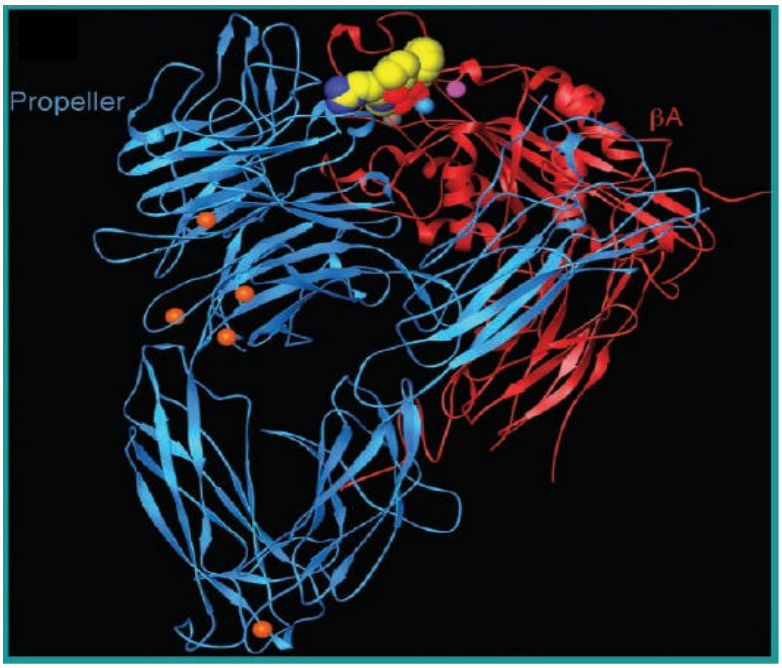

Fig. 9 Crystal structure of αvβ3 in complex with c(RGDf[NMeV]) (Xiong J.P., et al., 2004).

The crystal structure shown that the peptide is inserted in a space between the β propeller and the β I domain on the receptor head. The aspartic and arginine lateral chains are direct in opposite direction. The arginine residue is inserted in a groove on the bottom of the beta propeller of the alpha subunit and its guanidium group interacts with Asp^{218} and Asp^{150} lateral chains through salt bridges. The second Asp carboxyl oxygen forms hydrogen bonds with the backbone amides of Tyr^{122} and Asn^{215} and inteact with MIDAS metallic ions. Contrary to the arginine residue that is partially exposed to the solvent, aspartic acid is completely inserted into the binding site. The Gly residue, which completes the prototype RGD ligand sequence, lies at the interface between the α and β subunits. It makes several hydrophobic interactions with αv, the most critical of which appears to be the contact with the carbonyl oxygen of Arg^{216}.
The remaining two residues of the pentapeptide face are away from the αβ interface and are not interact with the receptor. Selectivity between different subunits is achieved by the RGD sequence conformation.

1.2.2 Phisiological and pathological role

In the last decade, αvβ3 integrin attracted the attention of the scientific community as interesting target for development of new and selective systems for biotechnological applications. This receptor mediates many different biological processes such as intracellular signalling, cell migration, proliferation, and survival through interactions with the conserved Arg-Gly-Asp sequence of several plasma and matrix proteins (Harburger D. S., et al., 2009).
αvβ3 integrin is expressed on a variety of cell types including smooth muscle cells (SMC), endothelial cells (EC), osteoclasts, leucocytes, platelet and mesangimal cells and it plays a crucial role in many pathological events.
In osteoporosis, a chronic bone disease characterized by a decrease in bone mass resulting from accelerated osteoclast mediated bone resorption relative to formation (Nakamura I., et al., 2007), αvβ3 is expressed at high level in osteoclasts. In these cells, the receptor is implicated in the adhesion, activation, and migration on the bone surface as well as in osteoclast polarization. Therefore, inhibition of osteoclast-driven bone resorption by blocking αvβ3 integrin could be useful for the treatment of this disease.
αvβ3 integrin is also implicated in the rheumatoid arthritis (RA), a chronic and systemic inflammatory disorder that may affect many tissues and organs, but mainly attacks synovial joints. Moreover, this integrin is overexpressed on activated macrophages and osteoclasts and these cell types are found in abundance at sites of bone destruction in rheumatoid arthritis patients. In these cases, activated macrophages are markedly increased in both subchondral bone and inflamed synovial tissues, and osteoclasts are markedly increased in subchondral bone at sites of bone erosion and resorption. Consequently, osteoclast mediated bone resorption, macrophage dependent inflammation and inflammatory angiogenesis represent relevant pathogenic features of RA. Hence, these evidences support the view that inhibition of αvβ3 in the synovium of RA patients may have therapeutic benefits (Perdih A., et al., 2010).
Cell-matrix adhesion, migration and differentiation events that underlie restenosis after injury are mediated by αvβ3 integrin-ligand interactions. Different studies have shown that αvβ3 integrin mediates smooth muscle cell proliferation and accumulation in the arterial intima by the interaction with osteopontin that contributes to neointimal thickening in the setting of arterial ligation. Thereby, selective αvβ3 blockade could be an effective anti-restenosis strategy that limits neointimal growth and lumen stenosis following deep arterial injury in coronary angioplasty (i.e. PTCA) (Hodivala-Dilke K., et al., 2008).

1.2.3 αvβ3 and angiogenesis

Among the different diseases αvβ3 integrin is involved in the pathological angiogenesis was the most studied in the last years. Angiogenesis is the formation of new blood vessels starting from pre-existing capillaries. Physiologically this process verify during the embryo formation and, in adults, during menstruation, ovulation, pregnancy and wound healing.
The mechanism of angiogenesis is very complex. In a simplified overview (Figure 5), the angiogenesis starts with the release of angiogenic factors which bind to their receptors on the membrane of ECs, allowing the transmission of the signal that leads to the transcription of several genes. Following angiogenic stimulus, the ECs express integrins, in particular αvβ3 which participates to the activation of vascular endothelial growth factor receptor-2 (VEGFR-2), providing a survival signal to the proliferating vascular cells during new vessel growth. Since a functional vascular network is formed, it is necessary that the new-formed vessel is remodelled to form a mature vessel. At this propose, platelets release the Platelet-derived growth factor (PDGF) as it stimulates the requirement of pericytes and smooth muscle cells which stabilise the morphology of the vessel and prevent the regression of endothelial cells (Harper J., 2006; Nyberg P., et al., 2008; Cristofanilli M. et al., 2002).

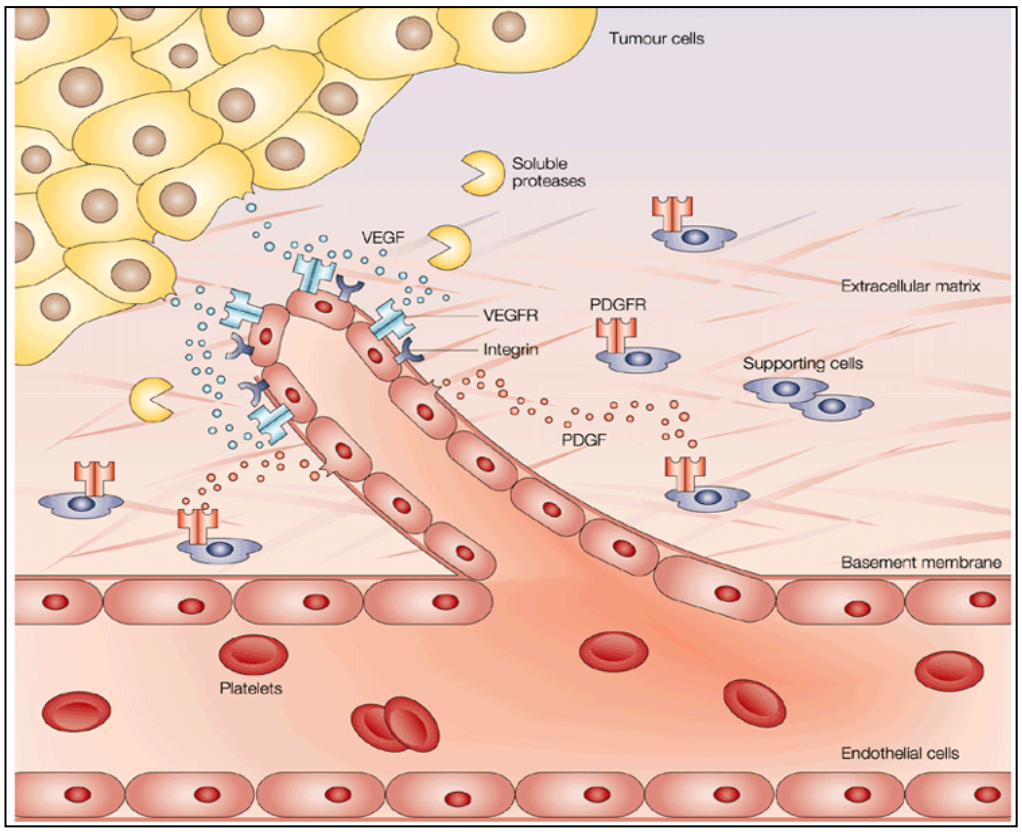

Fig.5 A simple scheme of the angiogenesis processes (Cristofanilli M., et al., 2002).

Angiogenesis is regulated by the equilibrium between pro-angiogenic and anti-angiogenic factors (Table 2).

Pro-angiogenic factors	Inhibitors and antiangiogenic factors
VEGF	mAbs to VEGF VEGFR, RTK inhibitors
bFGF	Suramin, Suradistas, IFNα
αvβ3	Angiostatin,Thrombospondin
HGF	Angioarrestin
TP	TPI, 2dLr
NPY	PF4

TAB. 2 Factors affecting EC proliferation and migration (Bou¨ıs D., 2006).

The shift from this equilibrium (angiogenic switch), under specific stimuli such as hypoxia, is related to several human diseases (pathological angiogenesis) (Figure 6). The overexpression of antiangiogenic-factors, such as angiostatin or thrombospondin, is associated with chronic injury due to inhibition of capillaries growth and prolonged bleeding consequent to inhibition of platelets aggregation (Mu W., et al., 2009). Instead, the prevalence of pro-angiogenic factor such as VEGF or αvβ3 integrin is associated with cancer, proliferating retinopathy and psoriasis (Folkman J., 2001).

To date, it was greatly reported that $\alpha v\beta 3$ integrin receptor seems to be most closely associated with another integrin in angiogenesis process, $\alpha v\beta 5$, playing an important role in tumour-induced angiogenesis. αvβ5 is widely expressed in many malignant tumour cells while αvβ3 has a relatively limited cellular distribution compared with that of αvβ5. In particular, $\alpha v\beta 3$ integrin is normally expressed on mature endothelial cells but it is highly expressed on the activated ECs, in several tumour forms, including melanomas, ovarian and lung carcinomas, osteosarcomas, neuroblastomas, glioblastomas, and breast cancer.

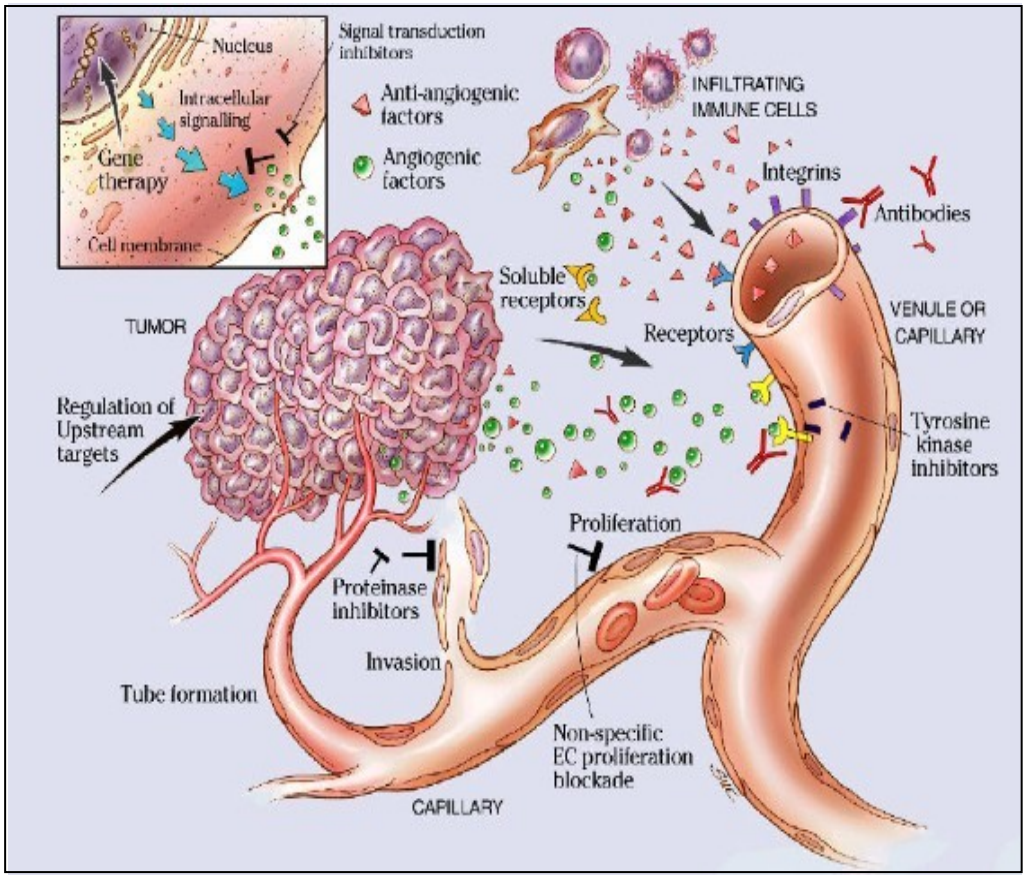

Fig. 6 A simple scheme of the tumor angiogenesis processes (www.wentek.com/jean/research.htm).

Therefore, the development of new compounds that can discriminate between αvβ3 and αvβ5 is required to target αvβ3-mediated processes for diagnostic or therapeutic applications. For this reason in last decade a variety of different compounds able to modulate αvβ3 biological activity was synthesised (Bachmann I.M., et al., 2008).

1.3 αvβ3 INTEGRIN: A THERAPEUTIC AND DIAGNOSTIC APPROACH

1.3.1 αvβ3 integrin: synthetic ligands

Most cancer drugs fail in clinical studies not because they are ineffective in killing cancer cells but because they cannot be administered in doses high enough to contrast the tumour without severely harming the patient.
For this reason in recent years the design of high selective ligands represented a great challenge in cancer therapy. In particular, in biotechnological field, selective ligands could be used to deliver specifically therapeutic and diagnostic molecules into tumour cells.
Many compounds as αvβ3 ligands were developed such as small organic molecules, peptidomimetics, cyclic and linear peptides. Specific monoclonal antibodies, as the human monoclonal antibody LM609 (named Vitaxin) now in phase II clinical trials for the antiangiogenic therapy of colorectal cancer, was also developed (Wilder R.L., et al., 2002).
However, antibody-based compounds, despite the development of chimeric and engineered molecules, suffer of several limitations because of the long circulation half-life, the high background activity, the poor tumour penetration, and the no uniform intratumoral distribution. For these reasons, peptide-based probes, despite the lack of absolute integrin selectivity, are preferred because of small size, preparation by chemical and biological methods, functionalization and conjugation, low toxicity, low immunogenicity, a high affinity and specificity for receptors.
Since different integrins recognise different proteins containing RGD sequences, the contest of the RGD sequence (flanking residues, three dimensional presentation and individual features of the integrin binding pockets) determines the specificity and the efficacy of interaction. For this reason, the actually available molecules in the literature were designed also thanks to information derived from Cilengitide-αvβ3 integrin complex structure that stressed the conformational features of the RGD sequence and the main contacts essential for the receptor interaction.
In 1999 Kesselr and co-workers designed and characterized the Cilengitide, the pentapeptide c(RGDf[NMe]V), (Dechantsreiter M.A., et al., 1999). This molecule is one of the most potent αvβ3 antagonist and is now in phase III clinical trial as antiangiogenic molecule for the treatment of glioblastoma by inhibiting angiogenesis.
Biological assays experienced that the Cilengitide, although not able to discriminate between αvβ3 and αvβ5 shows a higher affinity for αvβ3 respect with αvβ5 (IC_{50} = 3.2 nM and 1.7 nM respectively) (Liu Z., et al., 2008).

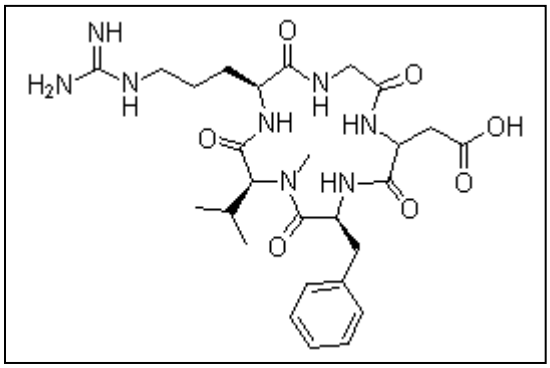

Fig. 10 Cilengitide structure

In 2003 was developed the molecule S247, a peptidomimetic compound able to bind αvβ3 integrin with high affinity (IC_{50}= 0.4nM) and that was demonstrated both in vitro and in vivo that decreases colon cancer metastasis and angiogenesis (Reinmuth N., et al., 2003).
In 2004 Lark and co-workers designed and characterized a new orally active Arg-Gly-Asp peptidomimetic vitronectin receptor antagonist named SB 265123 for prevention of bone loss in osteoporosis. Even if, SB 265123 inhibits αvβ3-mediated cell adhesion with an IC_{50} =60 nM, the compound binds both αvβ3 and the closely related integrin αvβ5 with high affinity (K_i 3.5 and 1.3 nM, respectively), moreover binds, even if weakly, to the related RGD-binding integrins αIIbβ3 (K_i >1 μM) and α5β1 (K_i >1 μM) (Lark M.W., et al., 2004).

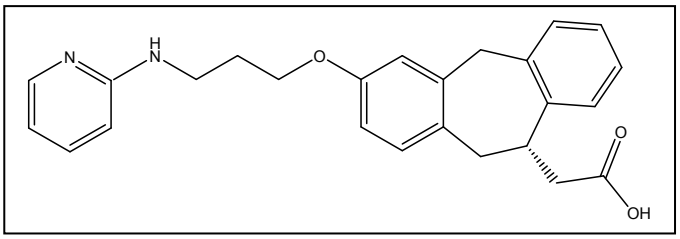

Fig. 11 SB 265123 structure ((Lark M. W., et al., 2004).

Moreover, Scolastico and co-workers in 2006 have synthesised a small library of cyclic RGD pentapeptide mimics incorporating stereoisomeric 5,6- and 5,7-fused bicyclic lactams some of them are reported in (Figure12).

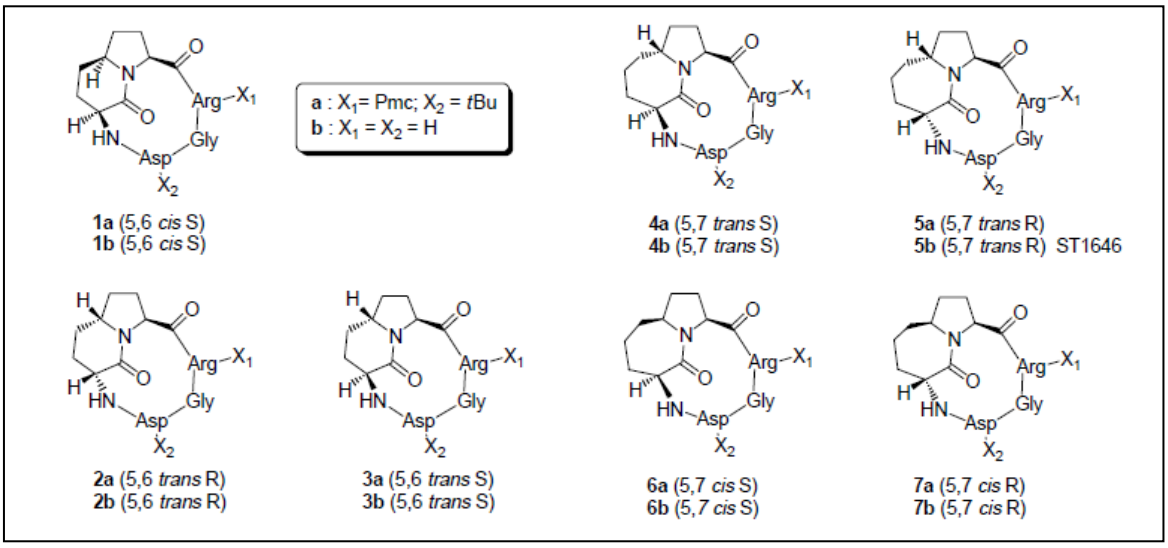

Fig. 12 Cyclic RGD pentapeptide mimics cyclo(Arg-Gly-Asp-Lactam) 1–7. The ring size and the stereochemistry at the bridgehead (cis or trans) and at the C3 (S or R) carbon of the bicyclic lactam are reported in parentheses (Belvisi L., et al., 2006).

In 2009 the same team developed cyclic RGD-containing azabicycloalkane peptides (Figure 13A), and amide and ester derivative of these compunds suitable for target drug delivery and diagnostic applications (Figure 13B).

These molecules shown have a major affinity for target integrins, compared with the ligands of first generation reported above (IC_{50} of 53.7nM and between 30 and 100μM respectively) (Manzoni L., et al., 2009).

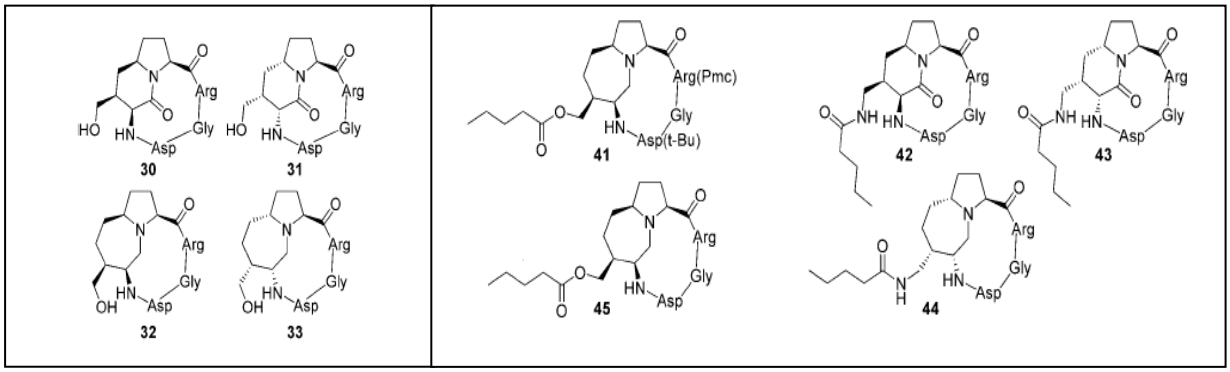

Fig. 13 Synthesis of pseudopeptides based on azabicycloalkane scaffold (A). Synthesis of the amide derivatives 42–44 and ester 45 (B) (Manzoni L., et al., 2009).

Another interesting application of αvβ3 ligands is in diagnostic field.
In the last years, the development of radiolabelled peptides for imaging of a variety of tumours, infection/inflammation and thrombus has seen a new era in nuclear medicine. Due to their small size, peptide molecules exhibit favourable pharmacokinetic characteristics, such as rapid uptake in target tissue and rapid blood clearance, which potentially allow images to be acquired at ones after the administration of the radioactive compounds.
In this contest, radiolabeled cRGD peptides in combination with nuclear imaging techniques such as positron emission tomography (PET) and single photon emission computed tomography (SPECT) have been extensively studied for imaging of αvβ3 expression in experimental tumours (Dijkgraaf I., et al., 2010).
Furthermore in the field of angiogenic research, non-invasive monitoring of molecular processes in the angiogenic cascade will be of great interest for investigation on the mechanisms of angiogenesis basic science, as well as clinical settings where it could help in planning and controlling antiangiogenic therapies.
The lead compound in this field is the radiolabeled Cilengitide's analogue, developed by Kessler and co-workers in 2001, shown in figure 14.

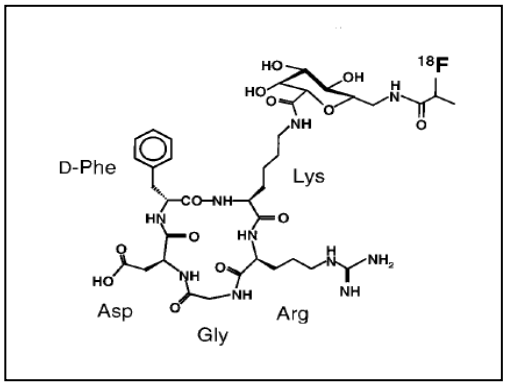

Fig.14 Schematic structure of [^{18}F]Galacto-RGD (Haubner R., et al., 2001).

It was obtained through ^{18}F-labeling of the RGD-containing glycopeptide cyclo(-Arg-Gly-Asp-DPhe-Lys(sugar amino acid)-) with 4-nitrophenyl 2-[^{18}F]fluoropropionate. The obtained compound was biologically evaluated. In particular *in vitro* binding assays showed that the inhibitory peptide was able to fully suppress the binding of the ligands (vitronectin or fibrinogen) to the isolated immobilized receptors (αIIbβ3, αvβ5, and αvβ3) and that the binding kinetics followed a classic sigmoid path.
The IC_{50}s of [^{18}F]Galacto-RGD were 5 (αvβ3), 1.000 (αvβ5), and 200-1200-fold higher affinity for αvβ3 than for αvβ5 and aIIbb3,respectively.
Other interesting compounds was synthesised using [^{18}F]Galacto-RGD, a glycosylated cyclic pentapeptide with the sequence cyclo(-Arg-Gly-Asp-DPhe-Lys(SAA)-) (SAA=sugar amino acid) developed to permit a non-invasive determination of αvβ3 integrin expression in vivo (Beer A.J., et al., 2008) (Figure 15).

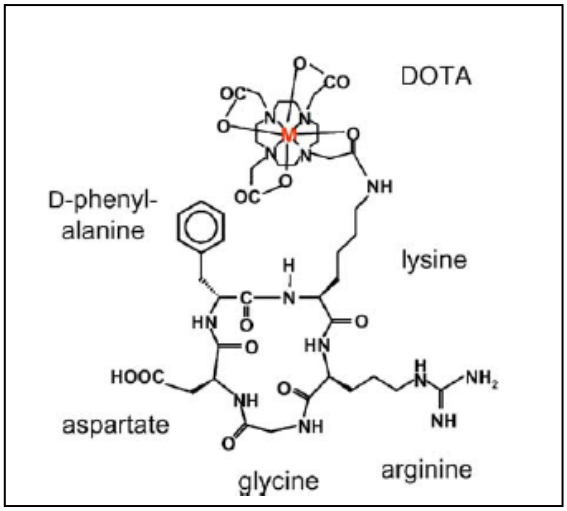

Fig. 15 Schematic structure of the radiolabelled DOTA-RGD peptides. Depending on the isotope used, the metal is hexacoordinated with pseudoctrahedral cis geometry (M=68Ga) or octacoordinated with twisted square antiprismatic coordination geometry (M=111In; as presented at the scheme) (Beer A.J., et al., 2008).

The main drawback of all reported molecule is a low selectivity for αvβ3 although they show a high affinity for the receptor. To overcome this limit, in 2006 a new potent and selective peptide, named RGDechi, able to bind the integrin αvβ3 with a comparable affinity to Cilengitide but with improved selectivity was reported in literature (Del Gatto A., et al., 2006) (Figure 16).

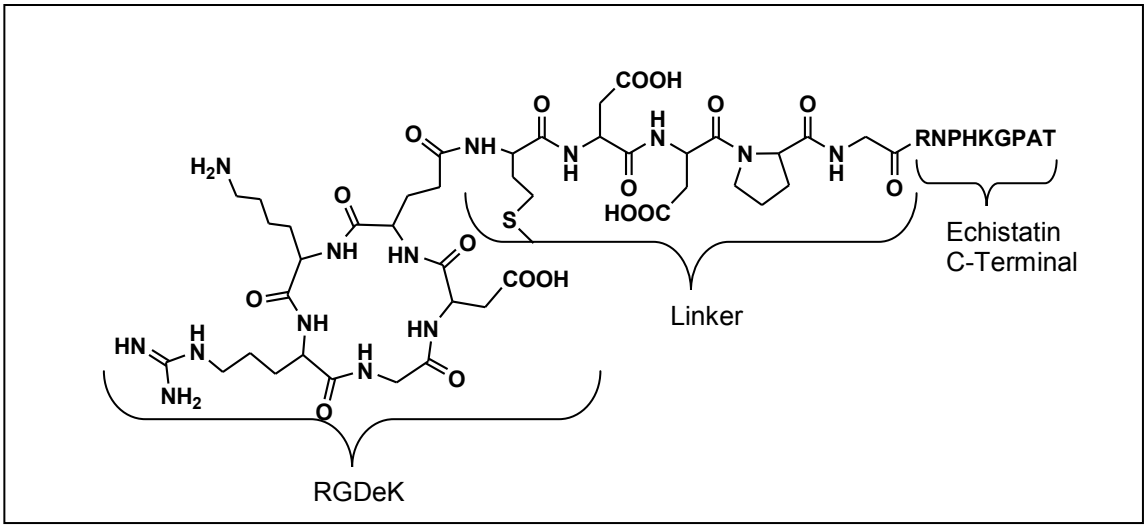

Fig. 16 RGDechi pepide (Del Gatto A., et al., 2006)

RGDechi was designed starting from the Cilengitie-avb3 complex structure. It is a chimeric bifunctional peptide, including a cyclic RGD pentapeptide covalently linked by an amino acidic spacer to the C-terminus domain of the Echistatin, a natural antagonist of αvβ3 integrin extracted from the venom of the snake *Echis Carinatus*. *In vitro* and *in vivo* studies demonstrated that RGDechi is able to discriminate between αvβ3, αvβ5 and αIIbβ3 (Del Gatto A., et al., 2006). Considering the advantages of the radiolabeled peptides application in diagnostic field and the high selectivity of RGDechi peptide, the same research group designed and synthesised an RGDechi analogue suitable for diagnostic and therapeutic applications, named RGDechiHCit (Figure 17) (Zannetti A., et al., 2009). RGDechiHCit presents a residue of homocitrulline, an unnatural amino acid residue related to lysine, in substitution of the Lys^1 of RGDechi peptide to permit the selective labelling of the lysine at the cyclic portion. PET and SPECT imaging *in vivo* studies confirmed that the peptide selectively localizes on αvβ3 expressing tumor cells in xenograft animal model (Zannetti A., et al., 2009).

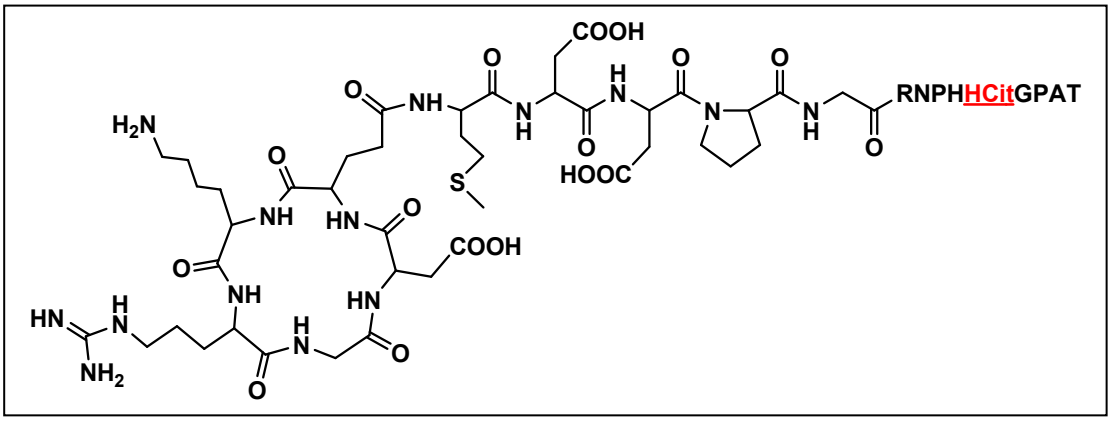

Fig.17 RGDechiHCit peptide (Zannetti A., et al., 2009).

1.3.2 αvβ3 integrin: ligands for drug delivery systems

Recenly, an explosive development of vectors (i.e. micelles, liposomes, etc…) to improve the delivery of drug or tracers in targeted tissues has been reported in literature (Wu H.C., et al., 2010; Gao C.,et al., 2009). In particular, nanoparticles (NP) are playing a pivotal role in providing new types of targeted delivery systems.
Drug delivery based on NP consists of three essential molecules: 1) nanostructure as vehicle; 2) drug conjugated to the nanoparticles; 3) ligands linked to the nanoparticles which binds with high affinity target cells.
Several peptides was used as ligands to obtain selective nanosystems suitable for therapeutic and diagnostic applications.
In 2006 Winter at al. developed αvβ3 integrin-targeted paramagnetic nanoparticles functionalised with Fumagillin, a natural antimicrobic and antiangiogenic biomolecule, that inhibit angiogenesis in atherosclerosis animal model (hyperlipidemic rabbit) and are suitable for MRI (magnetic resonance imaging) (Winter P.M., et al., 2006).
Moreover, in 2007 Lesniak et al., synthesized a stable and clinically relevant dendrimer based nanodevice (ND) cRGD-BT(biotine)-ND that exhibits superior binding to the αvβ3 integrin, when either compared to the same free cRGD peptide or to the biotinylated nanodevice without covalently attached peptide (Lesniak W.G., et al., 2007).
Likewise, in 2008 the synthesis of αvβ3 integrin targeted paramagnetic perfluorocarbon nanoparticle formulated to deliver selectively the rapamycin, an immunosuppressant drug used to prevent rejection in organ transplantation, was reported.
Many biological studies have shown that this nanosystem prepared for diagnostic applications, also inhibits stenosis after balloon injury (Waters E. A., et al., 2008).
Among nanostructured materials, gold nanoparticles (AuNP) also known as “nanogold” are particularly interesting for their intrinsic properties (Bhattacharya R., et al., 2007).
Nanogold are aggregates of sub-micrometre-sized particles of gold (1-100nm) in a fluid, usually water with an unique optical propriety: the Plasmonic resonance. This physical effect is due to the resonant coupling of incident light to the collective oscillation mode of the conduction electrons in the noble metal nanoparticles and is responsible for the commonly observed enhancement in the optical absorption. It may also accompany a strong scattering as a secondary process, usually when the particle size is larger than a few tens of nanometers (Duncan B., et al., 2010). The magnitude of the scattering efficiency and the relative contribution to the total extinction have been shown to vary with the particle size and shape, metal composition, and surrounding medium. The optical scattering is useful in imaging methods to detect conjugated biosystems and has been used in the diagnostics of cancer cells (Melancon M., et al., 2009). For small particles, optical absorption has a dominant effect and the absorbed light energy generally undergoes a thermal dissipation process giving rise to localized heat, which constitutes a basis of biomedical therapeutic applications.
Gold nanoparticles presents many other advantages. They are inert and non toxic, have low immunogenicity, can be easily synthesised in different sizes ranging from 1 nm to 150 nm and ready functionalized generally through thiol linkages. Moreover, their photophysical properties could trigger drug release at remote place (Ghosh P., et al., 2008).

However, nanogold present also a relevant limit: they are not stable in solution and so tend to give aggregates. To prevent the particles from aggregating, some sort of stabilizing agents that cover the nanoparticle surface (Rautaray D., et al., 2004). Moreover, it is known that gold nanoparticles can be functionalised with various organic ligands to create organic-inorganic hybrids with advanced functionality. For example, the use of peptide sequences based on the GC repeats as stabilizing agents for the preparation of monolayer gold nanoparticles was recently reported in literature (Krpetić Z., 2009).
Controlling the surface chemical composition and mastering its modification at the nanometer scale are critical issues for high-added value applications involving nanoparticles. The creation of specific surface sites on nanoparticles for selective attachment of ligand as targeting agents able to recognize tumor molecular markers is considered a promising starting point for their applications in the field of drug delivery. The repertoire of molecules that can be used as targeting agents is greatly expanded, since many ligands (antibody, peptides, proteins etc...) can be anchored on nanoparticles to create higher affinity via multivalent binding to tumor biomarkers. This capped system can be considered a good scaffold for functionalization of molecules suitable for tumour selective targeting delivery.

1.4 THE AIM OF THE WORK

In the last decade, αvβ3 integrin, due to its main role in many pathologies such as tumour angiogenesis, focused the attention of the scientific community as interesting target for development of new and selective systems for biotechnological applications. However, even if all $\alpha v\beta 3$ ligands reported in the literature have a good affinity for this receptor, they present a low selectivity and bind, even if with lower affinity, also other integrin receptors structurally homologues of $\alpha v\beta 3$ such as $\alpha v\beta 5$ integrin (Smith J.W., et al., 2003; Eskens F.A., et al. 2003). Only recently, a cyclic peptide named RGDechiHCit, able to bind with high affinity and selectivity αvβ3 integrin overexpressed on tumor cells was reported in literature (Del Gatto, 2006 Zannetti A., al., 2009). Since no information was available about the antiangiogenic activity of this peptide, a first aims of this PhD thesis have been the study of RGDechiHCit effect on neovascularisation process (in collaboration with the department of clinic medicine, cardiovascular ad immunological science, University "Federico II" of Naples Italy) and study the degradation of this molecule in serum to solve this issue and evaluate the biotechnological application of this molecule as antagonist of αvβ3 integrin.

αvβ3 integrin represents a great challenge also in the field of nanotechnologies for development of selective drug delivery systems. So a further object of this work has been the design and synthesis of a new peptide encompassing the RGD motif, critical for a selective binding of αvβ3 integrin, for gold nanoparticles (AuNP) delivery. Subsequently, we characterised both the RGD peptide and the targeted gold nanoparticles by spectroscopic techniques. The ability of RGD containing nanosystem in comparison with non functionalized NP to penetrate inside glioblastoma target cells was also tested.

2 MATERIALS AND METHODS

2.1 MATERIALS

Polypropylene reaction vessels and sintered polyethylene frits were supplied by Alltech Italia. F=DPhe amino acid, MeIm, TFA and scavengers were purchased from Fluka; Novasyn TGA, Novasyn TGR and 2-Chlorotrityl chloride resin, coupling reagents and all amino acids were from Novabiochem. DIPEA was purchased from Romil; piperidine from Biosolve; $PhSiH_3$ and $Pd(PPh_3)_4$ from Sigma-Adrich.

2.2 PEPTIDE SYNTHESIS

2.2.1 RGDechiHCit synthesis

The RGDechiHCit linear precursor with amino acidic sequence, H-KRGDeMDDPGRNPH*HCit*GPAT-OH, was synthesised using the Fmoc solid-phase strategy (0.1 mmol) (Figure 18). The synthesis was carried out using all standard amino acids except for Fmoc-D-Glu-OAll, to insert the D-Glu residue in the peptide sequence by its carboxyl side chain and the Fmoc-HCit to functionalise selectively the Lys[1] of peptide for therapeutic and diagnostics applications.
The first amino acid was bound to the resin by treatment with Fmoc-Thr(tBu)-OH (5 equiv.)/MSNT (5equiv.)/MeIm (3.75 equiv.) in DCM for 3 h.
The Fmoc deprotection step was performed with 30% piperidine in DMF for 10 min and active ester-coupling reactions were carried out under a 10-fold excess of amino acid and HBTU (9.8 equiv.)/HOBT (9.8 equiv.)/DIPEA (20 equiv.) in DMF.

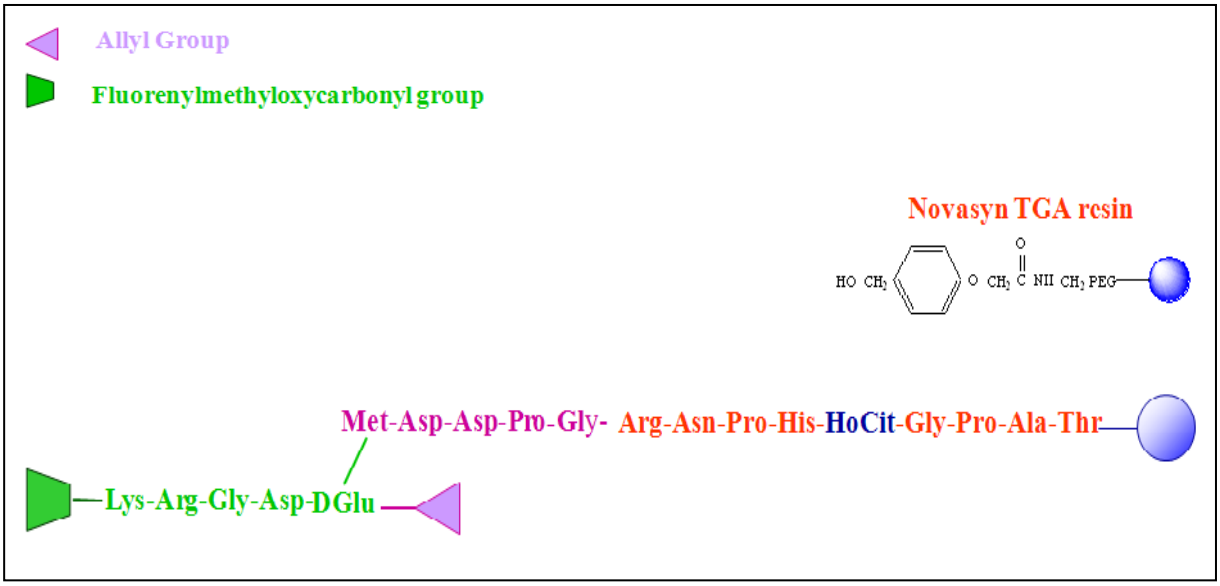

Fig 18 RGDechiHCit linear precursor

During the RGDechiHCit synthesis, before the Fmoc deprotection of Lys[1], a selective alpha-carboxyl deprotection of the D-Glu residue from the allyl group was carried out by treatment of the peptidyl resin with $PhSiH_3$ (24equiv.)/$Pd(PPh_3)_4$ (0.25equiv.) in DCM (Figure 19).

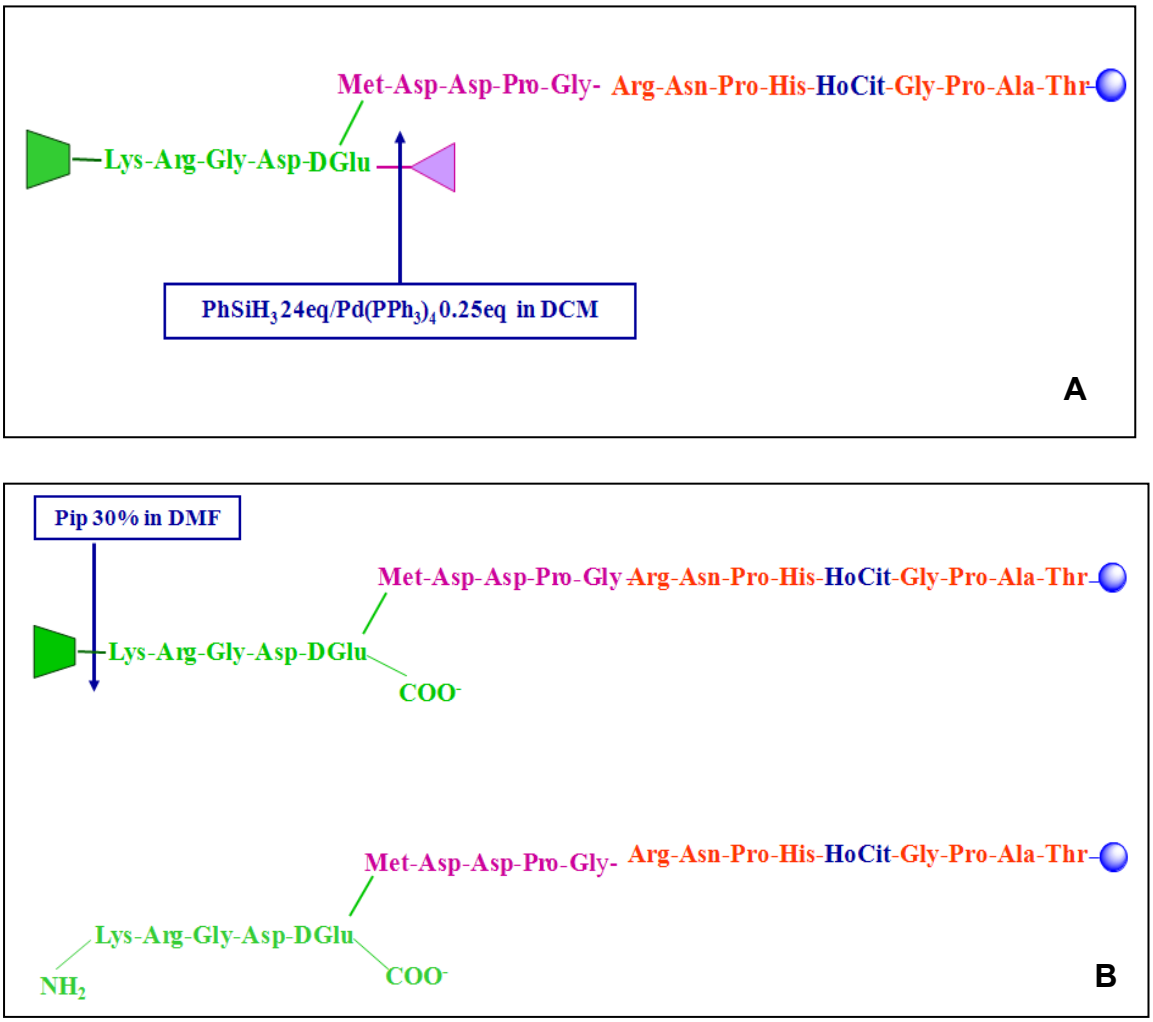

Fig 19 RGDechiHCit linear precursor selective allylic group remotion (A). Fmoc Lys[1]deprotection (B).

The final cyclization between αNH of Lys and αCO of D-Glu was performed on solid phase with PyBop (1.5equiv.)/HOBT(1.5equiv.)/DIPEA (2equiv.) in DMF (Figure 20)

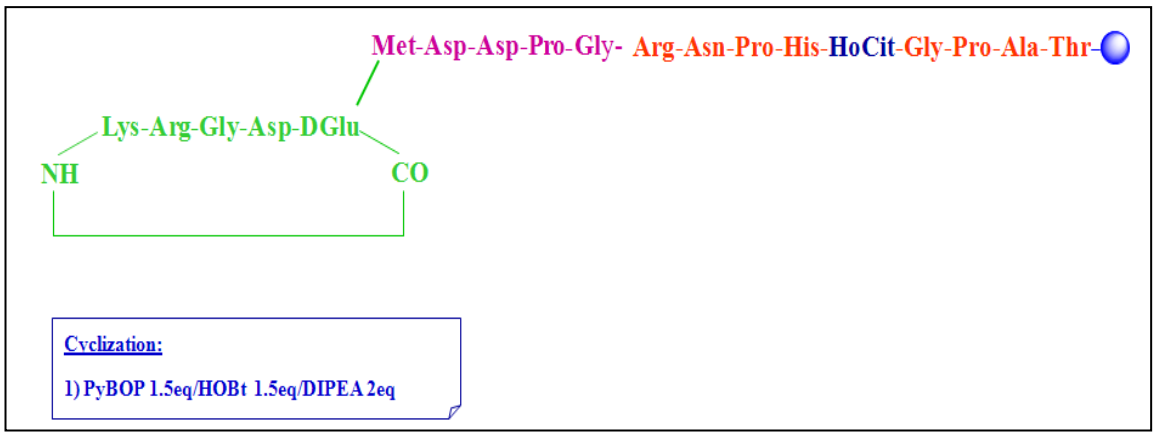

Fig 20 RGDechiHCit cyclisation scheme.

The peptide were cleaved off from the resin and deprotected using a mixture of TFA/ H_2O /EDT/TIS (94:2.5:2.5:1 v/v/v/v).
The resin was filtered, and the peptide was precipitated using cold anhydrous diethyl ether. The crude product was purified by preparative RP-HPLC on the Shimadzu LC-8A system, equipped with an UV-Vis detector SPD-10A using a Phenomenex C18 column (21 x 250 mm; 15µm; 300 Á) and a linear gradient of H_2O (0.1%TFA)/CH_3CN (0.1%TFA) from 5 to 70% of CH_3CN (0.1%TFA) in 30 min at flow rate of 20ml/min. The purified peptide was characterized using LC-MS (Finnigan Surveyor MSQ) using a Phenomenex Jupiter Proteo C12 column (150x 2.00 mm; 4µm; 90Á). The method developed at 0.2mL/min with a linear gradient of H_2O 0.05% TFA/ CH_3CN 0.05% TFA, from 5% to 70% for 30 min.

2.2.2 c(RGDf[NMe]V) synthesis

The synthesis of the Cilengitide (0.1 mmol), (RGDf[NMe]V), was performed using the Fmoc chemistry and the 2-Chlorotrityl chloride resin as solid support. The resin loading was reduced from 1.16 mmol/g to 0.26 mmol/g by MeOH (4ml for 2 minutes) to prevent inter peptides cyclization side reactions. The linear protected peptide was assembled with the Gly residue at the C-terminus to prevent racemisation and steric hindrance during the cyclization step (Dechantsreiter M.A., et al., 1999). The first amino acid (1 eqiv.) was dissolved in dry THF (approx. 5 ml). The mixtrure was added to the resin and was stirred for 120 min. At the end of this time, the resin was washed 3 times with DCM /MeOH/DIPEA (17:2:1 v/v/v); DCM (3x1min); DMF(3x1min); DCM (2x1min). The Fmoc deprotection step was performed with 30% piperidine in DMF for 10 min and active ester-coupling reactions were carried out under a 10-fold excess of amino acid and HBTU (9.8 equiv.)/HOBT (9.8 equiv.)/DIPEA (20 equiv.) in DMF (Figure 21).

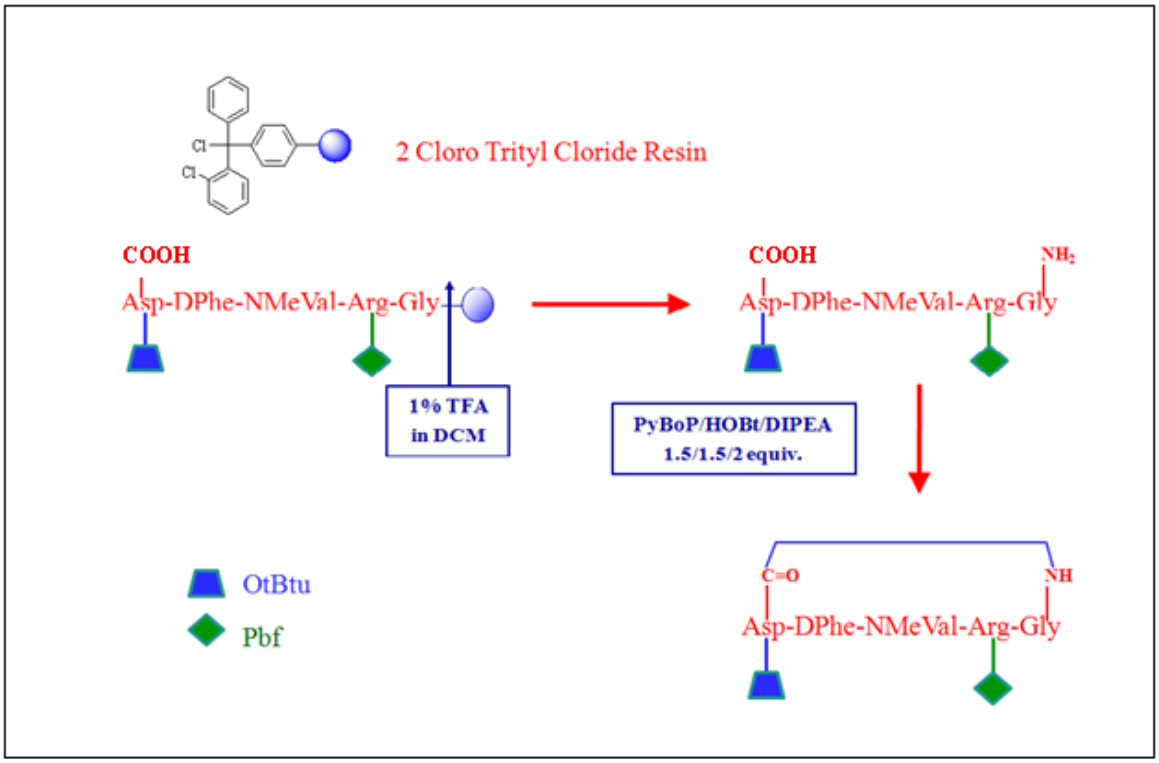

Fig 21 Cilengitide cyclisation scheme.

At the end of the synthesis, the protected peptide was cleved from the resin using diluite TFA (1%) in DCM. The mixture was added to the solid support and was shaked for 2 minutes. The solution was filters by appling nitrogen pressure into a flask containing 10% pyridine in methanol (2 ml). This step was repeated for 10 times and at the end, the residual protected peptide was washed out from the resin with 3x30 ml DCM, 3x30 ml MeOH, and the filtrates were analysed by TLC.
Then, the filtrates containing the product were combined and and evaporated under reduced pressure to 5% of the volume. Finally, was added water (40 ml) to the residue and the mixture obtained was cooled with ice to aid precipitation of the product.

This last, was isolated by filtration through a sintered glass funnel and was dryed in an desiccator.
At this point, the protected peptide was cyclisated in solution (1.25 x 10^{-3}M) in DMF via in situ activation using PyBop, HOBt and DIPEA (1.5/1.5/2 eqiv) as cyclisation reagents.
Final deprotection was achieved with TFA using a mixture of TFA/ H_2O /EDT/TIS (94:2.5:2.5:1 v/v/v/v). The crude product was purified by preparative RP-HPLC on the Shimadzu LC-8A system, equipped with an UV-Vis detector SPD-10A using a Phenomenex C18 column (21 x 250 mm; 15µm; 300 Å) and a linear gradient of H_2O (0.1%TFA)/CH_3CN (0.1%TFA) from 5 to 70% of CH_3CN (0.1%TFA) in 30 min at flow rate of 20ml/min. The purified peptide was characterized by LC-MS (Finnigan Surveyor MSQ) using a Phenomenex Jupiter Proteo C12 column (150x 2.00 mm; 4µm; 90Å). The method developed at 0.2mL/min with a linear gradient of H_2O 0.05% TFA / CH_3CN 0.05% TFA from 5% to 70% for 30 min.

2.3 *In vitro* STUDIES

All *in vitro* studies were performed using bovine aortic EC (BAEC) and vascular smooth muscle cells (VSMC) cultured in Dulbecco's modified Eagle's medium (DMEM; Sigma-Aldrich, Milano, Italy) as previously described and validate (Iaccarino G., et al., 2004). All experiments were performed in triplicate.

2.3.1 Cell proliferation assay

Cells were seeded at density of 10000 per well in six-well plates, serum starved, pre-incubated overnight with c(RGDf-[NMe]V), or RGDechiHCit (10^{-6}M) and then stimulated with 5% fetal bovine serum (FBS). Cell number was measured at 3, 6, 12, 24 h after stimulation as previously described (Santulli G., et al., 2009).

2.3.2 DNA synthesis

Cells were serum-starved for 24 h and then incubated in DMEM with [^{3}H]thymidine and 5% FBS. After 3, 6, 12, 24 h [^{3}H]thymidine incorporation was assessed as previously described (Santulli G., et al., 2009).

2.3.3 Endothelial Matrigel assay

The formation of network-like structures by EC on Matrigel® (BD Biosciences, Bedford, MA, USA) was performed as previously described and validated (Santulli G., et al., 2009).
Tubule formation was defined as a structure exhibiting a length four times its width. Network formation was observed using an inverted phase-contrast microscope (Zeiss). As negative control Phenylephrine (10^{-7}M) was used. Representative fields were taken, and the average of the total number of complete tubes formed by cells was counted in 15 random fields by two independent investigators.

2.3.4 Western blot

Immunoblot analyses were performed as previously described and validated (Illario M., et al., 2005).
Serine-tyrosine phosphorylated ERK1/2 (extracellular signal regulated kinase; Cell Signaling Technology, Danvers, MA, USA), total ERK (Santa Cruz Biotechnology, Santa Cruz, CA, USA), pCaMKII (Santa Cruz Biotechnology), CaMKII (Santa Cruz Biotechnology) were visualized with specific antibodies, anti-rabbit and anti-goat horseradish peroxidase-conjugated secondary antibody (Santa Cruz Biotechnology) and standard chemiluminescence (Pierce) on autoradiographic films. Autoradiographies were then digitalized and densitometry quantification performed using dedicated software (ImageQuaNT; Molecular Dynamics). Levels of VEGF, were determined by immunoprecipitation of VEGF (protein A/G agarose beads conjugated with a rabbit polyclonal antibody raised against VEGF (Santa Cruz Biotechnology) visualized by a goat polyclonal IgG (Santa Cruz Biotechnology). Experiments were performed in triplicate to ensure reproducibility. Data are presented as arbitrary densitometry units after normalization for the total corresponding protein or actin as internal control (Ciccarelli M., et al., 2008).

2.3.5 Peptides processing in serum and plasma

About 8 µl of a 1 mg/ml solution of RGDechiHCit peptide and of Cilengitide were incubated at 37° C with 20 µl human serum and plasma. Samples withdrawn after 1, 2, 4 and 24 h were, centrifuged for 1 min at 10,000 × g (Bracci L., et al., 2003).
These solutions were analyzed by LC-MS using a Phenomenex C_{18} column (250x 2 mm; 5 µm; 300 Å) and a linear gradient of H_2O (0.05%TFA)/CH_3CN (0.05%TFA) from 10% to 80% of CH_3CN in 30 min at flow rate of 0.2 ml/min.

2.4 *In vivo* STUDIES

2.4.1 Wound Healing

Wound healing assay was performed on 14-week-old (weight 293±21 g) normotensive WKY male rats (Charles River Laboratories, Milan, Italy; n=18), and Matrigel plugs experiments were carried out on 16-week-old (weight 33±4 g) c57BL/6 mice (Charles River Laboratories, Milan, Italy; n=13). All animal procedures were performed in accordance with the *Guide for the Care and Use of Laboratory Animals* published by the National Institutes of Health in the United States (NIH Publication No. 85- 23, revised 1996) and approved by the Ethics Committee for the Use of Animals in Research of “Federico II” University (Illario M, et al., 2005).
The rats (n=18) were anesthetized using vaporized isoflurane (4%, Abbott) and maintained by mask ventilation (isoflurane 1.8%). The dorsum was shaved by applying a depilatory creme (Veet, Reckitt-Benckiser, Milano, Italy) and disinfected with povidone iodine scrub. A 20 mm diameter open wound was excised through the entire thickness of the skin, including the *panniculus carnosus* layer, as described and validated [5, 26]. Pluronic gel (30%) containing (10^{-6} M) c(RGDf-[NMe]V) (n=6), RGDechiHCit (n=7), or saline (n=5) was placed directly onto open wounds, then covered with a sterile dressing. Two operators blinded to the identity of the sample measured wound areas every day, for 8 days. Direct measurements of wound region were determined by digital planimetry (pixel area), and subsequent analysis was

performed using a computer-assisted image analyzer (ImageJ software, version 1.41, National Institutes of Health, Bethesda, MD, USA). Wound healing was quantified as a percentage of the original injury size. After eight days, rats were euthanized and dorsal skin was collected, fixed by immersion in phosphate buffered saline (PBS, 0.01M, pH 7.2-7.4)/formalin and then embedded in paraffin to be processed for immunohistology, as described (Takahashi S.,et al., 2010).

2.4.2 Matrigel Plugs

Mice (n=13), anesthetized as described above, were injected subcutaneously midway on the dorsal side, using sterile conditions, with 0.2 ml of Matrigel® (BD Biosciences, Bedford, MA, USA), mixed with 10^{-6}M VEGF and 10^{-5}M c(RGDf-[NMe]V) (n=4), 10^{-6}M VEGF and 10^{-5}M RGDechiHCit (n=5), or 10^{-6}M VEGF alone (n=4). After seven days, mice were euthanized and the implants were isolated along with adjacent skin to be fixed in 10% neutral-buffered formalin solution and then embedded in paraffin. All tissues were cut in 5 µm sections and slides were counterstained with a standard mixture of hematoxylin and eosin. Quantitative analysis was done by counting the total number of endothelial cells, identified by lectin staining, as previously described (Takahashi S., et al., 2010) in the Matrigel plug in each of 20 randomly chosen cross-sections per each group, at ×40 magnification, using digitized representative high resolution photographic images, with a dedicated software (Image Pro Plus; Media Cybernetics, Bethesda, MD, USA).

2.5 DATA PRESENTATION AND STATISTICAL ANALYSIS

All data are presented as the mean value±SEM. Statistical differences were determined by one-way or two-way ANOVA and Bonferroni post hoc testing was performed where applicable.
A p value less than 0.05 was considered to be significant. All the statistical analysis and the evaluation of data were performed using GraphPad Prism version 5.01 (GraphPad Software, San Diego, CA, USA).

2.6 FUNCTIONALISED GOLD NANOPARTICLES

2.6.1 $RGD(GGC)_2$, $RGD(GC)_2$ and $(GC)_2$ design and synthesis

The peptides $RGD(GGC)_2$, $RGD(GC)_2$, and $(GC)_2$ were synthesized using the Fmoc solid-phase strategy (0.1 mmol) using all standard amino acids except for Fmoc-Glu-OAll. Peptide sequences are reported in Table 3.

Peptide	**Sequence**
$RGD(GGC)_2$	$_c$(RGDfE)GGCGGCG-NH_2
$RGD(GC)_2$	$_c$(RGDfE)AGCGGCG-NH_2
$(GC)_2$	Ac-GGCGGCG-NH_2

TAB. 3 $RGD(GGC)_2$; $RGD(GC)_2$; $(GC)_2$ sequences

Active ester-coupling reactions were carried out under a 5-fold excess of amino acid, incused the first residue of Gly, and HBTU (9.8 equiv.)/HOBT (9.8 equiv.)/DIPEA (20 equiv.) in DMF.
The Cyst residues, 5-fold excess, was coupled without preactivation using HBTU/TMP(5eqiv./5eqiv.) for 90 min to prevent racemisation (Han Y., et al.,1997).
The Fmoc deprotection step was performed with 30% piperidine in DMF for 10 min and. During the synthesis, before the Fmoc deprotection of the last amino acid, a selective deprotection of the Glu residue from the allyl group was carried out by treatment of the peptidyl resins with $PhSiH_3$ (24equiv.)/$Pd(PPh_3)_4$ (0.25equiv.) in DCM Figure 22 A). The final cyclization between αNH of Arg and αCO of D-Glu was performed on solid phase with PyBop, HOBt and DIPEA (1.5/1.5/2 eqiv.) as cyclisation reagents (Figure 22 B).

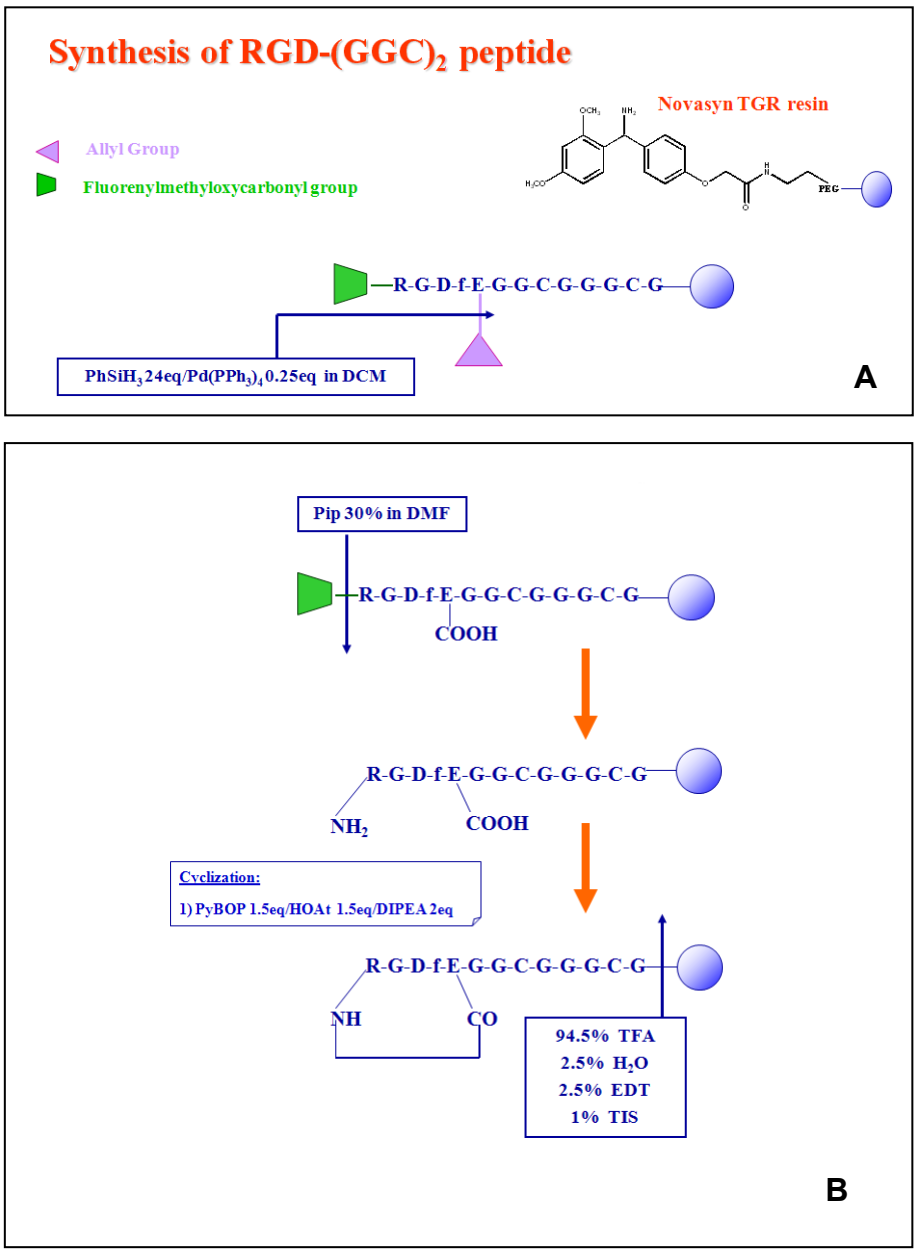

Fig. 21 RGD(GGC)$_2$ deallylation scheme (A); RGD(GGC)$_2$ cyclisation scheme(B).

N-terminal acetylation of the peptide $(GC)_2$ was carried out with a mixture of acetic anhydride/DIPEA/ HOBT (0.5M/0.5M/0.125M) in DMF two times for 10 min.
All the peptides were cleaved off from the resin and deprotected using a mixture of TFA/ H_2O /EDT/TIS (94:2.5:2.5:1 v/v/v/v).
The resins were filtered, and the peptide was precipitated using cold anhydrous diethyl ether. The crude products were purified by preparative RP-HPLC on the Shimadzu LC-8A system, equipped with an UV-Vis detector SPD-10A using a Phenomenex C18 column (21 x 250 mm; 15µm; 300 Å) and a linear gradient of H_2O (0.1%TFA)/CH_3CN (0.1%TFA) from 5 to 70% of CH_3CN (0.1%TFA) in 30 min at flow rate of 20ml/min. The purified peptides were characterized using LC-MS (Finnigan LCQ DECA XP MAX) using a Phenomenex Jupiter Proteo C12 column (150x 2.00 mm; 4µm; 90Å). The method developed at 0.2mL/min with a linear gradient of H_2O 0.05% TFA/ CH_3CN 0.05% TFA, from 5% to 70% of CH_3CN for 30 min.

2.6.2 Preparation of functionalized gold nanoparticles

For preparation of $RGD(GC)_2$ and $(GC)_2$ functionalised gold nanoparticles (named $RGD(GC)_2$AuNPs and$(GC)_2$AuNPs respectively) an aqueous solution of $NaAuCl_4$ ($5\cdot10^{-2}$M) and proper volumes of the corresponding peptide aqueous solution ($5\cdot10^{-4}$M) were mixed in six test-tubes containing 5 mL of H_2O mQ, under vigorous magnetic stirring. Au:stabiliser peptide:agent molar ratios have been carefully set up following the quantities and molar ratios reported in table 4.

№	n (mmol)	Volume (µL)	Molar ratios (Au:L:BH_4^-)
1	$2.4\cdot10^{-5}$	27.9	1:0.01:2
2	$1.2\cdot10^{-5}$	14	1:0.005:2
3	$2.4\cdot10^{-6}$	2.8	1:0.001:2
4	$2.4\cdot10^{-5}$	28	1:0.01:1
5	$1.2\cdot10^{-5}$	14	1:0.005:1
6	$2.4\cdot10^{-6}$	2.8	1:0.001:1

TAB. 4 Peptide quantities and molar ratios

For setting the minimal amount of the needed peptide for an efficient stabilization of Au nanoparticles, series of probes have been carried out varying the molar ratio of peptide: metallic Au. Aqueous solution of $NaAuCl_4$ (52 µL, C= $4.64\cdot10^{-2}$M and 47 µL, C= $5.07\cdot10^{-2}$M) and the corresponding volumes of the peptide aqueous solutions were added in six test-tubes containing 5 mL of mQ water under vigorous stirring (Porta F., et al., 2008). An aqueous solution of $NaBH_4$ 0.1M ($5\cdot10^{-3}$ mmol) was used as reducing agent and it was added after 5 min from the previous addition. Colourful sols were immediately formed. The colours of the obtained sols varied from bluish to red depending on the molar ratio from the component

2.6.3 UV characterization

The peptides and the functionalised gold nanoparticles UV-VIS characterisation was performed using a spettrophotometer Jasco V550 and standard UV-VIS quartz cuvettes (Hellman) with a 1cm path length and a volume of 500 µl. The data were collected with a speed scan of 100nm/min and data pitch of 1nm.
The samples were prepared by dissolving the compounds to a concentration of 1.8 x 10^{-5}M in H_2O. The spectra were acquired in the range of 200-800nm.

2.6.4 ATR-FTIR characterization

ATR-FTIR analysis was performed on a JASCO FT/IR-4100 spectrometer from 2300 to 500 cm^{-1}. For the ATR-FTIR analysis, the samples of gold colloids were freeze-dried, and the analysis of the free peptide and $RGD(GC)_2$ stabilized gold particles was performed on solid state.

2.6.5 NMR characterization

NMR samples consist of 1 mg of RGD peptide or 0.5 mg of $RGD(GC)_2$AuNPs nanoparticles and $(GC)_2$ nanoparticles dissolved in 600 µl of a H_2O/D_2O (90:10) mixture. NMR spectra for resonance assignments of the RGD peptide were collected at 25°C on a Varian *UNITYINOVA* 600 spectrometer, equipped with a 5-mm triple resonance probe and triple-axis pulsed-field gradients, located at the "Institute of Biostructures and Bioimaging" (CNR, Naples, Italy). Proton resonances were assigned using a standard protocol based on comparison of 2D [^{1}H, ^{1}H] TOCSY (Griesinger et al 1988) (mixing time: 70 ms) and 2D [^{1}H, ^{1}H] ROESY (Bax and Davis, 1985) (mixing times: 150 and 200 ms) experiments. 2D spectra were generally recorded with 64 scans, 256 FIDs in t_1, 2048 data points in t_2.
NMR spectra (1D proton and 2D [^{1}H, ^{1}H] TOCSY (70 ms mixing time)) of a dispersion of $RGD(GC)_2$AuNPs and $(GC)_2$AuNPs were recorded on the Varian *UNITYINOVA* 600 spectrometer equipped with a cold probe, by acquiring 512-2048 and 256 scans for 1D and 2D experiments respectively.
Water signal was suppressed by means of either the WATERGATE PFG (Piotto et al 1992) or the DPFGSE (Double Pulsed Field Gradient Selective Echo) techniques (Dalvit, 1998). Proton resonances were referenced to the water signal at 4.75 ppm.
Spectra were processed with the Varian software VNMRJ 1.1D and analyzed with NEASY (Bartels et al 1995) as implemented in CARA.

2.6.6 TEM characterization

Transmission electron microscopy (TEM) micrographs of the colloidal dispersions were obtained using a FEI Tecnai Spirit instrument operated at an accelerating voltage of 120 kV.
Carbon-supported copper grids were used to support the colloidal dispersions. Specimens for imaging by TEM were prepared by evaporating a droplet (100ul) of gold nanoparticle solutions ($8x10^{-5}$M) onto carbon-coated copper grids. A histogram of the particle size distribution and the average particle diameter were obtained by measuring about 200 particles (Porta F., et al., 2008).

2.6.7 Cellular uptake

For cellular uptake studies, U-87 MG cells have been used, kindly donated by Dr. Maura Francolini of the Dept. of Pharmacology, Chemotherapy and Medical Toxicology of Milan, Italy. Glioblastoma is the highest differentiated form of astrocytic brain tumors; in most cases it is irresponsive to radiation and chemotherapy. U-87 MG (malignant glioma) cells are used as an vitro model of human glioblastoma cells to investigate the cytotoxic effect of chemo-therapeutic drugs towards cancer cells.
Cells were grown on coverslip in Dulbecco's modified Eagle's medium (Gibco, Paisley, Scotland) supplemented with 10% heat-inactivated foetal calf serum (Gibco), 1% L-glutamine (Eurobio), 100 UI/ml penicillin G and 100 g/ml streptomycin and maintained at 37°C in a humid atmosphere of 5% CO_2 in air. After treatment with $2x10^{-3}$M of AuRGD for 5, 20, 60, 120, and 180 min the supernatant was removed, and sprayed with CryoSpray® in order to fix the cells. Subsequently, a cover glass slide with fixed cells was placed onto a microscopy glass slide containing 10 μl of Gel Mount® aqueous-based mounting medium. Prepared glass slides were glued and kept in freezer/dark room before microscopy observations. In the described protocol, use of 4% paraformaldehyde or glutharaldeide fixative solution is avoided in order to remove any false signals during confocal microscopy observations (Krpetić Z, et al.,2009).

3 RESULTS AND DISCUSSION

3.1 PEPTIDES: DESIGN, SYNTHESIS AND CHARACTERISATION

3.1.1 Synthesis and Characterization of RGDechiHCit

The peptide RGDechiHCit was designed on the bases of the RGDechi peptide (Del Gatto A., et al., 2006).
It presents a residue of homocitrulline, an unnatural amino acid residue related to lysine, in substitution of the Lys[1].
RGDechiHCit was synthesised on solid phase using the Fmoc chemistry as previously described. On solid phase cyclisation step was optimised using a minor dilution ($2x10^{-4}$M) compared with which reported in literature (Del Gatto A., et al., 2006) and was obtained with a yield of 30% and a purity of 99%.
The purified peptide (theoretical MW=2100.1 Da) was characterized using LC-MS, which gave the expected molecular ion peak $[M + H]^+$ of 2100.3 and an ion $[M+ 2H]^{+2}$of 1050 respectively as showed in figure 23 A and B.

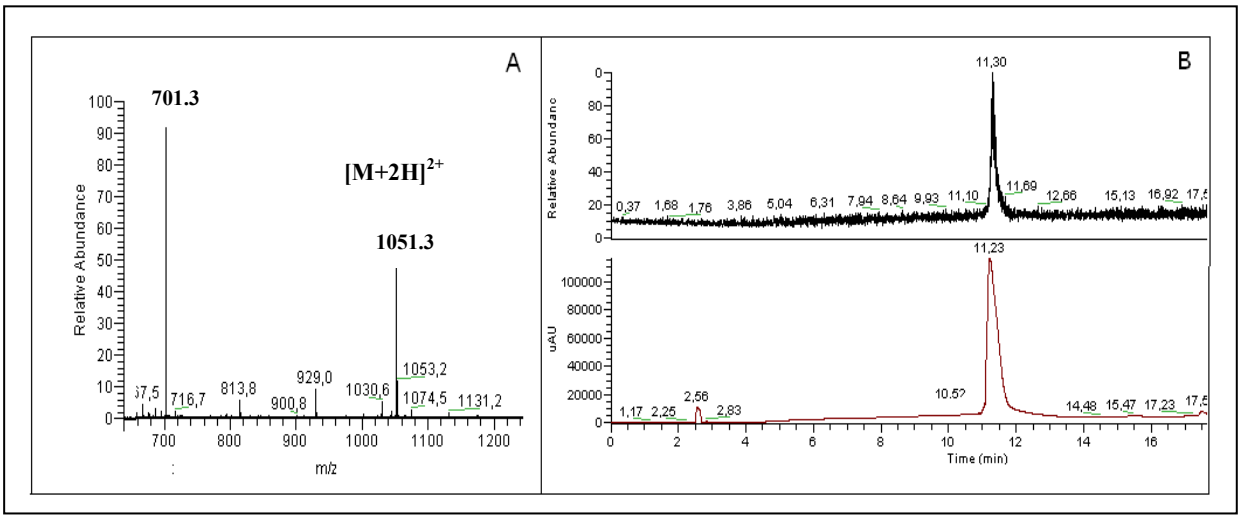

Fig. 23 RGDechiHCit eptide mass spectrum (A); TIC profile and HPLC spectrum (B).

3.1.2 Synthesis and Characterization of c(RGDf[NMe]V)

To have a peptide as positive control in RGDechiHCit biological studies, we synthesised the Cilengitide, having sequence c(RGDf[NMe]V).
Its synthesis was performed on liquid phase as previously described. The peptide was obtained with a final yeald of 49% and a purity of 99%. The purified peptide (theoretical MW=589 Da) was characterized by LC-MS, which gave the expected molecular ion peak $[M + H]^+$ of 589 as showed in figure 24A and B.

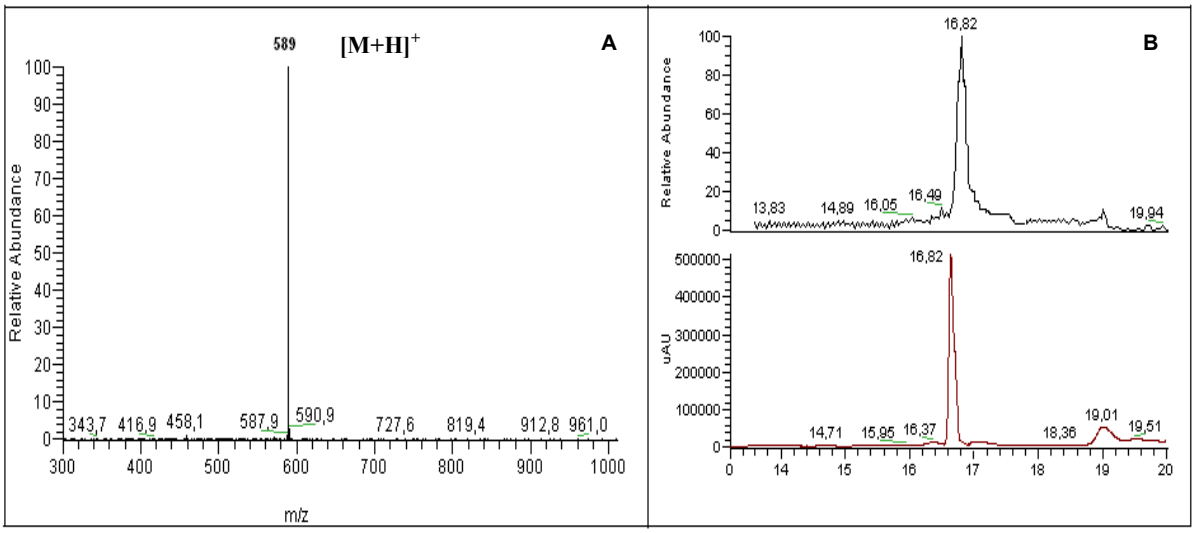

Fig. 24 c(RGDf[NMe]V) peptide mass spectrum (A); TIC profile and HPLC spectrum (B).

3.2 PEPTIDES IN SERUM STABILITY EVALUATION

RGDechiHCit and c(RGDf[NMe]V) peptides stabilities were evaluated in serum. The degradation of the peptides were followed by LC/MS. The reversed-phase high performance liquid chromatography (RP-HPLC) of RGDechiHCit before the serum incubation showed a single peak at t_r=11.82 min corresponding to the complete sequence (theoretical MW=2100.1 Da) as indicated by the $[M+H]^+$, $[M+2H]^{2+}$ and $[M+3H]^{+3}$ molecular ion adducts in the MS spectrum (Figure 25A). After 1h, chromatography showed two peaks, ascribable to RGDechiHCit and to a fragment of the complete sequence (theoretical MW=1929.1Da), respectively, as confirmed by MS spectrum. Finally, after 24h a further peak at t_r=10.93 min corresponding to another RGDechiHCit degradation product (theoretical MW=1775.8 Da) appeared, as indicated by the molecular ion adducts in the MS spectrum, although the peaks attributed to the RGDechiHCit and to the first fragment were still present (Figure 25 B). Considering the obtained fragment we hypothesized that RGDechiHCit peptide was cleaved by a Prolyl peptidase: a serine protease subfamily that cleaves peptide bonds at the C-terminal side of proline residues. Its activity is confined to action on oligopeptides of less than 10 kDa.

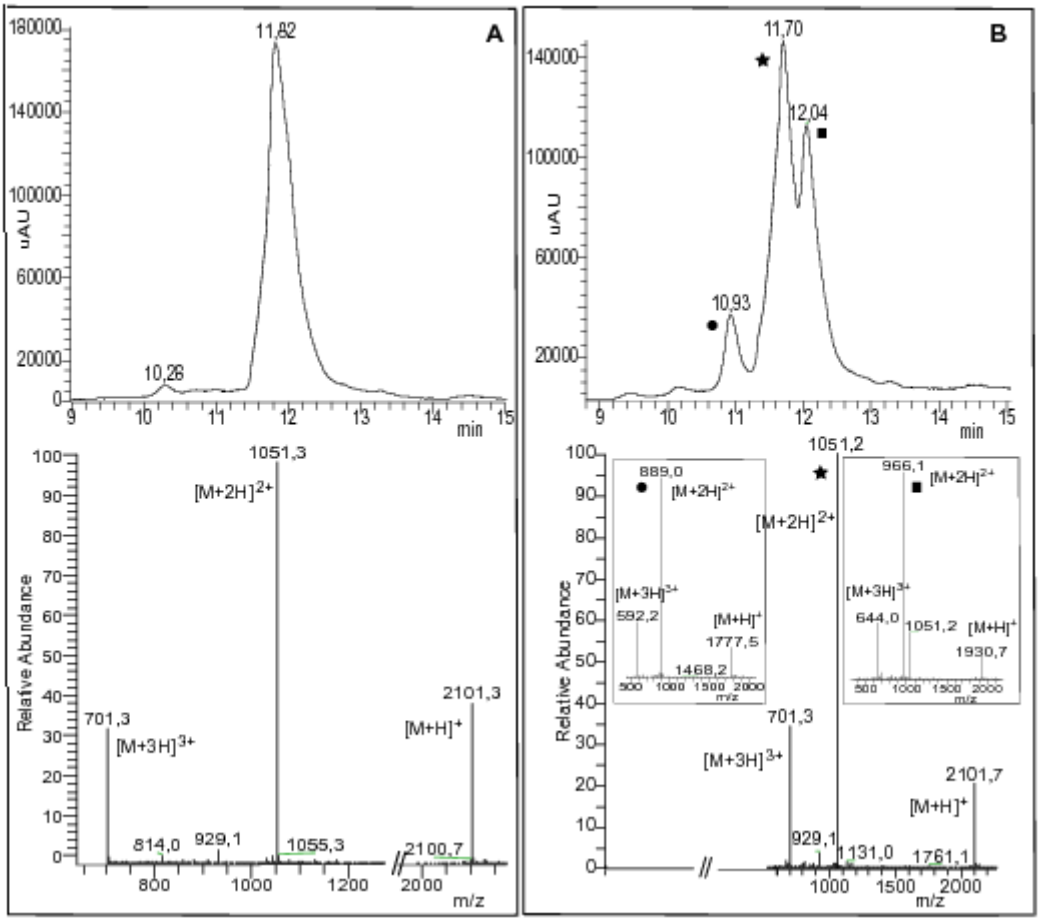

Fig. 25: RGDechiHCit after incubation in human serum at t=0 (A) and after 24h (B).

In contrast with RGDechiHCit, c(RGDf[NMe]V) showed high stability in serum. The RP-HPLC profile of the peptide before the incubation showed a single peak at t_r=16.64 min, ascribable to the complete sequence by the MS spectrum (Figure 26A). After 24h of incubation chromatogram and mass profiles failed to identify any degradation product (Figure 26 B).

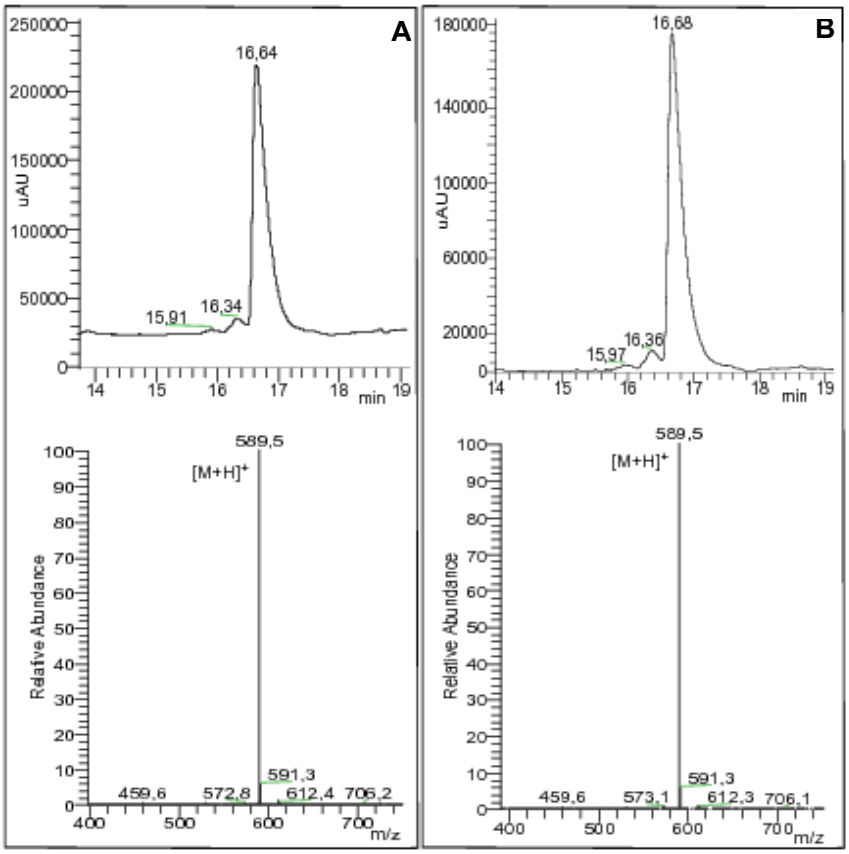

Fig. 26 c(RGDf[NMe]V) after incubation in human serum at t=0 (A) and after 24h (B).

Since RGDechiHCit showed a low stability, we replenished antagonists every six hours in experiments involving chronic exposure.

3.3 RGDechiHCit ANTIANGIOGENIC ACTIVITY: *in vitro* STUDIES

3.3.1 Cell proliferation and DNA synthesis

Angiogenesis is intimately associated to EC proliferation. Therefore, we explored the effects of RGDechiHCit and c(RGDf[NMe]V) on hFN-stimulated EC. In this cellular setting, after 6 hours, both $\alpha_v\beta_3$ integrin antagonists inhibited in a comparable way the ability of hFN to induce proliferation (hFN: +1.98±0.6; hFN+RGDechiHCit: +0.58±0.24; hFN+c(RGDf[NMe]V): +0.6±0.38 fold over basal; $p<0.05$, ANOVA) as depicted in figure 27A. After 20 hours such inhibitory effect was less marked (Figure 27A). In VSMC there was only a trend of an anti-proliferative effect for these peptides, due to the less evident action of hFN in this specific cellular setting (hFN: +1.21±0.1; hFN+RGDechiHCit: +0.93±0.07; hFN+c(RGDf[NMe]V): +0.9±0.09 fold over basal; NS; Figure 27A). The effects of RGDechiHCit and c(RGDf[NMe]V) on EC and VSMC proliferation were also measured by assessing the incorporation of [^{3}H]Thymidine in response to hFN.
This assay confirmed the anti-proliferative action of both these peptides, which is more evident after 6 hours and in ECs (hFN: +1.84±0.24; hFN+RGDechiHCit: +1.02±0.2; hFN+c(RGDf[NMe]V): +1.09±0.07 fold over basal; $p<0.05$, ANOVA; Figure 27B).

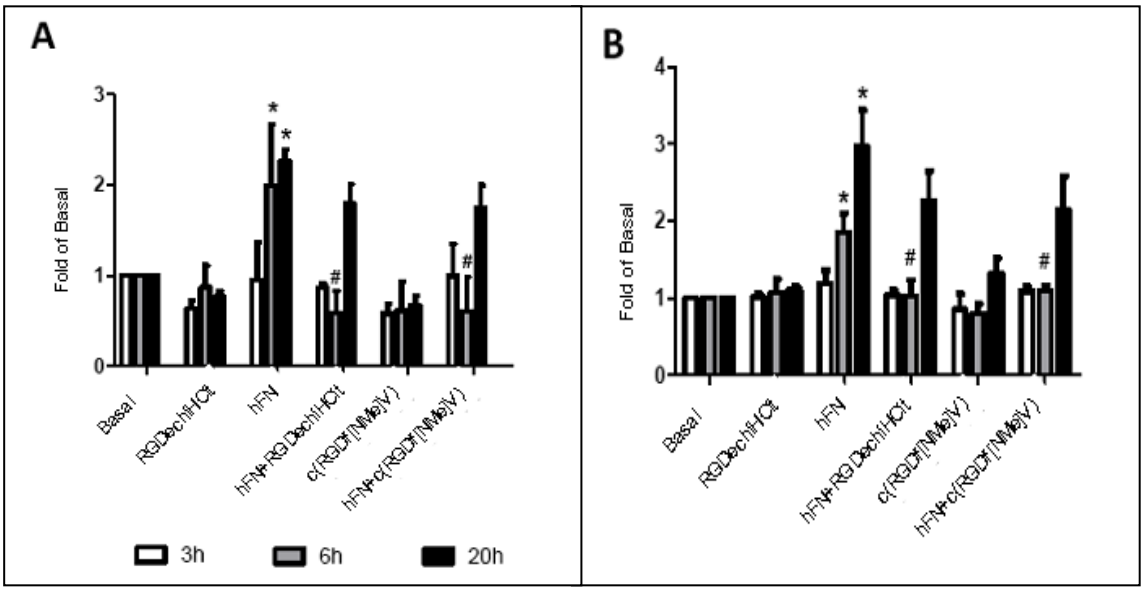

Fig. 27 *In vitro* effects of c(RGDf[NMe]V) and RGDechiHCit on cell proliferation (**Panel A**) and DNA synthesis assessed by [^{3}H]thymidine incorporation (**Panel B**) in bovine aortic endothelial cells (EC). Given alone, c(RGDf[NMe]V) or RGDechiHCit did not affect EC proliferation. Neverteless, incubation with these $\alpha_V\beta_3$ integrin antagonists inhibited in a comparable way EC proliferation in response to the mitogenic stimulus, hFN. All experiments depicted in this figure were performed from three to six times in duplicate (*= $p<0.05$ vs Basal, #= $p<0.05$ vs hFN).

On the contrary, the effect of RGDechiHCit on VSMC did not reach statistical significance in comparison with the c(RGDf[NMe]V) used as control (Figure 28B).

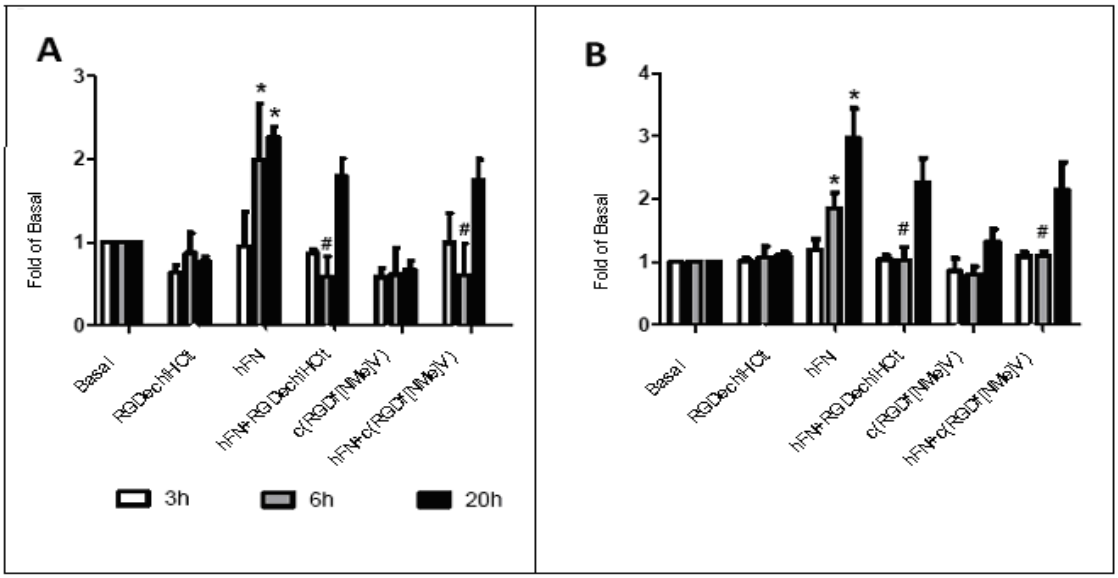

Fig. 28 *In vitro* effects of c(RGDf[NME]V) and RGDechiHCit on vascular smooth muscle cell (VSMC) cell proliferation (**Panel A**) and DNA synthesis assayed by [^{3}H]thymidine incorporation (**Panel B**). In this cellular setting, hFN induced a mitogenic stimulus, appreciable especially at 20h. c(RGDf[NMe]V) but not RGDechiHCit at that time-point induced an attenuation of such proliferative response. All experiments were performed from three to five times in triplicate (*= $p<0.05$ vs Basal; #= $p<0.05$ vs hFN).

3.3.2 Effects on cellular signal transduction

Since hFN-mediated activation of ERK2 is linked to angiogenesis (Eliceri B.P., et al., 1998; Illario M., et al., 2005), we analyzed the ability of RGDechiHCit and c(RGDf[NMe]V) to inhibit hFN-induced phosphorylation of ERK2 in EC and VSMC. In accordance with the results on cell proliferation and [^{3}H]Thymidine incorporation, in EC both RGDechiHCit and c(RGDf[NMe]V) significantly inhibited the hFN-induced phosphorylation of mitogen-activated protein ERK2 (Figure 29A). Also, in VSMC, there was no significant inhibition of ERK2 phosphorylation by the RGDechiHCit compund c(RGDf[NMe]V) (Figure 29B).

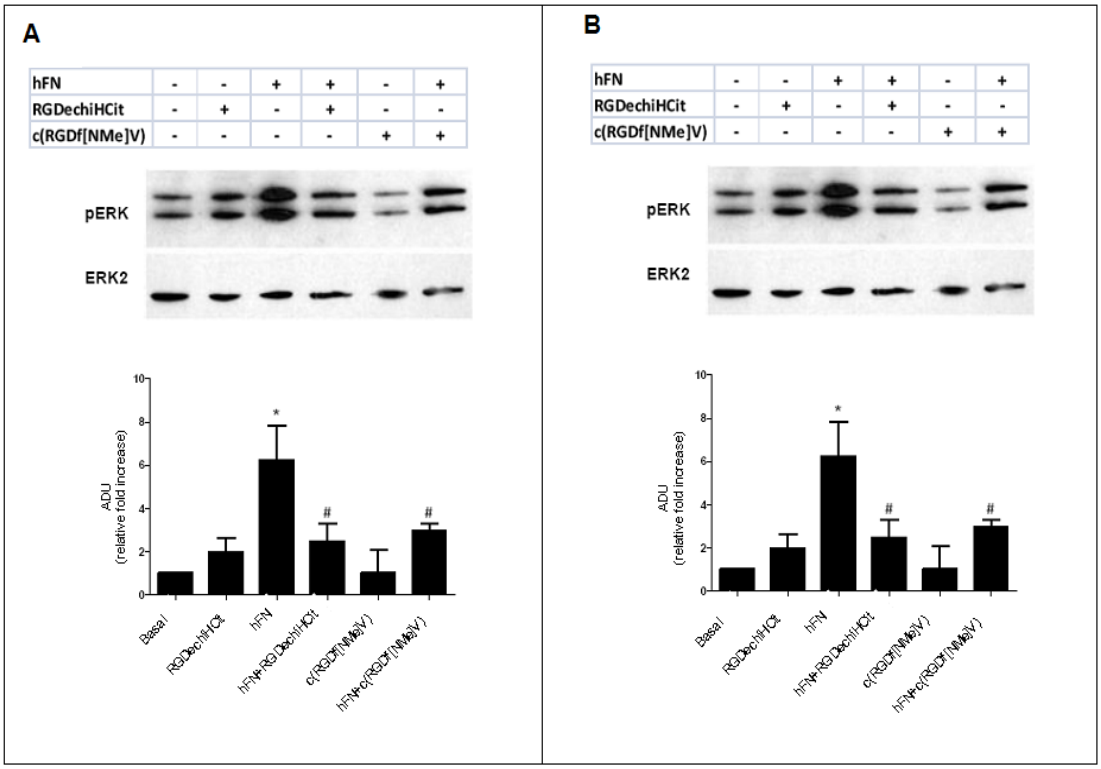

Fig 29 **Panel A**: *In vitro* effects of c(RGDf[NMe]V) and RGDechiHCit on EC signal transduction. Extracellular signal regulated kinase (ERK)/mitogen-activated protein kinase activation: western blot of activated (phosphorylated: pERK) ERK2 after hFN-stimulation. Equal amounts of proteins were confirmed via blotting for total ERK. Densitometric analysis (bar graph) showed that hFN stimulation caused ERK activation (*= p<0.05 vs Basal) and that treatment with $\alpha_V\beta_3$ antagonists blunted such activation (#= p<0.05 vs hFN). Error bars show SEM. Representative blots are shown in the inset. *In vitro* effects of c(RGDf[NMe]V) and RGDechiHCit on VSMC signal transduction were represented in **Panel B**. Extracellular signal regulated kinase (ERK)/mitogen-activated protein kinase activation: western blot of activated (phosphorylated: pERK) ERK2 after hFN-stimulation. Blots were then stripped and reprobed for either total ERK as a loading control. Densitometric analysis (bar graph) showed that hFN induced ERK phosphorylation (*= p<0.05 vs Basal) and that treatment with c(RGDf[NMe]V) but not RGDechiHCit decreased such activation (#= p<0.05 vs hFN). Error bars show SEM. Representative blots are presented in the inset.

3.3.3 Evaluation of VEGF expression

Angiogenesis is largely dependent on ERK2 activation, which in turn promotes cellular proliferation and expression of VEGF. This cytokine promotes infiltration of inflammatory cells, proliferation of ECs and VSMCs and sustains the proangiogenic phenotype (Mahabeleshwar G.H., et al., 2007).
The early release (6 hours) of the cytokine is therefore an important readout when studying angiogenesis *in* vitro. On these grounds, we assessed the expression levels of this pivotal proangiogenetic factor in EC after 6 hours of stimulation with hFN. hFN induces VEGF release and such response was blunted by incubation with either integrin antagonist, as depicted in figure 30 (hFN: +18.9±1.02; hFN+RGDechiHCit: +2.44±0.76; hFN+c(RGDf[NMe]V): +3.19±0.73 fold over basal, ADU; $p<0.05$, ANOVA).

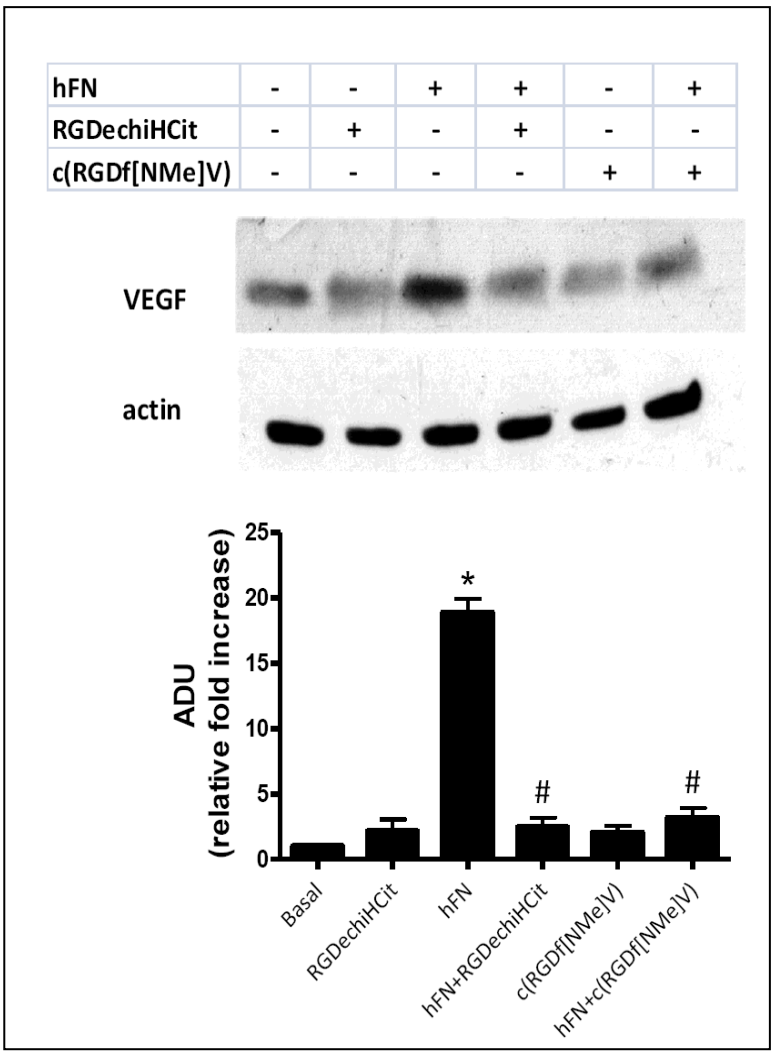

Fig. 30 VEGF production in bovine aortic endothelial cells (ECs) measured by Western blot (inset). Shown are VEGF levels after 6 hours of serum starvation. Equal amount of proteins were verified by blotting for actin. Quantification of western blot from all experiments demonstrated that hFN was able to increase VEGF production (*= $p<0.05$ vs Basal), while after c(RGDf[NMe]V) or RGDechiHCit treatment VEGF levels returned to basal conditions (#= $p<0.05$ vs hFN). All data derived from three different experiments performed in duplicate. The results were expressed as fold increased with respect to the basal condition in untreated samples. Error bars show SEM

3.3.4 Endothelial Matrigel assay

The formation of capillary-like tube structures in the ECM by ECs is a pivotal step in angiogenesis and is also involved in cell migration and invasion (Iaccarino G., et al., 2005). To evaluate any potential antiangiogenic activity of our novel integrin antagonist, *in vitro* angiogenesis assays were conducted by evaluating hFN-induced angiogenesis of ECs on Matrigel.
As shown in Figure 31, when ECs were plated on wells coated with Matrigel without the addition of hFN, they showed formation of only a few spontaneous tube structures (17.4±1.2 branches per 10000 μm^2). On the other hand, when the cells were plated on Matrigel with the addiction of hFN, cells formed a characteristic capillary-like network (42.8±4.4 branches per 10000 μm^2; $p<0.05$ vs Basal, ANOVA).
In the presence of RGDechiHCit or c(RGDf[NMe]V), the extent of tube formation hFN-induced was significantly reduced (10.03±1.44; 14.11±3.9, respectively; $p<0.05$ vs hFN alone, ANOVA; Figure 31).

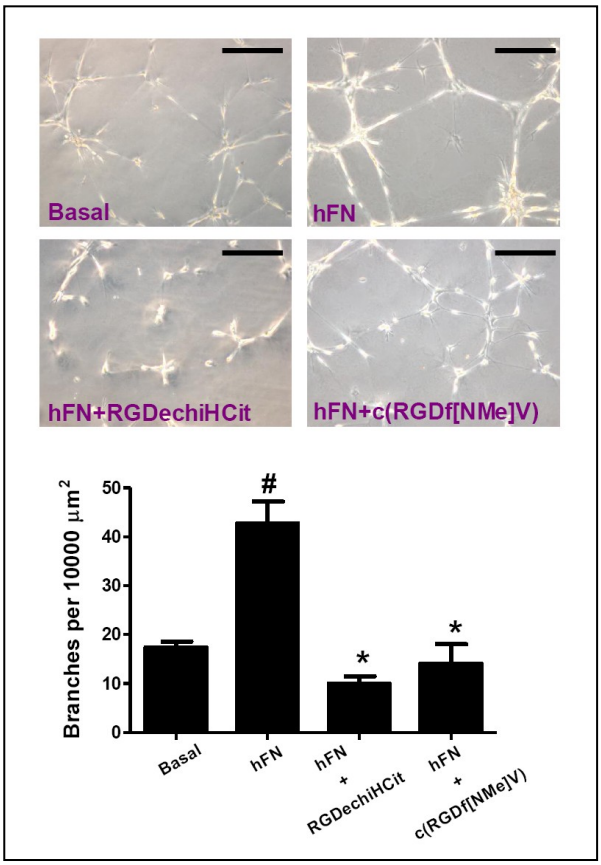

Fig. 31 Representative phase contrast photomicrographs of bovine aortic endothelial cells (ECs) are shown plated on Matrigel. Both c(RGDf[NMe]V) and RGDechiHCit inhibited hFN-induced tube formation. Microscopy revealed numbers of network projections (branches) formed in each group after 12 h of incubation. Data from three experiments in triplicate are summarized in the graph (*=$p<0.05$ vs Basal; #= $p<0.05$ vs hFN). Error bars show SEM. The black bar corresponds to 100 µm.

Looking at *in vitro* studies results, it is possible affirm that RGDechiHCit ability to inhibit hFN-induced cell proliferation is comparable to that of c(RGDf[NMe]V), although the half-life is quite reduced.
A major evidence that is brought up by our results is the peculiar selectivity of RGDechiHCit towards EC as compared to c(RGDf[NMe]V). Indeed, RGDechiHCit fails to inhibit VSMC proliferation in vitro, opposite to c(RGDf[NMe]V).
We believe that this feature is due to the selectivity of such a novel compound toward $\alpha v\beta 3$. In fact, VSMCs express $\alpha v\beta 3$ only during embryogenesis meanwhile when these cells are in culture express other integrins which may be blocked by c(RGDf[NMe]V).
On the contrary, $\alpha v\beta 3$ is expressed by ECs (Lu H., et al., 2006) thus conferring RGDechiHCit selectivity toward this cell type.

3.4 RGDechiHCit ANTIANGIOGENIC ACTIVITY: *in vivo* STUDIES

3.4.1 Wound healing

The examination of full-thickness wounds in the back skin showed that both RGDechiHCit and c(RGDf[NMe]V) slowed down healing (Figure 32). At a macroscopic observation, the delay in the wound healing in treated rats was evident, with raised margins, more extensive wound debris and scab, that persisted for at least 7 days after surgery.
Moreover, histological analysis showed that while control rats presented a dermal scar tissue consisting of a well defined and organized fibrous core with minimal chronic inflammatory cells, skin wounds exposed to RGDechiHCit or c(RGDf[NMe]V) exhibited a retarded repair pattern. Indeed, there was an intense inflammatory infiltrate, extended from the wound margin into the region of the *panniculus carnosus* muscle and hypodermis. Moreover, the basal epidermis was disorganized and epidermal cell growth failed to achieve re-epithelialization, as shown in figure 32.

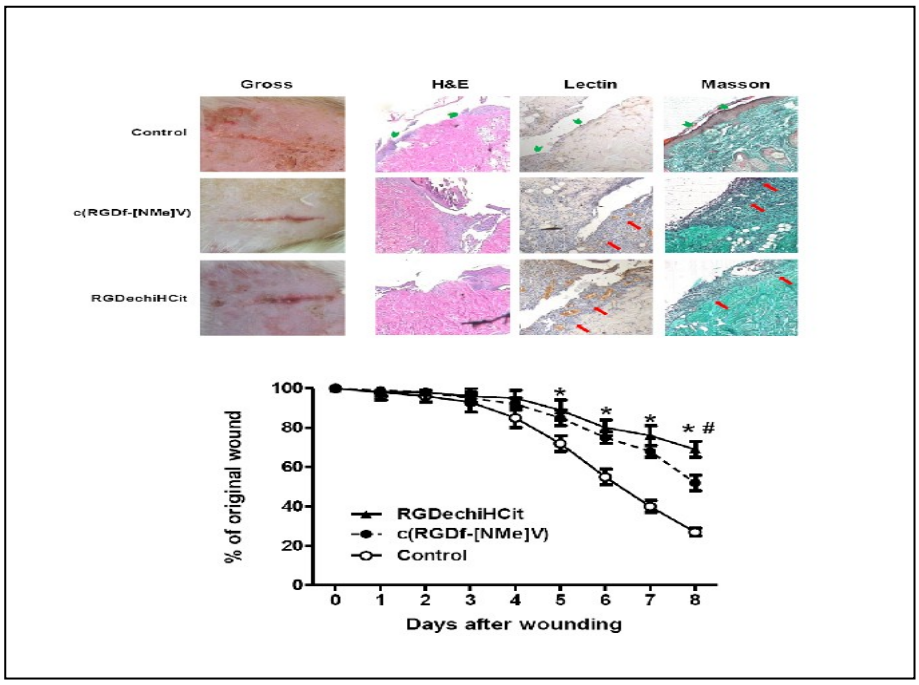

Fig. 32 Both c(RGDf[NMe]V) and RGDechiHCit slowed down the closure of full thickness punch biopsy wounds. Three to five rats were analyzed at each time point. Gross appearance (representative digital photographs) after 5 days of the wound treated with pluronic gel containing c(RGDf-[NMe]V), RGDechiHCit (10^{-6}M) or saline. Diagram of the kinetics of wound closure; *=p<0.05 vs Control; #=p<0.05 vs c(RGDf-[NMe]V, ANOVA). Error bars show SEM. Histological analysis revealed a retarded repair pattern in treated rats, which is consistent with inhibition of angiogenesis in the granulation tissue. Representative sections of excised wounds; 5 µm, ×20 objective (Hematoxylin & Eosin, Lectin immunohistochemical staining, Masson's trichrome). In control animals, epidermal cells. growth achieved complete re-epitalization (green arrowheads) and there is a well defined and organized fibrous core of scar tissue. Both in c(RGDf[NMe]V) and RGDechiHCit treated rats there is a chronic inflammatory infiltrate (red arrows) and lectin staining shows (in brown) the presence of vessels in the granulation tissue.

3.4.2 Matrigel plugs

After injection, Matrigel implants containing the angiogenic stimulant VEGF (10^{-5} M) formed a plug into which ECs can migrate. Matrigel pellets evidenced a significant lower EC infiltration, identified through means of immunohistological lectin staining, in c(RGDf[NMe]V) and RGDechiHCit treated plugs respect to VEGF alone (VEGF+RGDechiHCit: 0.211±0.034; VEGF+c(RGDf[NMe]V): 0.185±0.027 fold over VEGF alone; $p<0.05$, ANOVA), as depicted in figure 33.

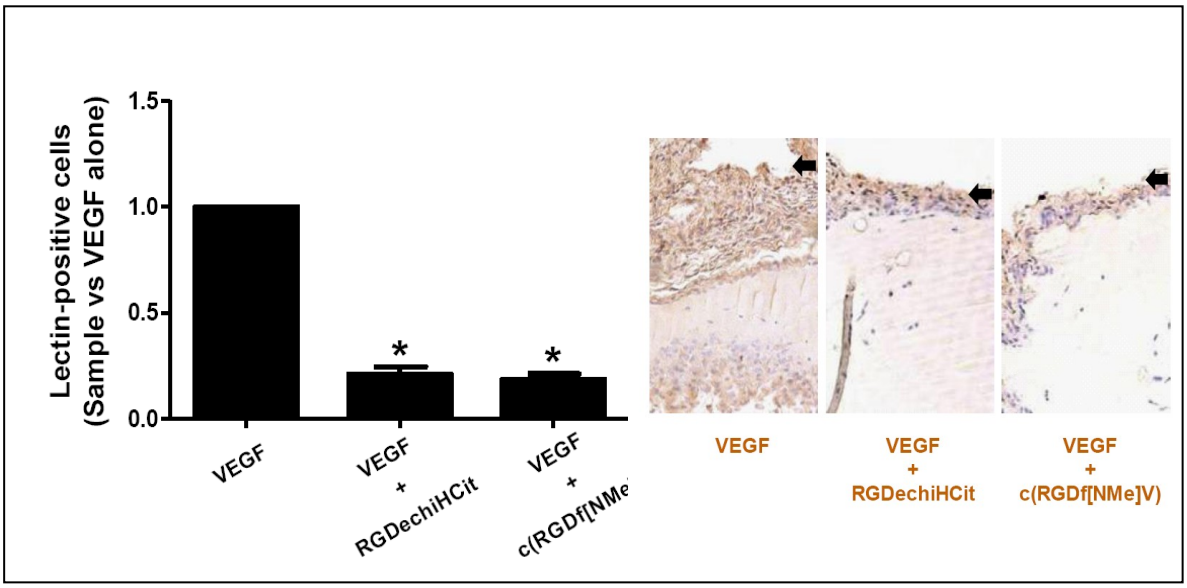

Fig. 33 Representative immunohistochemical sections (5 μm) of Matrigel plugs subcutaneously injected, at ×20 magnification. ECs were identified by lectin staining, that gave a brown reaction product, as described in Methods. Both c(RGDf[NMe]V) and RGDechiHCit treatment reduced the number of invading cells from the edge to the core of implanted Matrigel plug. Analysis was conducted in 20 randomly chosen cross-sections per each group. *=$p<0.05$ vs VEGF. Error bars show SEM.

Our data suggest that inhibition of the endothelial integrin system is sufficient to inhibit angiogenesis. It is possible to deduce that the higher specificity of RGDechiHCit for the endothelium would result in a lower occurrence of side effects than the use of less selective inhibitors.
This is only an indirect evidence, that needs further investigation in more specific experimental setups. Indeed, of the wide spectrum of integrins that are expressed on the surface of ECs, $\alpha v\beta 3$ receptor has been identified as having an especially interesting expression pattern among vascular cells during angiogenesis, vascular remodeling, tumor progression and metastasis (Castel S., et al., 2000). The relevance of this molecule in angiogenesis and its potential as therapeutic agent has been, therefore, well estabilished (Laitinen I., et al., 2009) and in this thesis it was shown that RGDechiHCit activity is highly critical for ECs hFN stimulated proliferation.

3.5 FUNCTIONALISED GOLD NANOPARTICLES: DESIGN, SYNTHESIS AND CHARACTERISATION

3.5.1 Design and synthesis of RGD(GGC)$_2$ and RGD(GC)$_2$ peptides

RGD(GGC)$_2$ peptide (Figure 34) is a chimeric molecule of 12 aminoacids that contains two parts encompassing a RGD-sequence and a GGC-motif for both integrin targeting and nanoparticle capping effect, respectively.
The RGD-motif was derived from the c(RGDfK) peptide, a $\alpha v\beta 3$ antagonist, where the lysine residue was mutated in glutamic acid one to allow the conjugation to the GGC-motif by its γ-carboxylic group. (GGC)$_2$ is an analog of the previously reported capping agent GC15 (Krpetića Z., et al., 2009), containing 7 aminoacid residues (Ac-AGCGGCG-NH$_2$).

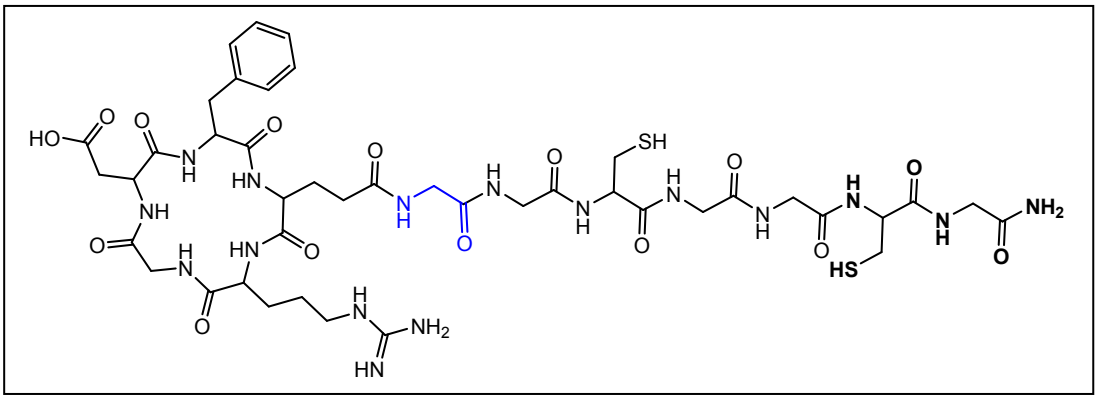

Fig.34 RGD(GGC)$_2$ peptide

LC-MS analysis were performed during the peptide elongation. In particular we obtained an unexpected LC-MS spectrum of the peptide after the Fmoc deprotection from the glutamic acid residue because the peptide molecular weight, was less 58 uma respect to the theoretical value (fugure 35). This mass corresponded to the allyl alcohol molecular weight and indicated that the allylic group may be eliminated during the Fmoc deprotection step with the formation of a cycle between the Gly^{6}and Glu^5 (glutarimide cyclo) as recently reported in literature (Zhu J., et al., 2008) (Figure 35).

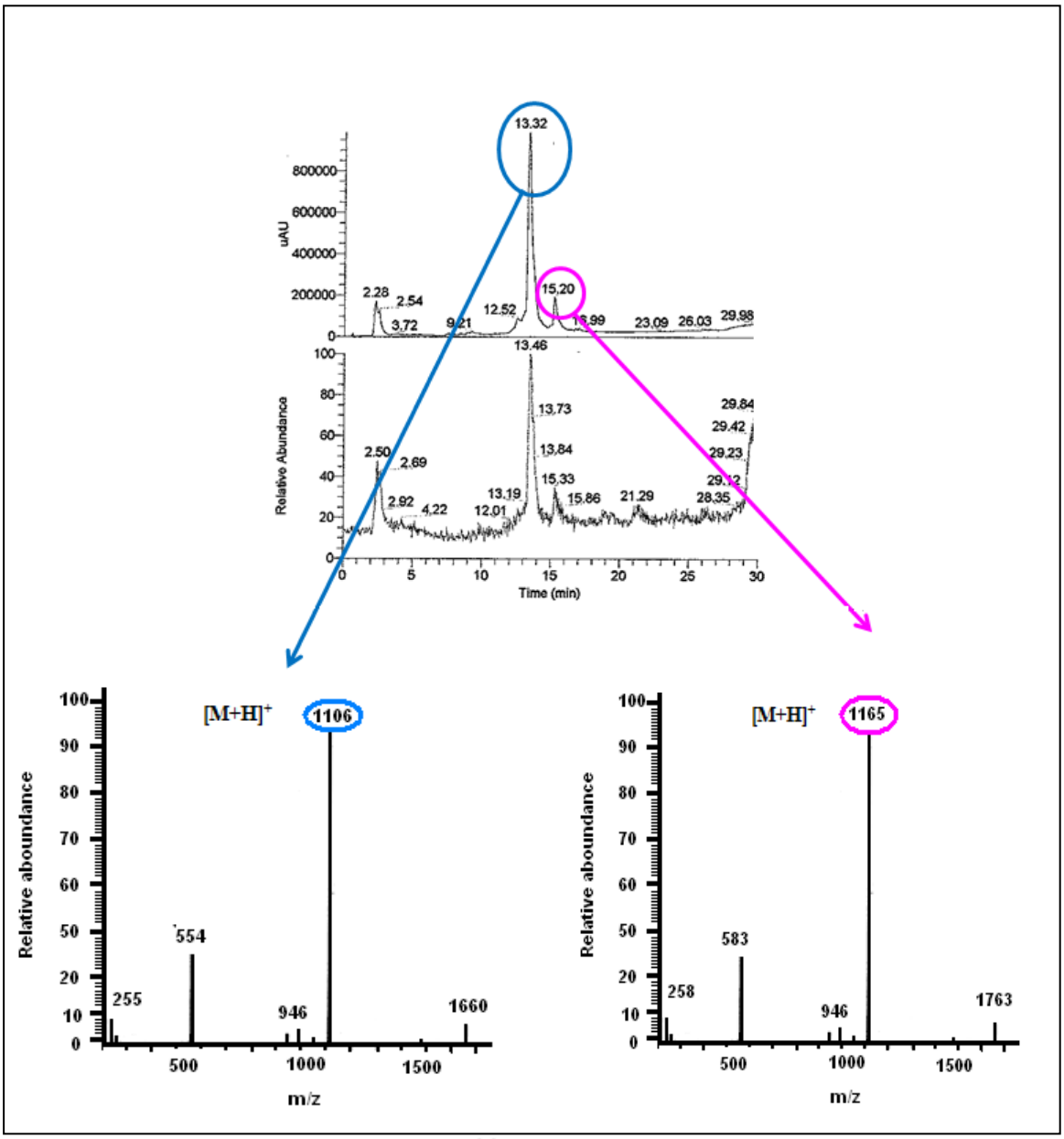

Figure 35 LC-MS of RGD(GGC)$_2$ after Fmoc deprotection from the glutamic acid residue. Two peaks are visible in HPLC profile. The most abundant peak (blue line) shows a molecular weight less 58 uma respect to the theoretical value present in minor quantity (pink line).

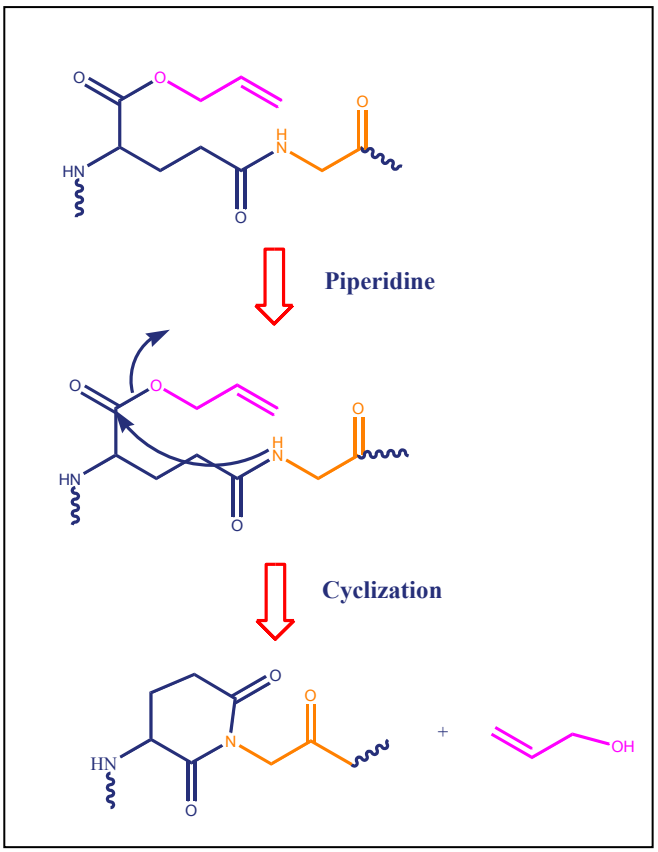

Fig. 36 Glutarimide formation between Glu^5 (blue residue)e Gly^6(yellow residue (Zhu J., et al., 2008).

This problem was overcame by the substitution of the Gly^6 residue with an alanine to prevent the glutarimide formation. The new obtained peptide was named $RGD(GC)_2$ (see Figure 37).

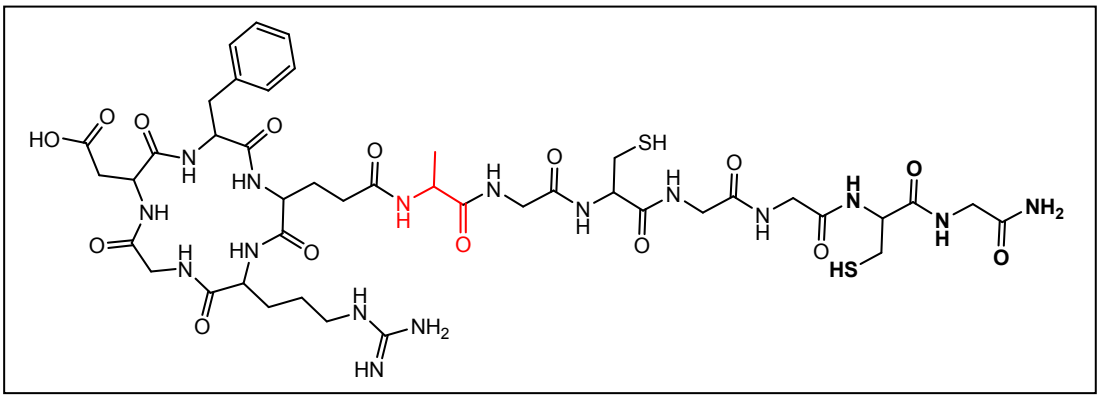

Fig.37 $RGD(GC)_2$ peptide.

During the synthesis of $RGD(GC)_2$, we had a further unexpected problem. Indeed, the final peptide LC-MS spectrum showed two peaks corresponding to the same molecular weight.
After a careful study, we deduced that this issue may be due to cysteine residues racemisation (Han Y., et al., 1997).

It is well known that the racemization process is based on a competition between the amino acid activation reaction, rearrangement of the activated species to a 5(4*H*)-oxazolone, base-catalyzed abstraction of the amino acid α-proton (enolization) from either the activated species directly or a from the oxazolone, and acylation of the activated species and/or the oxazolone with an incoming amine nucleophile.
The presence of base gives dual and opposite effects, because base catalyzes both more rapid acylation and leads to more rapid epimerization. Those activation protocols that involve the presence of base are likely to result in measurable cysteine racemization. As might be expected, the level of racemization decreases by using weaker base. Moreover, all of these phenomena are exacerbated with preactivated cysteine.
On the bases of this knowledge we substituted the DIPEA with the weaker base TMP in coupling reaction and avoided the amino acid preactivation.
The final RGD$(GC)_2$ peptide was obtained with a final yield of 25% and a purity of 99%. The identity of the peptide was confirmed by LC-MS wich gave the uspected molecular mass value $[M + H]^+$ of 1099 and an ion $[M + 2H]^{+2}$of 550.5 (Figure 38A and B).

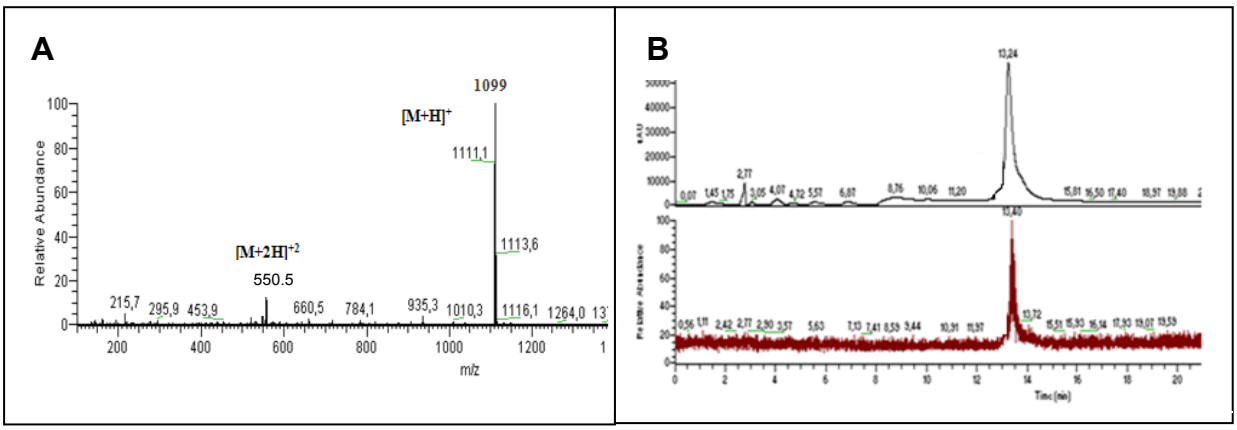

Fig. 38 RGD$(GC)_2$ peptide mass spectrum (A); RGD $(GC)_2$ HPLC spectrum and TIC profile.

Finally, we have synthesized a linear and aspecific peptide named $(GC)_2$ reported in figure 39, to have a negative control peptide in cellular uptake studies.

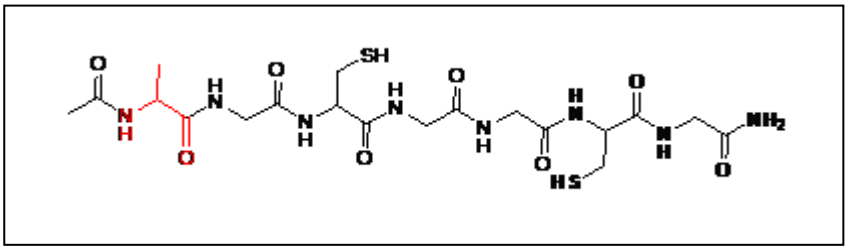

Fig. 39 $(GC)_2$ linear peptide

It was obtained using the standard Fmoc chemistry, as reported above for RDGgold, with a yield of 98% and a purity of 99% (Figure 40 B). The identity of the peptide was confirmed by mass value of $[M + H]^+$ of 562.5 for linear peptide $(GC)_2$ as showed in figure 40A.

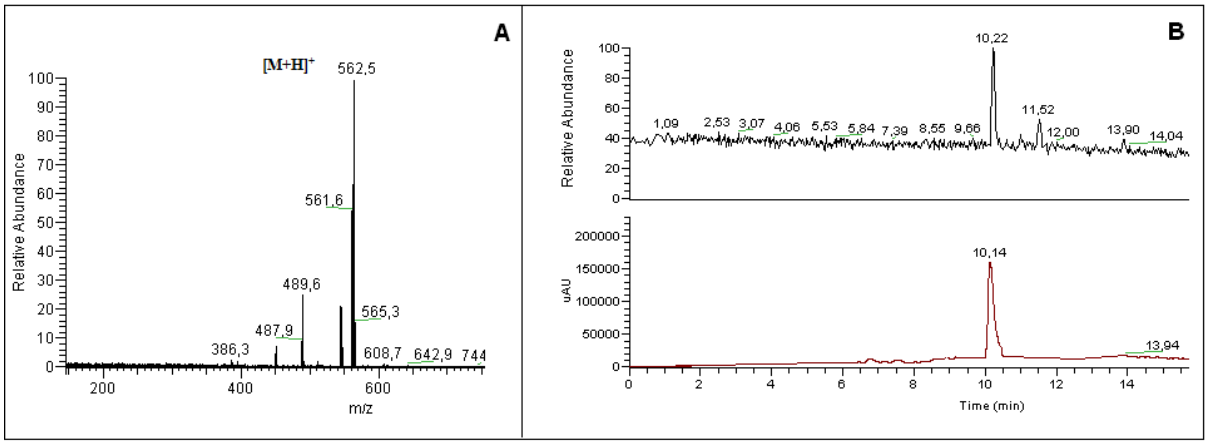

Fig. 40 RGD$(GC)_2$ peptide mass spectrum (A); RGD $(GC)_2$ HPLC spectrum and TIC profile.

3.5.2 UV and TEM characterisation

The UV-Vis spectrum of the gold capped nanosystem obtained (Figure 41A) shows a plasmon absorption band at 520 nm typical for gold particles of about 8 nm size and the TEM image of the peptide coated gold particles indicates a narrow size distribution centered at this size too (Figure 41B). The type of aggregation of particles on the sample grid observed here is fairly common for charged particles derived from hydrosols and does not suggest that particles are aggregated in solution. Sol stability is shown by the absence of any variation of the spectrum profile in 1 hr.

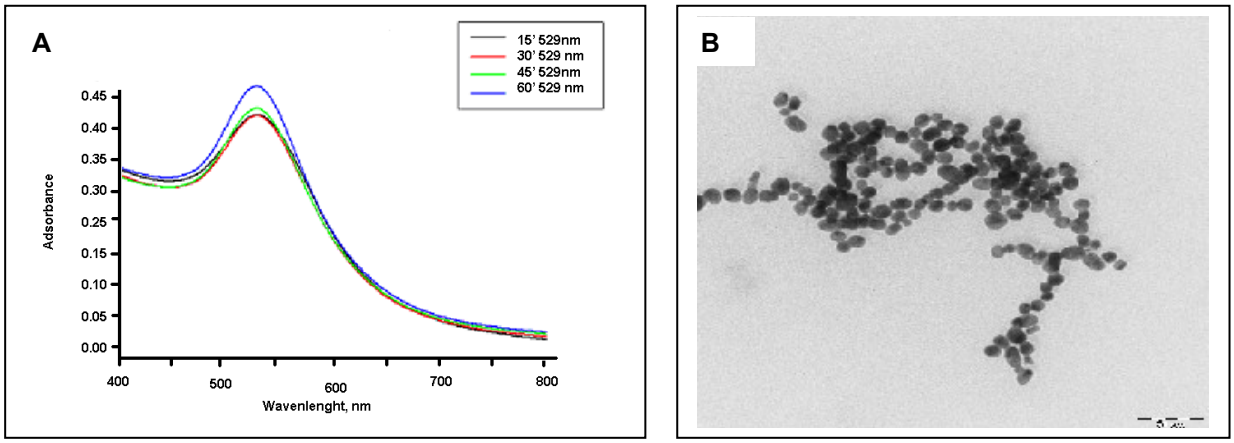

Fig. 41 UV characterization of complex RGD$(GC)_2$AuNPs from 15 to 60 minutes (A). TEM analysis of functionalised obtained nanosystem (B).

3.5.3 FTIR characterisation

We have confirmed the binding of $RGD(GC)_2$ to the gold nanoparticles by FTIR spectroscopy: the signals obtained was compared to those of the free ligand in solution, and the formation of the ligand shell was deduced from the shift of main frequencies. A comparison between the FTIR spectrum of the free peptide and that of the peptide-protected particles is shown in figure 42.

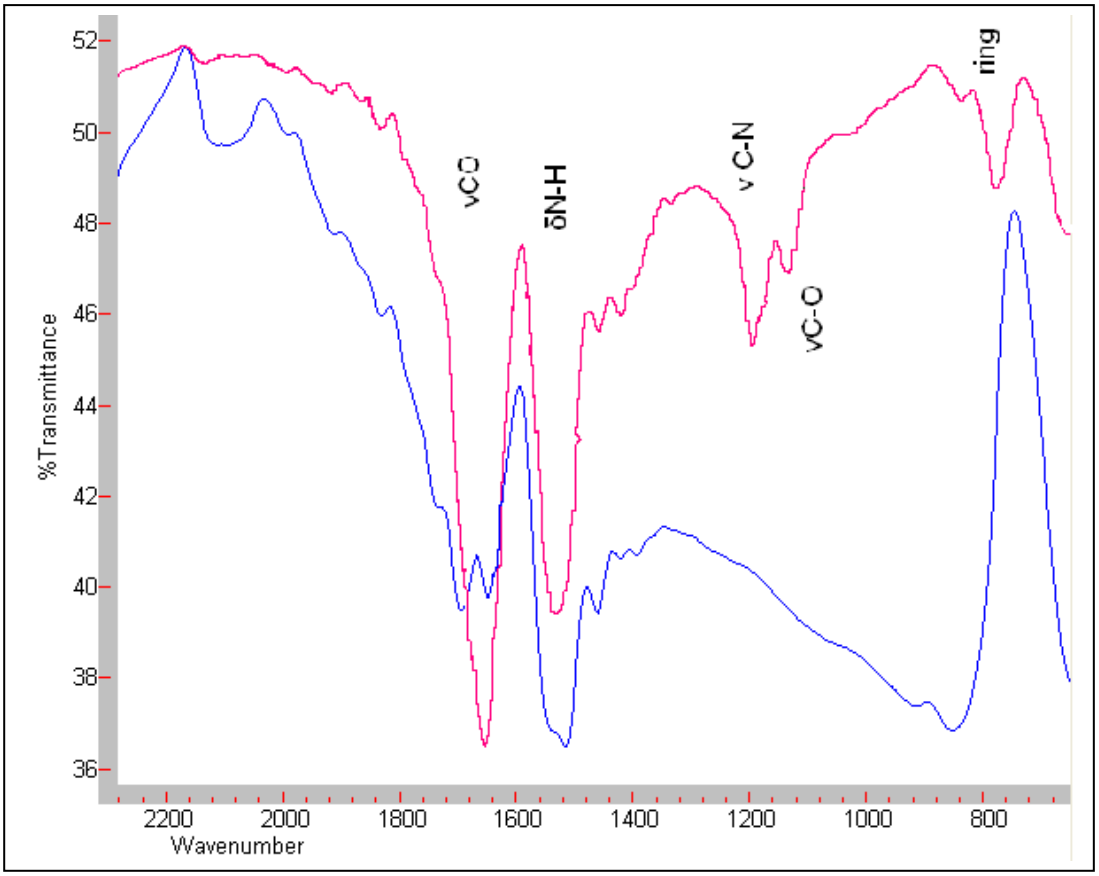

Fig. 42 FTIR spectrum of free $RGD(GC)_2$ peptide (red line) and $RGD(GC)_2$AuNPs (blue line) in 2300-500 cm^{-1} region.

It can be inferred from the spectra that the particles are bound to the peptide. This is concluded observing the vibrational bending modes related to the amidic groups and the carbonyl stretching absorption. Further studies to establish the groups involved in binding peptide-gold nanoparticles will be done.

3.5.4 NMR Characterisation

We implemented NMR spectroscopy to further verify the binding of the RGD peptide to the gold-nanoparticles and to identify key residues involved in this interaction. We first focused our attention on the RGD peptide in its apo form and assigned its proton resonances. Due to the fast tumbling of this small peptide, no NOE contacts could be observed in 2D [^{1}H, ^{1}H] NOESY experiments (Kumar et al., 1980) thus, we recorded 2D [^{1}H, ^{1}H] ROESY spectra (Bax and Davis, 1985).
By comparing 2D [^{1}H, ^{1}H] TOCSY and 2D [^{1}H, ^{1}H] ROESY experiments we were able to clearly identify all the different spin-systems for the residues of the RGD peptide and also sequentially assign most of them.
Then, we compared 1D proton and 2D [^{1}H, ^{1}H] TOCSY spectra of the RGD peptide with those of the same peptide attached to the gold nanoparticles and with those of an analogue peptide whose sequence is encompassing its C-terminal tail, i.e: $(CG)_2$, but is lacking the integrin binding motif. The strong interaction between peptide and AuNPs is already evident in the 1D spectra, where a large broadening of all the resonances of the peptides when attached to the nanoparticles can be observed (Figure 43).

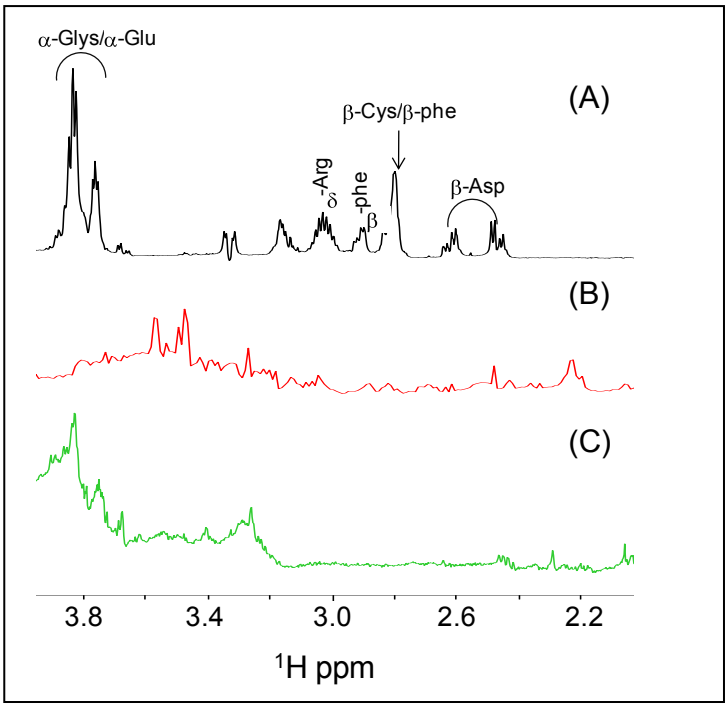

Fig. 43 Comparison of 1D proton spectra of the RGD peptide (A), RGD$(GC)_2$AuNPs nanoparticles (B) and $(GC)_2$AuNPs (C). An expansion of the region containing signals from side-chain protons is shown.

From figure 42 is also evident that a structural rearrangement takes place upon binding of the peptides to the nanoparticles. Chemical shifts changes are in fact widespread throughout the spectra in the aromatic-amide region and also in the region of the aliphatic side-chains.
Cysteines side chains appear highly affected by binding to the nanoparticles in fact signals from their H_α protons completely disappear (Figure 43).
The effect of the interaction with the large inorganic surface of the nanoparticles can be better seen in the 2D [^{1}H, ^{1}H] TOCSY spectra (Figure 44).

The large broadening of the resonances causes the disappearance of many spin systems and highly reduces the quality of the 2D spectra of the RGD peptide when bound to the nanoparticles. The use of a cold-probe allow us to partially overcome this problem. In fact, spin systems for alanine, arginine, aspartic acid and glutamic acid can be easily recognized whereas other spin systems are undergoing excessive line broadening (Figure 44).

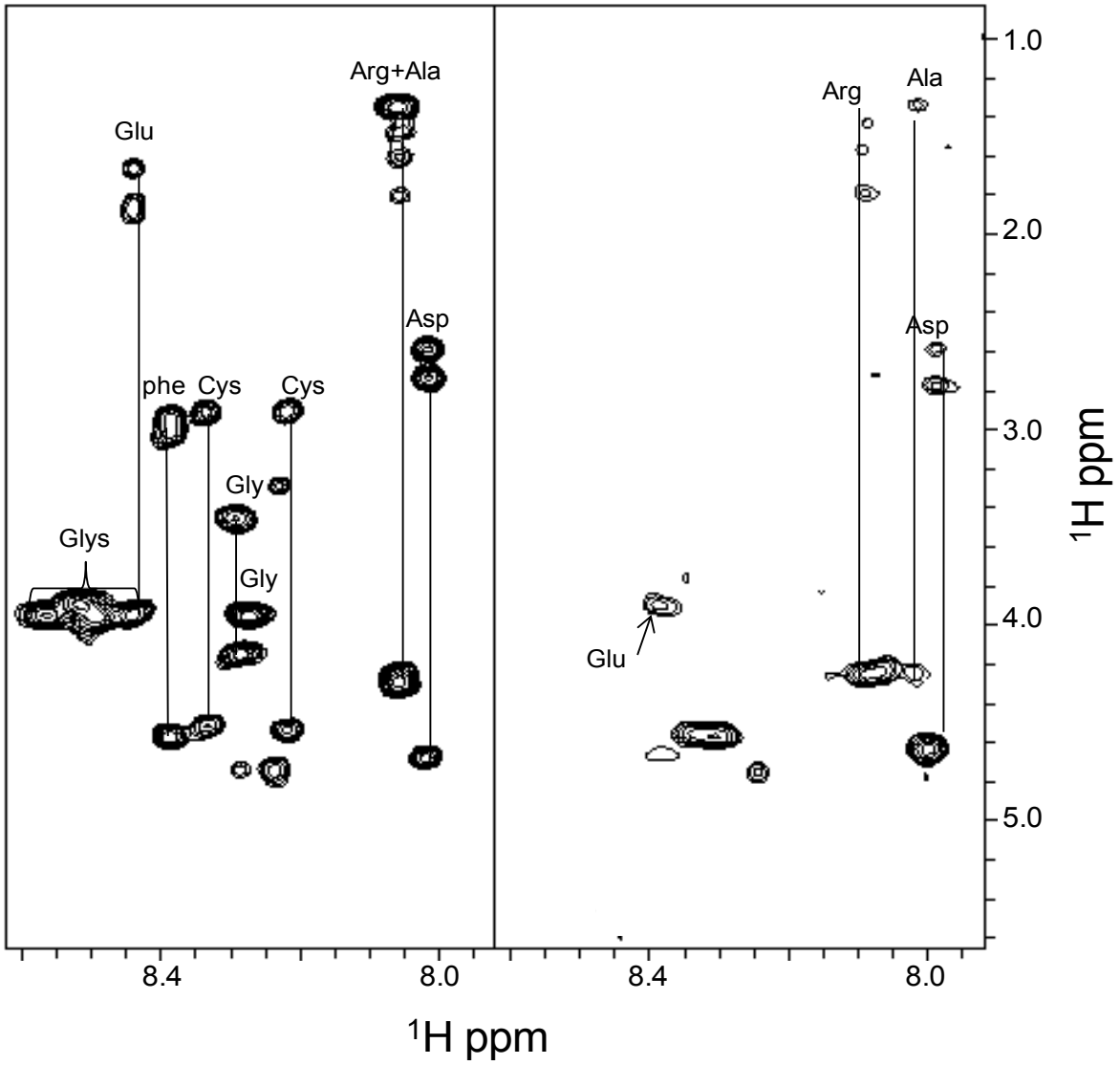

Fig. 44 Comparison of 2D [^{1}H, ^{1}H] TOCSY spectra of the RGD peptide (left panel) and RGD peptide attached to the Au-nanoparticles (right panel). The H_N-aliphatic protons correlation region is shown. Spin systems assignments are also reported.

It's worth noting that chemical shifts for the H_N of arginine as well as for the H_α protons of aspartic acid are clearly changing upon interaction of the peptide with the nanoparticles (Figure 44).

3.5.3 Cellular Uptake study

To investigate the cellular uptake of the RGD$(GC)_2$AuNPs in comparison with $(GC)_2$AuNPs, U-87 MG cells (malignant glioma) as model of human glioblastoma were used. To obtain images of the cells after incubation we performed confocal microscopy studies (Figure 45). In particular, we obtained A1 and B1 images in reflection modality in which the RGD$(GC)_2$AuNPs and the $(GC)_2$AuNPs intracellular distribution are shown (gold nanoparticles are artificially represented as red spots). Instead, images A2 and B2 showed, in transmission modality, the cells distribution. The superimposition of previous pictures, resulted in A3 and B3 images, demonstrated that both RGD$(GC)_2$AuNPs and $(GC)_2$AuNPs penetrated in target cells but RGD$(GC)_2$AuNPs are uptaken qualitatively more efficiently respect to $(GC)_2$AuNPs. The increased uptake of RGD$(GC)_2$AuNPs is likely due to receptor mediated endocytosis, a cellular uptake mechanism faster than the non specific endocytosis.

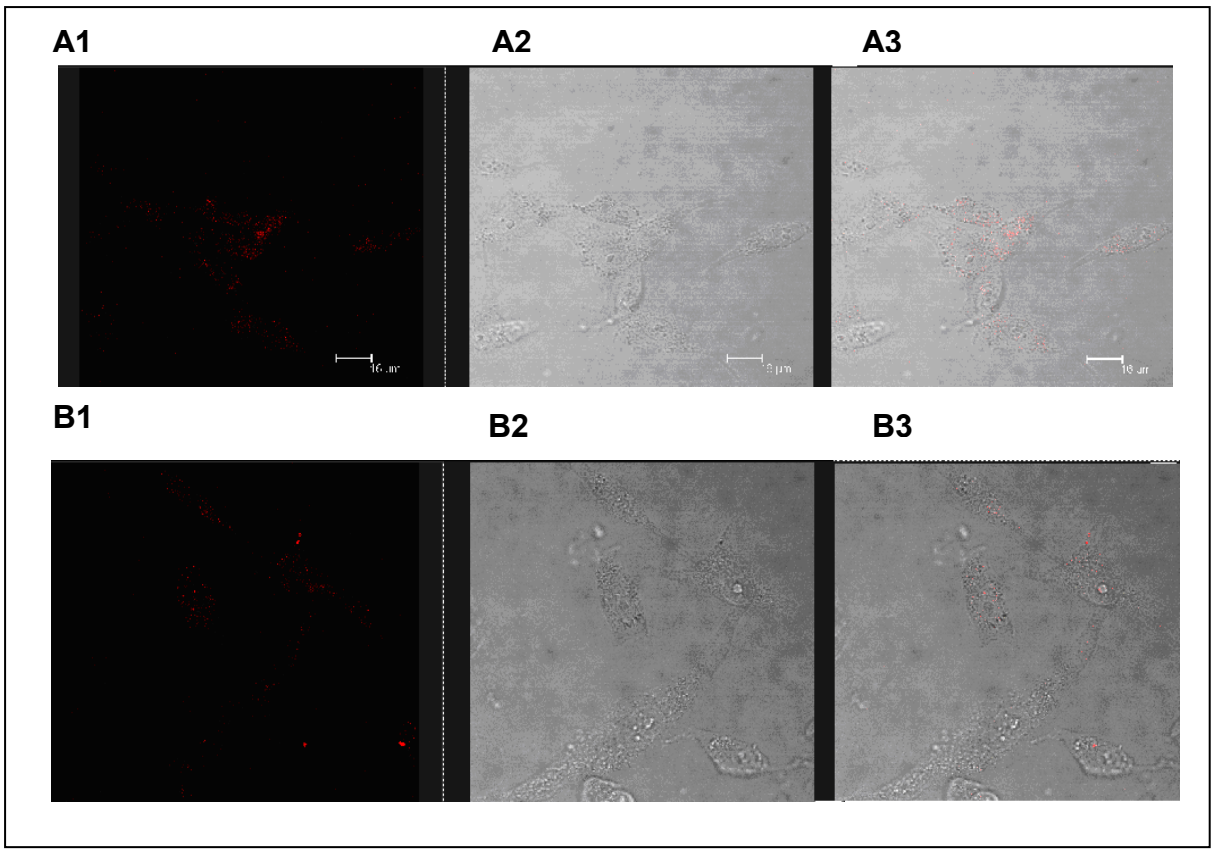

Fig. 45 RGD$(GC)_2$AuNPs and $(GC)_2$AuNPs (red spots) intracellular distribution by confocal reflection microscopy (A1 and B1); cellular distribution by confocal transmission microscopy (A2 and B2), superimposition of figure A1 and A2 and of figures B1 and B2 respectively (A3 and B3).

4 FUTURE PERSPECTIVES

The present PhD thesis demonstrated that the new and selective $\alpha v\beta 3$ integrin ligand, RGDechiHCit, recently designed and synthesized in our laboratory, has anti-angiogenic activity. Unfortunately, in vitro stability studies indicated this compound has a low half life in serum probably due to prolyl endopeptidase action.
To solve this problem we will modify the molecule for example by reducing the peptide bond to avoid the protease's cleavage. Another strategy could be to introduce a methyl group at the α-amino group of the residue flanking the proline to obtain a steric hindrance sufficient to inhibit the degradation by prolyl endopeptidase.
In parallel, starting from the results obtained on the RGD based gold nanoparticle (8-15nm), we will optimize the peptide sequence to improve its cellular uptake and obtain a new and selective delivery systems suitable for biotechnological applications. For this purpose a first strategy will be to insert an appropriate spacer between nanoparticles and the delivering peptide to leave a larger space for peptide-integrin interaction. Alternatively, we will insert the targeting motif, RGD, in the middle of two $(GC)_n$ sequences to favor the interaction with target receptor. The so obtained system will be used to deliver drug molecules, like platinum derivatives, suitable for cancer treatment (Nam J., et al., 2009). Moreover, we will functionalize the gold nanoparticles with opportunely chosen molecules helpful to induce intracellular nanoparticles aggregation (100nm) to obtain a system suitable for photothermal therapy. Finally, we will quantify the functionalized gold nanoparticles incorporated from the target cells measuring the pixel quantity (gold light in image) present in a representative cellular area (the same both for functionalised and not gold nanoparticles).

ACKNOWLEDGEMENTS

I would like to acknowledge all the wonderful people who were always behind me during my PhD experience. Especially Dr. Ivan de Paola, Dr. Luca Monfregola, Dr. Francesca Stanzione, Dr. Lucia De Rosa, Dr. Mariangela Castiglione and Dr. Alessandra Scannella who shared this experience with me being friends more than colleagues. I would like to say, in particular, to Dr. Laura Zaccaro and to Dr. Annarita Del Gatto “It would not have been possible to write this doctoral thesis without you!!”
And, last but not least, I would like to express my gratitude to the Prof. Ettore Benedetti that provide me the opportunity of fees due in this field.
ALL of you made those experiences very memorable….Thanks!!

Sincerely,
Mariarosaria De Simone

REFERENCES

Anderson D.C., Springer T.A., Leukocyte adhesion deficiency: an inherited defect in the Mac-1, LFA-1, and p150,95 glycoproteins, *Annu Rev Med*, 1987; 38:175-194.

Arnaout M.A., Goodman S.L. and Xiong J.P., Coming to grips with integrin binding to ligands, *Current opinion in Cell Biology*, 2002,14:641-652.

Astrof S., Hynes R.O., Fibronectins in vascular morphogenesis, *Angiogenesis*, 2009, 12:165-175.

Bachmann I.M., Ladstein R.G., Straume O., Naumov G.N., and Akslen L.A., Tumor necrosis is associated with increased integrin αvβ3 expression and poor prognosis in nodular cutaneous melanomas, *BMC Cancer*, 2008, 8:362.

Bartels C., Xia T., Billeter M., Gunthert P., Wüthrich K., The program XEASY for computer-supported NMR spectral analysis of biological macromolecules. *J. Biomol. NMR*, 1995, 6:1-10.

Bax A. and Davis D.G., Practical aspects of two-dimensional transverse NOE spectroscopy, *J. Magn. Reson.*, 1985, 63:207-213.

Bednarski M., Frausto R., Guccione S., Reisfeld R.A., Xiang R., Cheresh D.A., Tumor Regression by Targeted Gene Delivery to the Neovasculature, *Science*, 2002, 296:2404-2407.

Beer A.J., Grosu A.L., Carlsen J., Kolk A., Sarbia M., Stangier I., Watzlowik P., Wester H.J., Haubner R., and Schwaiger M., [^{18}F]Galacto-RGD Positron Emission Tomography for Imaging of αvβ3 Expression on the Neovasculature in Patients with Squamous Cell Carcinoma of the Head and Neck, *Clin Cancer Res*, 2007, 13:6610-6616.

Belvisi L., Bernardi A., Colombo M., Manzoni L., Potenza D., Scolastico C., Giannini G., Marcellini M., Pisano C., Targeting integrins: Insights into structure and activity of cyclic RGD pentapeptide mimics containing azabicycloalkane amino acids, *Bioorganic & Medicinal Chemistry*, 2006, 14:169-180.

Blindt R., Vogt F., Astafieva I., Fach C., Hristov M., Krott N., Seitz B., Kapurniotu A., Kwok C., Dewor M., A Novel Drug-Eluting Stent Coated With an Integrin-Binding Cyclic Arg-Gly-Asp Peptide Inhibits Neointimal Hyperplasia by Recruiting Endothelial Progenitor Cells, *Clinical Research Interventional Cardiology*, 2006, 47:1786-95.

Bous D., Kusumanto Y., Meijer C., Mulder N.H., Hospers G.A.P., A review on pro- and anti-angiogenic factors as targets of clinical intervention, *Pharmacological Research*, 2006, 53:89-103.

Bracci L., Falciani C., Lelli B., Lozzi L., Runci Y., Pini A., De Montis M.G., Tagliamonte A., and Neri P., Synthetic Peptides in the Form of Dendrimers Become Resistant to Protease Activity, *The Journal of Biological Chemistry*, 2003, 47:46590-46595.

Burkhart D.J., Kalet B.T., Coleman M.P., Post G.C. and Koch H.T., Doxorubicin-formaldehyde conjugates targeting αvβ3 integrin, *Eur J Nucl Med Mol Imaging*, 2008, 35:1489-1498.

Cao Q., Li Z.B., Chen K., Wu Z., He L., Neamati N., Chen X., Evaluation of biodistribution and anti-tumor effect of a dimeric RGD peptide paclitaxel conjugate in mice with breast cancer, *Eur J Nucl Med Mol Imaging*, 2008, 35:1489-1498.

Castel S., Pagan R., Garcia R., Casaroli-Marano R.P., Reina M., Mitjans F., Piulats J., Vilaro S., Alpha v integrin antagonists induce the disassembly of focal contacts in melanoma cells, *Eur J Cell Biol*, 2000, 79:502-512.

Choi Y., Kim E., Lee Y., Han M.H. and Kang I.C., Site-specific inhibition of integrin αvβ3-vitronectin association by a ser-asp-val sequence through an Arg-Gly-Asp-binding site of the integrin, *Proteomics*, 2010, 10:72-80.

Ciccarelli M., Santulli G., Campanile A., Galasso G., Cervero P., Altobelli G.G., Cimini V., Pastore L., Piscione F., Trimarco B., Iaccarino G., Endothelial alpha1-adrenoceptors regulate neo-angiogenesis, *Br J Pharmacol*, 2008*,* 153:936-946.

Cox D., Brennan M., Moran N., Integrins as therapeutic targets: lessons and opportunities, *Nature Reviews Drug Discovery*, 2010, 9:804-820.

Crawford T.N., Alfaro D.V., Kerrison J.B., Jablon E.P., Diabetic retinopathy and angiogenesis, *Curr Diabetes Rev,* 2009, 5:8-13.

Cristofanilli M., Charnsangavej C., Hortobagyi G.N., Angiogenesis modulation in cancer research: novel clinical approaches, *Nature Reviews Drug Discovery, 2002*, 1:415-426.

Dalvit C., Efficient multiple-solvent suppression for the study of the interaction of organic solvents with biomolecules, *J. Biomol NMR,* 1998, 11:437-444.

De Bono J.S., Ashworth A., Translating cancer research into targeted therapeutics, *Nature,* 2010, 467:543-549.

Dechantsreiter M.A., Planker E., Matha B., Lohof E., Holzemann G., Jonczyk A., Goodman S.L. and Kessler H., N-Methylated Cyclic RGD Peptides as Highly Active and Selective Integrin αVβ3 Antagonists, *J. Med. Chem.,* 1999, 42:3033-3040.

Del Gatto A., Zaccaro L., Grieco P., Novellino E., Zannetti A., Del Vecchio S., Iommelli F., Salvatore M., Pedone C. and Michele Saviano, Novel and Selective αVβ3 Receptor Peptide Antagonist: Design, Synthesis, and Biological Behavior, *J. Med. Chem.,* 2006, 49:3416-3420.

Desgrosellier J.S. and Cheresh D.A., Integrins in cancer: biological implications and therapeutic opportunities, *Nature,* 2010, 10:9-22.

Dijkgraaf I., Boerman O.C., Molecular imaging of angiogenesis with SPECT, *Eur J. Nucl. Med. Mol. Imaging,* 2010, 37:104-113.

Duncan B., Kim C., Rotello V.M., Gold nanoparticle platforms as drug and biomacromolecule delivery systems, *J. Control Release,* 2010, 50:3412-3416.

Eliceri B.P., Cheresh D.A., The role of alphav integrins during angiogenesis: insights into potential mechanisms of action and clinical development, *J. Clin. Invest.,* 1999,103:1227-1230.

Eskens F.A., Dumez H., Hoekstra R., et al., Phase I and pharmacokinetic study of continuous twice weekly intravenous administration of Cilengitide, a novel inhibitor of the integrins αVβ3 and αVβ5 in patients with advanced solid tumours, *Eur. J. Cancer,* 2003, 39:917-926.

Folkman J., Angiogenesis-dependent diseases, *Semin. Oncol.,* 2001, 28:536-42.

Friedlander M., Brooks P.C., Shaffer R.W., Kincaid C.M., Varner J.A., Cheresh D.A., Definition of two angiogenic pathways by distinct alpha v integrins, *Science,* 1995, 5241:1500-2.

Gao C., Izquierdo-Barba I., Nakase I., Futaki S., Juanfang R., Sakamoto K., Sakamoto Y., Kuroda K., Terasaki O., Che S., Mesostructured silica based delivery system for a drug with a peptide as a cell-penetrating vector, *Microporous and Mesoporous Materials*, 2009, 122:201-207.

Ghosh P., Han G., De M., Kim C.K., Rotello V.M., Gold nanoparticles in delivery applications, *Advanced Drug Delivery Reviews*, 2008, 60:1307-1315.

Griesinger C., Otting G., Wüthrich K., Ernst R.R., Clean TOCSY for proton spin system identification in macromolecules, *J. Am. Chem. Soc.,* 1988,110:7870-7872.

Han Y., Albericio F. and Barany G., Occurrence and Minimization of Cysteine Racemization during Stepwise Solid-Phase Peptide Synthesis, *J. Org. Chem.*, 1997, 62:4307-4312.

Harburger D.S. and Calderwood D.A., Integrin signalling at a glance, *Journal of Cell Science*, 2009, 122:159-163.

Harper J. and Moses M.A., Molecular regulation of tumour angiogenesis: mechanisms and therapeutic implications, *Biomedical and life science*, 2006, 96:223-268.

Hodivala-Dilke K., αvβ3 integrin and angiogenesis: a moody integrin in a changingenvironment, *Current Opinion in Cell Biology*, 2008, 20:514-519.

Huang X., El-Sayed M.A., Gold nanoparticles: Optical properties and implementations in cancer diagnosis and photothermal therapy, *Journal of Advanced Research*, 2010, 1:13-28.

Humphries M.J., McEwan P., Barton J.S., Buckley A.P., Bella J. and Mould A.P., Integrin structure: heady advances in ligand binding, but activation still makes the knees wobble, *Biochemical Sciences*, 2003, 6:313-320.

Hwang R. and Varner J., The role of integrins in tumor angiogenesis, *Angiogenesis and Anti-Angiogenic Therapy*, 2006, 18:991-1006.

Hynes R.O., Integrins: versatility, modulation, and signaling in cell adhesion, *Cell*, 1992, 69:11.

Iaccarino G., Ciccarelli M., Sorriento D., Cipolletta E., Cerullo V., Iovino G.L., Paudice A., Elia A., Santulli G., Campanile A., et al, AKT participates in endothelial dysfunction in hypertension, *Circulation*, 2004, 109:2587-2593.

Illario M., Cavallo A.L., Monaco S., Di Vito E., Mueller F., Marzano L.A., Troncone G., Fenzi G., Rossi G., Vitale M., Fibronectin-induced proliferation in thyroid cells is mediated by alphavbeta3 integrin through Ras/Raf-1/MEK/ERK and calcium/CaMKII signals, *J. Clin. Endocrinol. Metab.*, 2005, 90:2865-2873.

Jonkman M.F., Pas H.N., Nijenhuis M., Kloosterhuis G., Steege G., Deletion of a cytoplasmic domain of integrin beta4 causes epidemiolysis bullosa simplex, *J. Invest Dermatol*, 2002, 119: 1275-1281.

Koninga G.A., Fretz M.M., Woroniecka U., Storm G., Krijger G.C., Targeting liposomes to tumor endothelial cells for neutron capture therapy, *Applied Radiation and Isotopes*, 2004, 61:963-967.

Krpetić Z., Scarì G., Caneva E., Speranza G., Porta F., Gold nanoparticles prepared using cape aloe active components, *Langmuir*, 2009, 13:7217-21.

Krpetić Z., Nativo P., Porta F. and Brust M., A Multidentate Peptide for Stabilization and Facile Bioconjugation of Gold Nanoparticles, *Bioconjugate Chem.*, 2009, 20: 619-624.

Kumar A., Ernst R.R., Wuthrich K.A., Two-dimensional nuclear Overhauser enhancement (2D NOE) experiment for the elucidation of complete proton-proton cross-relaxation networks in biological macromolecules, *Biochem Biophys Res Commun*, 1998, 95:1-6.

Laitinen I., Saraste A., Weidl E., Poethko T., Weber A.W., Nekolla S.G., Leppanen P., Yla-Herttuala S., Holzlwimmer G., Walch A., et al: Evaluation of alphavbeta3 integrin-targeted positron emission tomography tracer 18F-galacto-RGD for imaging of vascular inflammation in atherosclerotic mice, *Circ Cardiovasc Imaging*, 2009, 2:331-338.

Lark M.W., Stroup G.B., Hwang S., MJames H.I., Rieman D.J., Drake F.H., Bradbeer J.N., Mathur A., Growen M., Design and Characterization of Orally Active Arg-Gly-Asp Peptidomimetic Vitronectin Receptor Antagonist SB 265123 for Prevention of Bone Loss in Osteoporosis, *J. PET*, 2004, 291:612-617.

Legate K.R., Wickström S.A. and Fässler R., Genetic and cell biological analysis of integrin outside-in signalling, *Genes Dev.*, 2009, 23:397-418.

Lesniak W.G., Kariapper M.S.T., Nahir B.M., Tan W., Hutson A., Balogh L.P. and Khan M.K., Synthesis and Characterization of PAMAM Dendrimer Based Multifunctional Nanodevices for targeting αvβ3 Integrins, *Bioconjug Chem.*, 2007, 18: 1148-1154.

Lim Y., Kwon O.J., Lee E., Kim P.H., Yun C.O. and Lee M., A cyclic RGD-coated peptide nanoribbon as a selective intracellular nanocarrier, *Org. Biomol. Chem.*, 2008, 6:1944-1948.

Liu Z., Wang F., and Chen X., Integrin αvβ3-Targeted Cancer Therapy, *Drug Dev Res.*, 2008, 69:329-339.

Liu Z., Wang Fand Chen X., Integrin αvβ3-Targeted Cancer Therapy, *Drug development research*, 2008, 69:329-339.

Lu H., Murtagh J., Schwartz E.L., The microtubule binding drug laulimalide inhibits vascular endothelial growth factor-induced human endothelial cell migration and is synergistic when combined with docetaxel (taxotere), *Mol Pharmacol*, 2006, 69:1207-1215.

Mahabeleshwar G.H., Feng W., Reddy K., Plow E.F., Byzova T.V., Mechanisms of integrin-vascular endothelial growth factor receptor cross-activation in angiogenesis, *Circ Res*, 2007, 101:570-580.

Manzoni L., Belvisi L., Arosio D., Civera M., Pilkington-Miksa M., Potenza D., Andrea Caprini., Araldi M.V., Monferini V., Mancino M., Podest F. and Scolastico C., Cyclic RGD-Containing Functionalized Azabicycloalkane Peptides as Potent Integrin Antagonists for Tumor Targeting, *Chem Med Chem*, 2009, 4:615-632.

Melancon M., Lu W. and Li C., Gold-Based Magneto/Optical Nanostructures: Challenges for In Vivo Applications in Cancer Diagnostics and Therapy, *Mater Res Bull.*, 2009, 34:415-421.

Moser M., Montanez E., Nakano T., Seo M., Backert S., Inoue I., Awata T., Katayama S., Komoda T., Fassler R., The fibronectin RGD motif is required for multiple angiogenic events during early embryonic development, *Arterioscler Thromb Vasc Biol*, 2010, 30:31.

Nair S., Ghosh K.K., Shetty S., Mohanty D., Glanzmann's thrombasthenia: updated, *Platelets*, 2002, 13:387-393.

Nam J., Won N., Jin H., Chung H. and Kim S., pH-Induced Aggregation of Gold Nanoparticles for Photothermal Cancer Therapy, *J. AM. CHEM. SOC.*, 2009, 131:13639-13645.

Nyberg P., Salo T., Kalluri R., Tumor microenvironment and angiogenesis, *Frontiers in Bioscience*, 2008, 13:6537-6553.

Pesho M.M., Bledzka K., Michalec L., Cierniewski C.S., Plow E.F., The Specificity and Function of the Metal-binding Sites in the Integrin β3 A-domain, *Journal of Biological Chemistry*, 2006, 32:23034-23041.

Piotto M., Saudek V., Sklenár V., Gradient-tailored excitation for single-quantum NMR spectroscopy of aqueous solutions, *J. Biomol*. NMR, 1992, 2:661-665.

Porta F., Krpetic´ Z., Prati L., Gaiassi A. and Scarì G., Gold-Ligand Interaction Studies of Water-Soluble Aminoalcohol Capped Gold Nanoparticles by NMR, *Langmuir*, 2008, 24:7061-7064.

Rautaray D., Kumar S.P., Wadgaonkar P.P. and Sastry M., Highly Versatile Free-Standing Nano-Gold Membranes as Scaffolds for the Growth of Calcium Carbonate Crystals, *Chem. Mater.*, 2004, 16:988-993.

Reardon D.A., Nabors L.B., Stupp R., Mikkelsen T., Cilengitide: an integrin-targeting arginine-glycine-aspartic acid peptide with promising activity for glioblastoma multiforme, *Expert Opin Investig Drugs*, 2008, 8:1225-35.

Reddy V.R., Currao A. and Calzaferri G., Gold and silver metal nanoparticle-modified AgCl photocatalyst for water oxidation to O2, J. Phys., 2007, 61:960-965.

Reinmuth N., Liu W., Ahmad S.A., Fan F., Stoeltzing O., Parikh A.A., Bucana D.C., Gallick G.E., Nickols M.A., Westlin W.F. and Ellis L.M., αvβ3 Integrin Antagonist S247 Decreases Colon Cancer Metastasis and Angiogenesis and Improves Survival in Mice, Cancer Research, 2003, 63:2079-2087.

Santulli G., Ciccarelli M., Palumbo G., Campanile A., Galasso G., Ziaco B., Altobelli G.G., Cimini V., Piscione F., D'Andrea L.D., et al: In vivo properties of the proangiogenic peptide QK, J. Transl Med, 2009, 7:41.

Santulli G., Basilicata M.F., De Simone M., Sorriento D., Anastasio A., Del giudice C., saviano M., Del Gatto A., Trimarco B., Pedone C., Zaccaro L., Iaccarino G., Evaluation of the anti angiogenic properties of the new selective αvβ3 integrin antagonist RGDechiHCit, (SUBMITTED on J. Transl. Med.).

Schiffelers R.M., Ansari A., Xu J., Zhou Q., Tang Q., Storm G., Molema G., Lu P.Y., Scaria P.V. and Woodle M.C., Cancer siRNA therapy by tumor selective delivery with ligand-targeted sterically stabilized nanoparticle, Nucleic Acids Res., 2004, 32:149-157.

Serini, G., Valdembri D., Bussolino F., Integrins and angiogenesis: A sticky business, Exp, Cell Res., 2005, 312:651-658.

Smith J.W., Cilengitide Merck, Curr Opin Investig Drugs, 2003, 4:741-745.

Spence H.J., Chen Y.J., Winder S.J., Muscular dystrophies, the cytoskeletron and cell adhesion, Bioassay, 2002, 24:542-552.

Suehiro K., Smith J.W., Plaw E.F., The Ligand Recognition Specificity of β3 Integrins, Journal of Biological Chemistry, 1996, 28:10365-10371.

Sugahara K.N., Teesalu T., Karmali P., Kotamraju V.R., Agemy L., Girard O.M., Mattrey F.R. and Ruoslahti E., Tissue-Penetrating Delivery of Compounds and Nanoparticles into Tumors, Cancer Cell ,2009, 16:510-520.

Tabatabai G., Weller M., Nabors B., Picard M., Reardon D., Mikkelsen T., Ruegg C., Stupp R., Targeting integrins in malignant glioma, Target Oncol, 2010, 3:175-81.

Takada Y., Simon S., The integrins, Genome Biology, 2007, 8:215.

Takagi J., Spriger A.T., Integrin activation and structural rearrangement, Immunological Reviews, 2002, 186:141-163.

Tucker G.C., Integrins: molecular targets in cancer therapy, Cur. Onc. Rep., 2006, 8:96-103.

Vanderslice P., Woodside D.G., Integrin antagonists as therapeutics for inflammatory diseases, Expert Opin Investig Drugs, 2006, 15:1235-1255.

Wang H., Chen K., Cai W., Li Z., He L., Kashefi A. and Chen X., Integrin-targeted imaging and therapy withRGD4C-TNF fusion protein, Mol Cancer Ther, 2008, 7:1044-1054.

Waters E.A., Chen J., Yang X., Zhang H., Neumann R., Santeford A., Arbeit J., Lanza G.M. and Wickline S.A., Detection of Targeted Perfluorocarbon Nanoparticle Binding Using 19F Diffusion Weighted MR Spectroscopy, Magn Reson Med., 2008, 60:1232-1236.

Wehrle-Haller B. and Imhof Beat., Integrin-dependent pathologies, Journal of pathology, 2003, 200:481-487.

Wilder R.L., Integrin αvβ3 as a target for treatment of, rheumatoid arthritis and related rheumatic diseases, Ann Rheum Dis, 2002, 61:1196-1199.

Winter P.M., Neubauer A.M., Caruthers S.D., Harris T.D., Robertson J.D., Williams T.A., Schmieder A.H., Lanza G.M., Endothelial alpha(v)beta3 integrin-targeted fumagillin nanoparticles inhibit angiogenesis in atherosclerosis, Arteriosclerosis, thrombosis, and vascular biology, 2006, 26:2103-2109.

Wu H.C., and Chang D., Peptide-Mediated Liposomal Drug Delivery System Targeting Tumor Blood Vessels in Anticancer Therapy, Journal of Oncology, 2010 16:1-8.

Xiao T., Junichi T., Coller B.S., Wang J. and Springer T.A., Structural basis for allostery in integrins and binding to fibrinogen-mimetic therapeutics, Nature, 2004, 432:59-67.

Xiong J.P., Stehle T., Goodman S.L. and Arnaout M.A., A Novel Adaptation of the Integrin PSI Domain Revealed from Its Crystal Structure, The Journal of Biological Chemistry, 2004, 39:40252-40254.

Xiong J.P., Mahalingham B., Alonso J.L., Borrelli L.A., Rui X., Anand S., Rysiok T., Müller-Pompalla D., Goodman S.L., Arnaout M.A., Crystal structure of the complete integrin αVβ3 ectodomain plus an alpha/beta transmembrane fragment, J. Cell Biol., 2009, 186:589-600.

Xiong J.P., Stehle T., Diefenbach B., Zhang R., Dunken R., Scott D.L., Joachimiak A., Goodman S.L., Arnaout M.A., Crystal structure of the extracellular segment of integrin αVβ3, Science, 2001, 294:339-345.

Zaccaro L., Del Gatto A., Pedone C., Saviano M., integrin receptor family: promising target for therapeutic and diagnostic applications, Current topics in Biochemisry, 2007, 2:45-56.

Zannetti A., Del Vecchio S., Iommelli F., Del Gatto A., De Luca S., Zaccaro L., Papaccioli A., Sommella J., Panico M., Speranza A., Grieco P., Novellino E., Saviano M., Pedone C. and Salvatore M., Imaging of αvβ3 Expression by a Bifunctional Chimeric RGD Peptide not Cross-Reacting with αvβ5, Clin. Cancer Res., 2009,15:16.

Zhaofei L., Fan W., Xiaoyuan C., Integrin αvβ3-Targeted Cancer Therapy, Drug Development Research, 2008, 69:329-339.

Zhu J., Marchant R.E., Solid-phase synthesis of tailed cyclic RGD peptides using glutamic acid: unexpected glutarimide formation, J. Pept. Sci., 2008, 14:690-6.

APPENDIX

COMMUNICATIONS

1) J. Sommella, A. Zannetti, F. Iommelli, A. Papaccioli, M.R. Panico, A. Del Gatto, **M. De Simone**, L. Zaccaro, M. Saviano, C. Pedone, M. Salvatore. “Immaging of alpha(v)bata(3) integrin expression with a 18-labeled RGD peptide and micro PET”, 11th Naples Workshop on Bioactive Peptides, Naples, Italy, May, 2008.

2) **M. De Simone**, L. Zaccaro, A. Del Gatto, F. Iommelli, A. Zannetti, S. Del Vecchio, M. Salvatore, C. Pedone, M. Saviano. “A New and Selective Antagonist for alpha(v)bata(3)Integrin Imaging”, Scuola Nazionale di Chimica Bioinorganica, Naples, Italy, September, 2008.

3) L. Zaccaro, A. Del Gatto, **M. De Simone**, S. De Luca, F. Iommelli, A. Zannetti, S. Del Vecchio, M. Salvatore, M. Saviano, C. Pedone. “New and selective radiolabeled alpha(v)bata(3) antagonists tracer in tumor diagnosis”, 50th Annual Meeting of the Italian cancer Society, Naples, Italy, October, 2008.

4) L. Zaccaro, A. Del Gatto, **M. De Simone**, J. Omikinschi, M. Saviano, C. Pedone. “New mimetic peptides of p53” XXIII SCI congress, Sorrento, Italy, July, 2008.

5) **M. De Simone**, S. Avvakunova, A. Del Gatto, M. Saviano, C. Pedone, F. Porta and L. Zaccaro. “Biomedical nanotecnologiy: preparation and characterization of new functionalised gold nanoparticles”, 12th Naples Workshop on Bioactive Peptides, Naples, Italy, June, 2010.

6) M. Panico, L. Zaccaro, L. Lang, A. Del Gatto, **M. De Simone**, M. Saviano, C. Pedone, B. Alfano and M. Salvatore. “Fluoro-active-peptides: optimization of radiolabelling synthesis”, 12th Naples Workshop on Bioactive Peptides, Naples, Italy, June, 2010.

7) **M. De Simone**, A. Del Gatto, S. Avvakumova, F. Porta, M. Saviano, C. Pedone, L. Zaccaro. “Gold nanoparticles stabilised by a GGC peptide terminated with a RGD motif”, 31st EPS Copenaghen, Danmark, September, 2010.

8) **M. De Simone**, A. Del Gatto, S. Avvakumova, J. Omichinski, P. Di Lello, M. Saviano, C. Pedone, L. Zaccaro. “Development of new mimetic peptides of p53”, 31st EPS Copenaghen, Danmark, September, 2010.

ATTENDED LABORATORY

From November 2007 to October 2010: Department of Biological Science CNR-IBB University of Naples “Federico II”- Naples, Italy.

ARTICLES IN PREPARATION

1) Optimisation of on solid phase cyclisation of RGD small peptide.
2) Development of a new RGD based peptide to functionalize gold nanoparticles.
3) Fluoro-active-RGDpeptides: optimization of radiolabelling synthesis.

SUMITTED ARTICLE (submitted on *Journal of Translational Medicine*).

Evaluation of the anti-angiogenic properties of the new selective $\alpha_v\beta_3$ integrin antagonist RGDechiHCit

Gaetano Santulli[1], Maria Felicia Basilicata[1], Mariarosaria De Simone[2], Daniela Sorriento[1], Antonio Anastasio[1], Carmine Del Giudice[1], Michele Saviano[3], Annarita Del Gatto[4], Bruno Trimarco[1], Carlo Pedone[2], Laura Zaccaro[4], Guido Iaccarino[*1]

[1] Department of Clinical Medicine, Cardiovascular & Immunologic Sciences, "Federico II" University of Naples, Italy;
[2] Department of Biological Sciences, "Federico II" University of Naples, Italy;
[3] Institute of Crystallography (Consiglio Nazionale delle Ricerche, CNR), Bari, Italy;

[4] Institute of Biostructures and Bioimaging (Consiglio Nazionale delle Ricerche, CNR), Naples, Italy.

Email addresses:
GS: gaetano.santulli@unina.it
MFB: basilicata.felicia@gmail.com
MRDS:mariarosaria.desimone2@unina.it
DS: danisor@libero.it
AA: antonio.anastasio@hotmail.it
CDG: delgiudicec@gmail.com
MS: msaviano@unina.it
ADG: annarita.delgatto@unina.it
BT: trimarco@unina.it
CP: carlo.pedone@unina.it
LZ: lzaccaro@unina.it
GI: guiaccar@unina.it

***: Corresponding Author*: Prof. Guido Iaccarino, M.D., Ph.D., Dipartimento di Medicina Clinica, Scienze Cardiovascolari ed Immunologiche, Università degli Studi di Napoli "Federico II". Via Pansini n° 5, Ed. 2; 80131 Napoli, Italy

Phone/fax: +39 081 7462220 e-mail: guiaccar@unina.i

Abstract

Integrins are heterodimeric receptors that play a critical role in cell-cell and cell-matrix adhesion processes. Among them, $\alpha_V\beta_3$ integrin, that recognizes the aminoacidic RGD triad, is reported to be involved in angiogenesis, tissue repair and tumor growth. We have recently synthesized a new and selective ligand of $\alpha_V\beta_3$ receptor, referred to as RGDechiHCit, that contains a cyclic RGD motif and two echistatin moieties.The aim of this study is to evaluate *in vitro* and *in vivo* the effects of RGDechiHCit. Therefore, we assessed its properties in cellular (endothelial cells [EC], and vascular smooth muscle cells [VSMC]) and animal models (Wistar Kyoto rats and c57Bl/6 mice) of angiogenesis.In EC, but not VSMC, RGDechiHCit inhibits intracellular mitogenic signaling and cell proliferation. Furthermore, RGDechiHCit blocks the ability of EC to form tubes on Matrigel. *In vivo*, wound healing is delayed in presence of RGDechiHCit. Similarly, Matrigel plugs demonstrate an antiangiogenic effect of RGDechiHCit. Our data indicate the importance of RGDechiHCit in the selective inhibition of endothelial $\alpha_V\beta_3$ integrin *in vitro* and *in vivo*. Such inhibition opens new fields of investigation on the mechanisms of angiogenesis, offering clinical implications for treatment of pathophysiological conditions such as cancer, proliferative retinopathy and inflammatory disease.

Introduction

Angiogenesis is a complex multistep phenomenon consisting of the sprouting and the growth of new capillary blood vessels starting from the pre-existing ones. It requires the cooperation of several cell types such as endothelial cells (ECs), vascular smooth muscle cells (VSMCs), macrophages, which should be activated, proliferate and migrate to invade the extracellular matrix and cause vascular remodeling [1, 2]. The angiogenic process is finely tuned by a precise balance of growth and inhibitory factors and in mammalians it is normally dormant except for some physiological conditions, such as wound healing and ovulation. When this balance is altered, excessive or defective angiogenesis occur and the process becomes pathological. Excessive angiogenesis gives also rise to different dysfunctions, including cancer, eye diseases, rheumatoid arthritis, atherosclerosis, diabetic nephropathy, inflammatory bowel disease, psoriasis, endometriosis, vasculitis, and vascular malformations [3]. Therefore the discovery of angiogenesis inhibitors would contribute to the development of therapeutic treatments for these diseases.

The integrins are cell adhesion receptors that mediate cell-cell and cell-matrix interactions and coordinate signaling allowing a close regulation of physiological phenomena including cellular migration, proliferation and differentiation. In particular, the α_V integrins, combined with distinct β subunits, participate in the angiogenic process. An extensively studied member of this receptor class is integrin $\alpha_V\beta_3$, that is strongly overexpressed in activated EC, melanoma, glioblastoma and prostate cancers and in granulation tissue, whereas is not detectable in quiescent blood vessels or in the dermis and epithelium of normal skin [4-6]. This integrin participates in the activation of vascular endothelial growth factor receptor-2 (VEGFR-2), providing a survival signal to the proliferating vascular cells during new vessel growth [7, 8] and also seems to be essential in the step of vacuolation and lumen formation [9]. It has been also reported that $\alpha_V\beta_3$ is under the tight control of VEGF: this integrin is not expressed in quiescent vessels [10], but VEGF induces $\alpha_V\beta_3$ expression *in vitro* and, interestingly, the VEGF and $\alpha_V\beta_3$ integrin expression are highly correlated *in vivo* [11, 12]. Therefore, $\alpha_V\beta_3$ should be considered a tumor and activated endothelium marker.

$\alpha_V\beta_3$ is able of recognizing many proteins of the extracellular matrix, bearing an exposed Arg-Gly-Asp (RGD) tripeptide [5, 13, 14]. Even if different integrins recognize different proteins containing the RGD triad, many studies have demonstrated that the aminoacids flanking the RGD sequence of high-affinity ligands appear to be critical in modulating their specificity of interaction with integrin complexes [15, 16].

Several molecules including peptides containing RGD motif [11] have been recently developed as inhibitors of $\alpha_V\beta_3$ integrin, in experiments concerning tumor angiogenesis, showing a reduction of functional vessel density associated with retardation of tumor growth and metastasis formation [6, 17]. So far, the pentapeptide c(RGDf[NMe]V), also known as cilengitide (*EMD 121974*), is the most active $\alpha_V\beta_3/\alpha_V\beta_5$ antagonist reported in literature [18, 19] and is in phase III clinical trials as antiangiogenic drug for glioblastoma therapy [15]. The development of more selective antiangiogenic molecule would help to minimize the side-effects and increase the therapeutic effectiveness.

We have recently designed and synthesized a novel and selective peptide antagonist, referred to as RGDechiHCit, to visualize $\alpha_V\beta_3$ receptor on tumour cells [20]. It is a chimeric peptide containing a cyclic RGD motif and two echistatin C-terminal moieties covalently linked by spacer sequence. Cell adhesion assays have shown that RGDechiHCit selectively binds $\alpha_V\beta_3$ integrin and does not cross-react with $\alpha_V\beta_5$ and $\alpha_{IIb}\beta_3$ integrins [20]. Furthermore, PET and SPECT imaging studies have confirmed that the peptide localizes on $\alpha_V\beta_3$ expressing tumor cells in xenograft animal model [21]. Since $\alpha_V\beta_3$ is also a marker of activated endothelium, the main purpose of this study was to evaluate *in vitro* and *in vivo* effects of RGDechiHCit on neovascularization. Thus, we first assessed the *in vitro* peptide properties on bovine aortic ECs, and then *in vivo*, in Wistar Kyoto (WKY) rats and c57BL/6 mice, the ability of this cyclic peptide to inhibit angiogenesis.

Methods

Peptides

RGDechiHCit was prepared for the *in vitro* and *in vivo* studies as previously described [20]. To test the biological effects of RGDechiHCit, we synthesized the cyclic pentapeptide c(RGDf[NMe]V), also known as cilengitide or *EMD 121974* [14, 19]. We also investigated RGDechiHCit and c(RGDf[NMe]V) peptides degradation in serum. Both peptides were incubated and the resulting solutions were analyzed by liquid chromatography/mass spectrometry (LC/MS) at different times. 20uL of human serum (Lonza, Basel, Switzerland) were added to 8 uL of a 1 mg/ml solution of either RGDechiHCit or c(RGDf[NMe]V) at 37° C. After 1, 2, 4 and 24h, samples were centrifuged for 1min at 10000g. Solutions were analyzed by LCQ Deca XP Max LC/MS system equipped with a diode-array detector combined with an elctrospray ion source and ion trap mass analyzer (ThermoFinnigan, San Jose, CA, USA), using a Phenomenex C_{18} column (250x 2 mm; 5µm; 300 Å) and a linear gradient of H_2O (0.1%TFA)/CH_3CN (0.1%TFA) from 10 to 80% of CH_3CN (0.1%TFA) in 30 min at flow rate of 200µL/min.

In vitro studies

In vitro studies were performed on cell cultures of ECs or VSMCs, cultured in Dulbecco's modified Eagle's medium (DMEM; Sigma-Aldrich, Milan, Italy) as previously described and validated [22, 23]. Cell culture plates were filled with 10 µg/cm^2 of human fibronectin (hFN, Millipore®, Bedford, MA, USA) as described [24]. All experiments were performed in triplicate with cells between passages 5 and 9.

Cell proliferation assay

Cell cultures were prepared as previously described [25]. Briefly, cells were seeded at density of 100000 per well in six-well plates, serum starved, pre-incubated at 37 °C for 30' with c(RGDf[NMe]V) or RGDechiHCit (10^{-6} M). Proliferation was induced using hFN (100 µg/ml). Cell number was measured at 3, 6 and 20 h after stimulation as previously described [26, 27].

DNA synthesis

DNA synthesis was assessed as previously described [27]. Briefly, cells were serum-starved for 24 h and then incubated in DMEM with [^{3}H]thymidine and 5% FBS. After 3, 6 and 20 h, cells were fixed with trichloracetic acid (0.05%) and dissolved in 1M NaOH. Scintillation liquid was added and [^{3}H]thymidine incorporation was assessed as previously described [27].

VEGF quantification

VEGF production was measured as previously described [26]. Briefly, ECs were seeded at a density of 600000 per well in six well plates, serum starved overnight, seeded with c(RGDf[NMe]V) or RGDechiHCit (10^{-6} M) and then stimulated with hFN for 6 hours. Cultured medium was collected and VEGF production was revealed by western blot.

Endothelial Matrigel assay

The formation of network-like structures by ECs on an extracellular matrix (ECM)-like 3D gel consisting of Matrigel® (BD Biosciences, Bedford, MA, USA), was performed as previously described and validated [27, 28]. The six-well multidishes were coated with growth factor-reduced Matrigel in according to the manufacturer's instructions. ECs (5×10^4) were seeded with c(RGDf[NMe]V) or RGDechiHCit (10^{-6} M), in the absence (negative control) or presence (100 µg/ml) of hFN [24]. Cells were incubated at 37°C for 24h in 1 ml of DMEM. After incubation, ECs underwent differentiation into capillary-like tube structures. Tubule formation was defined as a structure exhibiting a length four times its width [27]. Network formation was observed using an inverted phase-contrast microscope (Zeiss). Representative fields were taken, and the average of the total number of complete tubes formed by cells was counted in 15 random fields by two independent investigators.

Western blot

Immunoblot analyses were performed as previously described and validated [23, 28]. Mouse monoclonal antibodies to extracellular signal regulated kinase (ERK2) and phospho-ERK, anti-rabbit VEGF and actin were from Santa Cruz Biotecnology (Santa Cruz, CA, USA). Levels of VEGF were determined using an antibody raised against VEGF-165 (Santa Cruz Biotechnology) [26]. Experiments were performed in triplicate to ensure reproducibility. Data are presented as arbitrary densitometry units (ADU) after normalization for the total corresponding protein or actin as internal control [24].

In vivo studies

Wound healing assay was performed on 14-week-old (weight 293±21 g) normotensive WKY male rats (Charles River Laboratories, Calco (LC), Italy; n=18), and Matrigel plugs experiments were carried out on 16-week-old (weight 33±4 g) c57BL/6 mice (Charles River Laboratories, Milan, Italy; n=13). All animal procedures were performed in accordance with the *Guide for the Care and Use of Laboratory Animals* published by the National Institutes of Health in the United States (NIH Publication No. 85- 23, revised 1996) and approved by the Ethics Committee for the Use of Animals in Research of “Federico II” University [23].

Wound Healing

The rats (n=18) were anesthetized using vaporized isoflurane (4%, Abbott) and maintained by mask ventilation (isoflurane 1.8%) [29]. The dorsum was shaved by applying a depilatory creme (Veet, Reckitt-Benckiser, Milano, Italy) and disinfected with povidone iodine scrub. A 20 mm diameter open wound was excised through the entire thickness of the skin, including the *panniculus carnosus* layer, as described and validated [1, 28]. Pluronic gel (30%) containing (10^{-6} M) c(RGDf[NMe]V) (n=6), RGDechiHCit (n=7), or saline (n=5) was placed daily directly onto open wounds, then covered with a sterile dressing. Two operators blinded to the identity of the sample examined and measured wound areas every day, for 8 days. Direct measurements of wound region were determined by digital planimetry (pixel area), and subsequent analysis was performed using a computer-assisted image analyzer (ImageJ software, version 1.41, National Institutes of Health, Bethesda, MD, USA). Wound healing was quantified as a percentage of the original injury size. Eight days after wounding, rats were euthanized. Wounds did not show sign of infection. A portion of the lesion and adiacent normal skin were excised, fixed by immersion in phosphate buffered saline (PBS, 0.01 M, pH 7.2-7.4)/formalin and then embedded in paraffin to be processed for immunohistology, as described [1].

Matrigel Plugs

Mice (n=13), anesthetized as described above, were injected subcutaneously midway on the dorsal side, using sterile conditions, with 0.2 ml of Matrigel® basement matrix, mixed with 10^{-6}M VEGF and 10^{-5}M c(RGDf[NMe]V) (n=4), 10^{-6}M VEGF and 10^{-5}M RGDechiHCit (n=5), or 10^{-6}M VEGF alone (n=4). After seven days, mice were euthanized and the implanted plugs were harvested with adjacent tissue to be fixed in 10% neutral-buffered formalin solution and then embedded in paraffin. Invading ECs were quantified by analysis of lectin immunostained sections, as described [1, 2].

Histology

All tissues were cut in 5 µm sections and slides were counterstained with a standard mixture of hematoxylin and eosin. For Masson's trichrome staining of collagen fibers, useful to assess the scar tissue formation, slides were stained with Weigert Hematoxylin (Sigma-Aldrich, St. Louis, MO, USA) for 10 minutes, rinsed in PBS (Invitrogen) and then stained with Biebrich scarlet-acid fuchsin (Sigma-Aldrich) for 5 minutes. Slides were rinsed in PBS and stained with phosphomolybdic/phosphotungstic acid solution (Sigma-Aldrich) for 5 minutes then stained with light green (Sigma-Aldrich) for 5 minutes [30]. ECs were identified by lectin immunohistochemical staining (Sigma-Aldrich) [2] and quantitative analysis was performed using digitized representative high resolution photographic images, with a dedicated software (Image Pro Plus; Media Cybernetics, Bethesda, MD, USA) as previously described [28].

Data presentation and statistical analysis

All data are presented as the mean value±SEM. Statistical differences were determined by one-way or two-way ANOVA and Bonferroni post hoc testing was performed where applicable. A p value less than 0.05 was considered to be

significant. All the statistical analysis and the evaluation of data were performed using GraphPad Prism version 5.01 (GraphPad Software, San Diego, CA, USA).

Results

Peptides

RGDechiHCit and c(RGDf[NMe]V) peptides stabilities were evaluated in serum. The degradation of the peptides were followed by LC/MS. The reversed-phase high performance liquid chromatography (RP-HPLC) of RGDechiHCit before the serum incubation showed a single peak at t_r=11.82 min corresponding to the complete sequence (theoretical MW=2100.1 g mol^{-1}) as indicated by the $[M+H]^+$, $[M+2H]^{2+}$ and $[M+3H]^{+3}$ molecular ion adducts in the MS spectrum (Figure 1A). After 1h, chromatography showed two peaks, ascribable to RGDechiHCit and to a fragment of the complete sequence (theoretical MW=1929.1 g mol^{-1}), respectively, as confirmed by MS spectrum. Finally, after 24h a further peak at t_r=10.93 min corresponding to another RGDechiHCit degradation product (theoretical MW=1775.8 g mol^{-1}) appeared, as indicated by the molecular ion adducts in the MS spectrum, although the peaks attributed to the RGDechiHCit and to the first fragment were still present (Figure 1B).
In contrast with RGDechiHCit, c(RGDf[NMe]V) showed high stability in serum. The RP-HPLC profile of the peptide before the incubation showed a single peak at t_r=16.64 min, ascribable to the complete sequence by the MS spectrum (Figure 1C). After 24h of incubation chromatogram and mass profiles failed to identify any degradation product (Figure 1D).
Since RGDechiHCit showed a low stability, we replenished antagonists every six hours in experiments involving chronic exposure.

In vitro experiments
Cell proliferation and DNA synthesis

Because angiogenesis is intimately associated to EC proliferation, we explored the effects of RGDechiHCit and c(RGDf[NMe]V) on hFN-stimulated EC. In this cellular setting, after 6 hours, both $\alpha_v\beta_3$ integrin antagonists inhibited in a comparable way the ability of hFN to induce proliferation (hFN: +1.98±0.6; hFN+RGDechiHCit: +0.58±0.24; hFN+c(RGDf[NMe]V): +0.6±0.38 fold over basal; $p<0.05$, ANOVA) as depicted in Figure 2A. After 20 hours such inhibitory effect was less marked (Figure 2A). In VSMC there was only a trend of an anti-proliferative effect for these peptides, due to the less evident action of hFN in this specific cellular setting (hFN: +1.21±0.1; hFN+RGDechiHCit: +0.93±0.07; hFN+c(RGDf[NMe]V): +0.9±0.09 fold over basal; NS; Figure 3A).
The effects of RGDechiHCit and c(RGDf[NMe]V) on EC and VSMC proliferation were also measured by assessing the incorporation of [^{3}H]Thymidine in response to hFN. This assay confirmed the anti-proliferative action of both these peptides, which is more evident after 6 hours and in ECs (hFN: +1.84±0.24; hFN+RGDechiHCit: +1.02±0.2; hFN+c(RGDf[NMe]V): +1.09±0.07 fold over basal; $p<0.05$, ANOVA; Figure 2B). On the contrary, the effect of RGDechiHCit on VSMC did not reach statistical significance in comparison to the c(RGDf[NMe]V) used as control (Figure 3B).

Effects on cellular signal transduction

Since hFN-mediated activation of ERK2 is linked to angiogenesis [16, 24, 31], we analyzed the ability of RGDechiHCit and c(RGDf[NMe]V) to inhibit hFN-induced phosphorylation of ERK2 in EC and VSMC. In accordance with the results on cell proliferation and [^{3}H]Thymidine incorporation, in EC both RGDechiHCit and c(RGDf[NMe]V) significantly inhibited the hFN-induced phosphorylation of mitogen-activated protein ERK2 (Figure 2C). Also, in VSMC, there was no significant inhibition of ERK2 phosphorylation by the RGDechiHCit compund c(RGDf[NMe]V) (Figure 3C).

Evaluation of VEGF expression

Angiogenesis is largely dependent on ERK2 activation, which in turn promotes cellular proliferation and expression of VEGF. This cytokine promotes infiltration of inflammatory cells, proliferation of ECs and VSMCs and sustains the proangiogenic phenotype [12]. The early release (6 hours) of the cytokine is therefore an important readout when studying angiogenesis *in* vitro. On these grounds, we assessed the expression levels of this pivotal proangiogenetic factor in EC after 6 hours of stimulation with hFN. hFN induces VEGF release and such response was blunted by incubation with either integrin antagonist, as depicted in Figure 4 (hFN: +18.9±1.02; hFN+RGDechiHCit: +2.44±0.76; hFN+c(RGDf[NMe]V): +3.19±0.73 fold over basal, ADU; $p<0.05$, ANOVA).

Endothelial Matrigel assay

The formation of capillary-like tube structures in the ECM by ECs is a pivotal step in angiogenesis and is also involved in cell migration and invasion [26]. To evaluate any potential antiangiogenic activity of our novel integrin antagonist, *in vitro* angiogenesis assays were conducted by evaluating hFN-induced angiogenesis of ECs on Matrigel. As shown in Figure 5, when ECs were plated on wells coated with Matrigel without the addition of hFN, they showed formation of only a few spontaneous tube structures (17.4±1.2 branches per 10000 μm^2). On the other hand, when the cells were plated on Matrigel with the addiction of hFN, cells formed a characteristic capillary-like network (42.8±4.4 branches per 10000 μm^2; $p<0.05$ vs Basal, ANOVA). In the presence of RGDechiHCit or c(RGDf[NMe]V), the extent of tube formation hFN-induced was significantly reduced (10.03±1.44; 14.11±3.9, respectively; $p<0.05$ vs hFN alone, ANOVA; Figure 5).

In vivo experiments

Wound healing

The examination of full-thickness wounds in the back skin showed that both RGDechiHCit and c(RGDf[NMe]V) slowed down healing (Figure 6). At a macroscopic observation, the delay in the wound healing in treated rats was evident, with raised margins, more extensive wound debris and scab, that persisted for at least 7 days after surgery. Moreover, histological analysis showed that while control rats presented a dermal scar tissue consisting of a well defined and organized fibrous core with minimal chronic inflammatory cells, skin wounds exposed to RGDechiHCit or c(RGDf[NMe]V) exhibited a retarded repair pattern. Indeed, there was an intense

inflammatory infiltrate, extended from the wound margin into the region of the *panniculus carnosus* muscle and hypodermis. Moreover, the basal epidermis was disorganized and epidermal cell growth failed to achieve re-epithelialization, as shown in Figure 6.

Matrigel plugs

After injection, Matrigel implants containing the angiogenic stimulant VEGF (10^{-5} M) formed a plug into which ECs can migrate. Matrigel pellets evidenced a significant lower EC infiltration, identified through means of immunohistological lectin staining, in c(RGDf[NMe]V) and RGDechiHCit treated plugs respect to VEGF alone (VEGF+RGDechiHCit: 0.211±0.034; VEGF+c(RGDf[NMe]V): 0.185±0.027 fold over VEGF alone; $p<0.05$, ANOVA), as depicted in Figure 7.

Discussion

In the present study, we evaluated the anti-angiogenic properties of RGDechiHCit peptide *in vitro* on EC and VSMC cells and *in vivo* on animal models of rats and mice. The data here reported recapitulate the well-known antiangiogenic properties of c(RGDf[NMe]V), that was used as control. We previously described the design and synthesis of RGDechiHCit, a novel and selective ligand for $\alpha_V\beta_3$ integrin, containing a cyclic RGD motif and two echistatin *C*-terminal moieties [20]. *In vitro* studies showed that this molecule is able to selectively bind $\alpha_V\beta_3$ integrin and not to cross-react with other type of integrins. Furthermore, PET and SPECT imaging studies have confirmed that the peptide localizes on $\alpha_V\beta_3$ expressing tumor cells in xenograft animal model [21]. Given the presence in the molecule of the RGD sequence it was obvious to speculate that RGDechiHCit acted as an antagonist. Our report is the first evidence that our peptide acts as antagonist for $\alpha_V\beta_3$ integrin. Its ability to inhibit hFN-induced cell proliferation is comparable to that of c(RGDf[NMe]V), although the half-life is quite reduced.

A major evidence that is brought up by our results is the peculiar selectivity of RGDechiHCit towards EC, as compared to c(RGDf[NMe]V). Indeed, RGDechiHCit fails to inhibit VSMC proliferation *in vitro*, opposite to c(RGDf[NMe]V). We believe that this feature is due to the selectivity of such a novel compound towards $\alpha_V\beta_3$. Indeed, VSMCs express $\alpha_V\beta_3$ only during embryogenesis [31], but express other integrins which may be blocked by c(RGDf[NMe]V). On the contrary, $\alpha_V\beta_3$ is expressed by ECs [8], thus conferring RGDechiHCit selectivity toward this cell type. This issue is relevant cause the effect *in vivo* is similar between the two antagonists on wound healing and Matrigel plugs invasion. Indeed, our data suggest that inhibition of the endothelial integrin system is sufficient to inhibit angiogenesis. It is possible to speculate that the higher specificity of RGDechiHCit for the endothelium would result in a lower occurrence of side effects than the use of less selective inhibitors. This is only an indirect evidence, that needs further investigation in more specific experimental setups. Indeed, of the wide spectrum of integrins that are expressed on the surface of ECs, $\alpha_V\beta_3$ receptor has been identified as having an especially interesting expression pattern among vascular cells during angiogenesis, vascular remodeling, tumor progression and metastasis [6, 32, 33]. What is more, two pathways of angiogenesis have been recently identified based on the related but distinct integrins $\alpha_V\beta_3$ and $\alpha_V\beta_5$ [4]. In particular, $\alpha_V\beta_3$ integrin activates VEGF receptors and inhibition of β_3 subunit has been shown to reduce phosphorylation of VEGF receptors [7], thereby limiting the biological effects of VEGF [1]. Further, Mahabeleshwar and coworkers have shown the intimate interaction occurring between $\alpha_V\beta_3$ integrin and the VEGFR-2 in primary human EC [12]. The relevance of this molecule to angiogenesis and its potential as a therapeutic target has, therefore, been well established [34, 35] and in this report we show that its activity is highly critical for both hFN or VEGF-stimulated ECs proliferation.

Our results concerning RGDechiHCit in angiogenic processes are of immediate translational importance, because deregulation of angiogenesis is involved in several clinical conditions including cancer, ischemic, and inflammatory diseases (atherosclerosis, rheumatoid arthritis, or age-related macular degeneration) [34-36]. Therefore, the research for drugs able to modulate angiogenesis constitutes a crucial investigation field. Since RGDechiHCit is rapidly removed in serum it is possible to increase its effect by engineering the molecule to elongate its lifespan. In the present paper we circumvented this issue by increasing the times of application of the drug

both *in vitro* and *in vivo*, or by reducing the times of observation. This issue can be solved by the design use of a more stable peptidic structure of RGDechiHCit. Clearly, further investigations are also needed to fully understand the basic cell biological mechanisms underlying growth factor receptors and integrin function during angiogenesis. The knowledge of molecular basis of this complex mechanism remains a challenge of fascinating interest, with clinical implications for treatment of a large number of pathophysiological conditions including but not limited to solid tumors [17, 37], diabetic retinopathy [38, 39] and inflammatory disease [36].

Competing interests

The authors declare that they have no competing interests.

Authors'contributions

GS and GI designed research; GS, MFB, MDS, DS, AA, CGD and MS carried out the experiments; GS and GI performed the statistical analysis; GS, GI, ADG and LZ drafted the manuscript; GS, BT, CP and GI supervised the project; GS and MFB equally contributed to this work. All authors read and approved the final manuscript.

References

1. Santulli G, Ciccarelli M, Palumbo G, Campanile A, Galasso G, Ziaco B, Altobelli GG, Cimini V, Piscione F, D'Andrea LD, et al: **In vivo properties of the proangiogenic peptide QK.** *J Transl Med* 2009, **7:**41.
2. Bonauer A, Carmona G, Iwasaki M, Mione M, Koyanagi M, Fischer A, Burchfield J, Fox H, Doebele C, Ohtani K, et al: **MicroRNA-92a controls angiogenesis and functional recovery of ischemic tissues in mice.** *Science* 2009, **324:**1710-1713.
3. Desgrosellier JS, Cheresh DA: **Integrins in cancer: biological implications and therapeutic opportunities.** *Nat Rev Cancer* 2010, **10:**9-22.
4. Hood JD, Frausto R, Kiosses WB, Schwartz MA, Cheresh DA: **Differential alphav integrin-mediated Ras-ERK signaling during two pathways of angiogenesis.** *J Cell Biol* 2003, **162:**933-943.
5. Takahashi S, Moser M, Montanez E, Nakano T, Seo M, Backert S, Inoue I, Awata T, Katayama S, Komoda T, Fassler R: **The fibronectin RGD motif is required for multiple angiogenic events during early embryonic development.** *Arterioscler Thromb Vasc Biol* 2010, **30:**e1.
6. Castel S, Pagan R, Garcia R, Casaroli-Marano RP, Reina M, Mitjans F, Piulats J, Vilaro S: **Alpha v integrin antagonists induce the disassembly of focal contacts in melanoma cells.** *Eur J Cell Biol* 2000, **79:**502-512.
7. Soldi R, Mitola S, Strasly M, Defilippi P, Tarone G, Bussolino F: **Role of alphavbeta3 integrin in the activation of vascular endothelial growth factor receptor-2.** *Embo J* 1999, **18:**882-892.
8. Lu H, Murtagh J, Schwartz EL: **The microtubule binding drug laulimalide inhibits vascular endothelial growth factor-induced human endothelial cell migration and is synergistic when combined with docetaxel (taxotere).** *Mol Pharmacol* 2006, **69:**1207-1215.
9. Bayless KJ, Salazar R, Davis GE: **RGD-dependent vacuolation and lumen formation observed during endothelial cell morphogenesis in three-dimensional fibrin matrices involves the alpha(v)beta(3) and alpha(5)beta(1) integrins.** *Am J Pathol* 2000, **156:**1673-1683.
10. Brooks PC, Stromblad S, Sanders LC, von Schalscha TL, Aimes RT, Stetler-Stevenson WG, Quigley JP, Cheresh DA: **Localization of matrix metalloproteinase MMP-2 to the surface of invasive cells by interaction with integrin alpha v beta 3.** *Cell* 1996, **85:**683-693.
11. Abumiya T, Lucero J, Heo JH, Tagaya M, Koziol JA, Copeland BR, del Zoppo GJ: **Activated microvessels express vascular endothelial growth factor and integrin alpha(v)beta3 during focal cerebral ischemia.** *J Cereb Blood Flow Metab* 1999, **19:**1038-1050.
12. Mahabeleshwar GH, Feng W, Reddy K, Plow EF, Byzova TV: **Mechanisms of integrin-vascular endothelial growth factor receptor cross-activation in angiogenesis.** *Circ Res* 2007, **101:**570-580.
13. Xiong JP, Stehle T, Zhang R, Joachimiak A, Frech M, Goodman SL, Arnaout MA: **Crystal structure of the extracellular segment of integrin alpha Vbeta3 in complex with an Arg-Gly-Asp ligand.** *Science* 2002, **296:**151-155.
14. Aumailley M, Gurrath M, Muller G, Calvete J, Timpl R, Kessler H: **Arg-Gly-Asp constrained within cyclic pentapeptides. Strong and selective**

inhibitors of cell adhesion to vitronectin and laminin fragment P1. *FEBS Lett* 1991, **291:**50-54.
15. Schottelius M, Laufer B, Kessler H, Wester HJ: **Ligands for mapping alphavbeta3-integrin expression in vivo.** *Acc Chem Res* 2009, **42:**969-980.
16. Eliceiri BP, Klemke R, Stromblad S, Cheresh DA: **Integrin alphavbeta3 requirement for sustained mitogen-activated protein kinase activity during angiogenesis.** *J Cell Biol* 1998, **140:**1255-1263.
17. Bai J, Zhang J, Wu J, Shen L, Zeng J, Ding J, Wu Y, Gong Z, Li A, Xu S, et al: **JWA regulates melanoma metastasis by integrin alpha(V)beta(3) signaling.** *Oncogene* 2009.
18. Eskens FA, Dumez H, Hoekstra R, Perschl A, Brindley C, Bottcher S, Wynendaele W, Drevs J, Verweij J, van Oosterom AT: **Phase I and pharmacokinetic study of continuous twice weekly intravenous administration of Cilengitide (EMD 121974), a novel inhibitor of the integrins alphavbeta3 and alphavbeta5 in patients with advanced solid tumours.** *Eur J Cancer* 2003, **39:**917-926.
19. Dechantsreiter MA, Planker E, Matha B, Lohof E, Holzemann G, Jonczyk A, Goodman SL, Kessler H: **N-Methylated cyclic RGD peptides as highly active and selective alpha(V)beta(3) integrin antagonists.** *J Med Chem* 1999, **42:**3033-3040.
20. Del Gatto A, Zaccaro L, Grieco P, Novellino E, Zannetti A, Del Vecchio S, Iommelli F, Salvatore M, Pedone C, Saviano M: **Novel and selective alpha(v)beta3 receptor peptide antagonist: design, synthesis, and biological behavior.** *J Med Chem* 2006, **49:**3416-3420.
21. Zannetti A, Del Vecchio S, Iommelli F, Del Gatto A, De Luca S, Zaccaro L, Papaccioli A, Sommella J, Panico M, Speranza A, et al: **Imaging of alphavbeta3 expression by a bifunctional chimeric RGD peptide not cross-reacting with alphavbeta5.** *Clin Cancer Res* 2009, **15:**5224-5233.
22. Ciccarelli M, Cipolletta E, Santulli G, Campanile A, Pumiglia K, Cervero P, Pastore L, Astone D, Trimarco B, Iaccarino G: **Endothelial beta2 adrenergic signaling to AKT: role of Gi and SRC.** *Cell Signal* 2007, **19:**1949-1955.
23. Iaccarino G, Ciccarelli M, Sorriento D, Cipolletta E, Cerullo V, Iovino GL, Paudice A, Elia A, Santulli G, Campanile A, et al: **AKT participates in endothelial dysfunction in hypertension.** *Circulation* 2004, **109:**2587-2593.
24. Illario M, Cavallo AL, Monaco S, Di Vito E, Mueller F, Marzano LA, Troncone G, Fenzi G, Rossi G, Vitale M: **Fibronectin-induced proliferation in thyroid cells is mediated by alphavbeta3 integrin through Ras/Raf-1/MEK/ERK and calcium/CaMKII signals.** *J Clin Endocrinol Metab* 2005, **90:**2865-2873.
25. Iaccarino G, Smithwick LA, Lefkowitz RJ, Koch WJ: **Targeting Gbeta gamma signaling in arterial vascular smooth muscle proliferation: a novel strategy to limit restenosis.** *Proc Natl Acad Sci U S A* 1999, **96:**3945-3950.
26. Iaccarino G, Ciccarelli M, Sorriento D, Galasso G, Campanile A, Santulli G, Cipolletta E, Cerullo V, Cimini V, Altobelli GG, et al: **Ischemic neoangiogenesis enhanced by beta2-adrenergic receptor overexpression: a novel role for the endothelial adrenergic system.** *Circ Res* 2005, **97:**1182-1189.
27. Ciccarelli M, Santulli G, Campanile A, Galasso G, Cervero P, Altobelli GG, Cimini V, Pastore L, Piscione F, Trimarco B, Iaccarino G: **Endothelial alpha1-adrenoceptors regulate neo-angiogenesis.** *Br J Pharmacol* 2008, **153:**936-946.

28. Sorriento D, Ciccarelli M, Santulli G, Campanile A, Altobelli GG, Cimini V, Galasso G, Astone D, Piscione F, Pastore L, et al: **The G-protein-coupled receptor kinase 5 inhibits NFkappaB transcriptional activity by inducing nuclear accumulation of IkappaB alpha.** *Proc Natl Acad Sci U S A* 2008, **105:**17818-17823.
29. Sorriento D, Santulli G, Fusco A, Anastasio A, Trimarco B, Iaccarino G: **Intracardiac Injection of AdGRK5-NT Reduces Left Ventricular Hypertrophy by Inhibiting NF-{kappa}B-Dependent Hypertrophic Gene Expression.** *Hypertension* 2010, **56:**696-704.
30. Santulli G, Illario M, Palumbo G, Sorriento D, Cipolletta E, Trimarco V, Del Giudice C, Ciccarelli M, Trimarco B, Iaccarino G: **CaMK4 partecipates in the settings of the hypertensive phenotype: a human genome wide analysis supported by animal model.** *Eur Heart J* 2009, **30(Suppl.1):**161.
31. Astrof S, Hynes RO: **Fibronectins in vascular morphogenesis.** *Angiogenesis* 2009, **12:**165-175.
32. Zaccaro L, Del Gatto A, Pedone C, Saviano M: **Peptides for tumour therapy and diagnosis: current status and future directions.** *Curr Med Chem* 2009, **16:**780-795.
33. Verbisck NV, Costa ET, Costa FF, Cavalher FP, Costa MD, Muras A, Paixao VA, Moura R, Granato MF, Ierardi DF, et al: **ADAM23 negatively modulates alpha(v)beta(3) integrin activation during metastasis.** *Cancer Res* 2009, **69:**5546-5552.
34. Laitinen I, Saraste A, Weidl E, Poethko T, Weber AW, Nekolla SG, Leppanen P, Yla-Herttuala S, Holzlwimmer G, Walch A, et al: **Evaluation of alphavbeta3 integrin-targeted positron emission tomography tracer 18F-galacto-RGD for imaging of vascular inflammation in atherosclerotic mice.** *Circ Cardiovasc Imaging* 2009, **2:**331-338.
35. Furundzija V, Fritzsche J, Kaufmann J, Meyborg H, Fleck E, Kappert K, Stawowy P: **IGF-1 increases macrophage motility via PKC/p38-dependent alphavbeta3-integrin inside-out signaling.** *Biochem Biophys Res Commun* 2010, **394:**786-791.
36. Vanderslice P, Woodside DG: **Integrin antagonists as therapeutics for inflammatory diseases.** *Expert Opin Investig Drugs* 2006, **15:**1235-1255.
37. Tani N, Higashiyama S, Kawaguchi N, Madarame J, Ota I, Ito Y, Ohoka Y, Shiosaka S, Takada Y, Matsuura N: **Expression level of integrin alpha 5 on tumour cells affects the rate of metastasis to the kidney.** *Br J Cancer* 2003, **88:**327-333.
38. Crawford TN, Alfaro DV, 3rd, Kerrison JB, Jablon EP: **Diabetic retinopathy and angiogenesis.** *Curr Diabetes Rev* 2009, **5:**8-13.
39. Santulli RJ, Kinney WA, Ghosh S, Decorte BL, Liu L, Tuman RW, Zhou Z, Huebert N, Bursell SE, Clermont AC, et al: **Studies with an orally bioavailable alpha V integrin antagonist in animal models of ocular vasculopathy: retinal neovascularization in mice and retinal vascular permeability in diabetic rats.** *J Pharmacol Exp Ther* 2008, **324:**894-901.

Figure 2

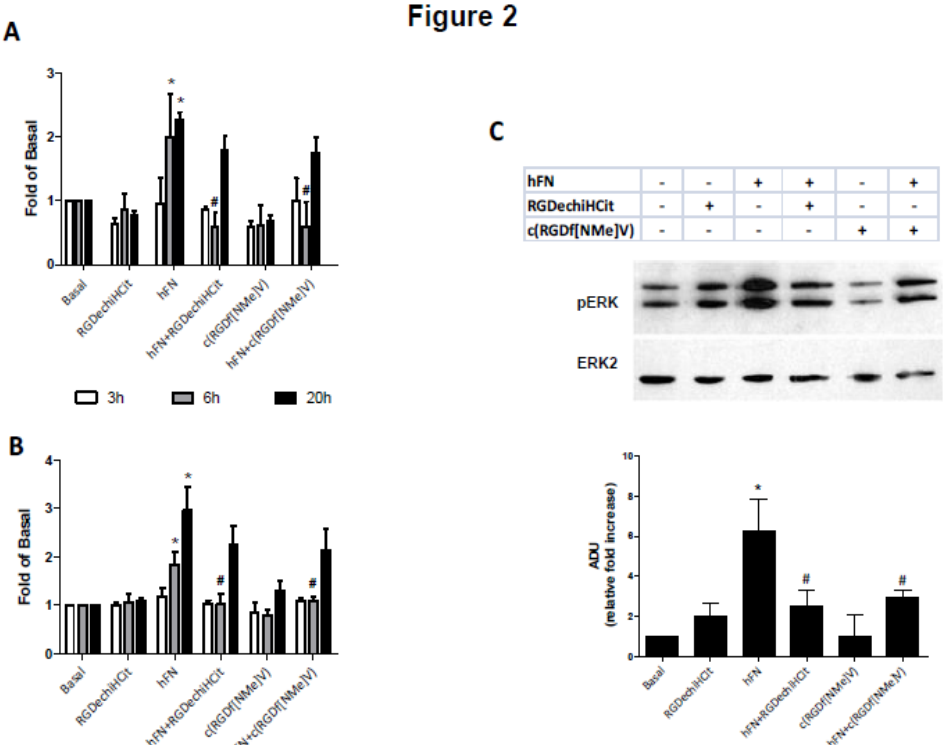

Figure 3

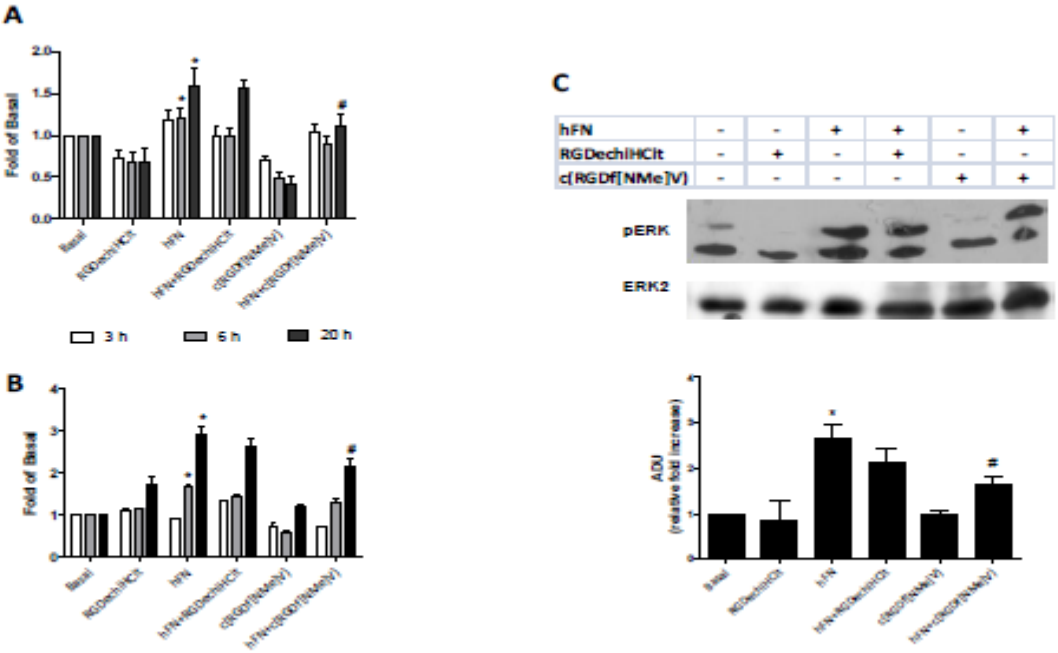

Figure 4

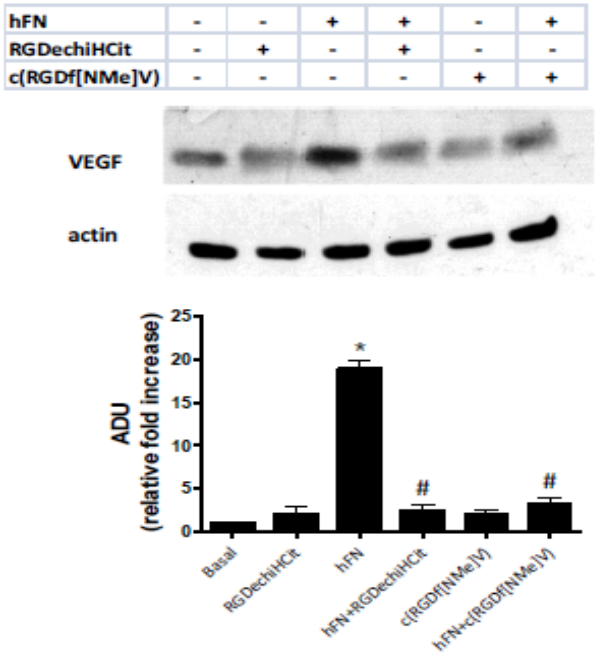

Figure 5

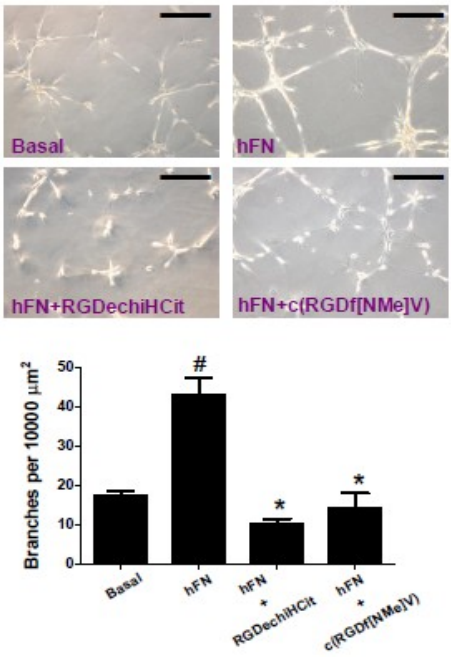

Figure 6

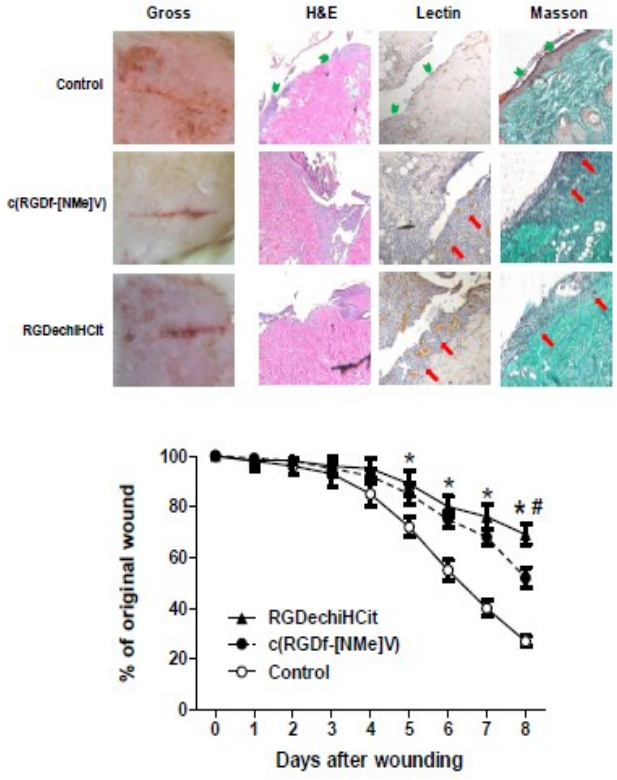

Figure 7

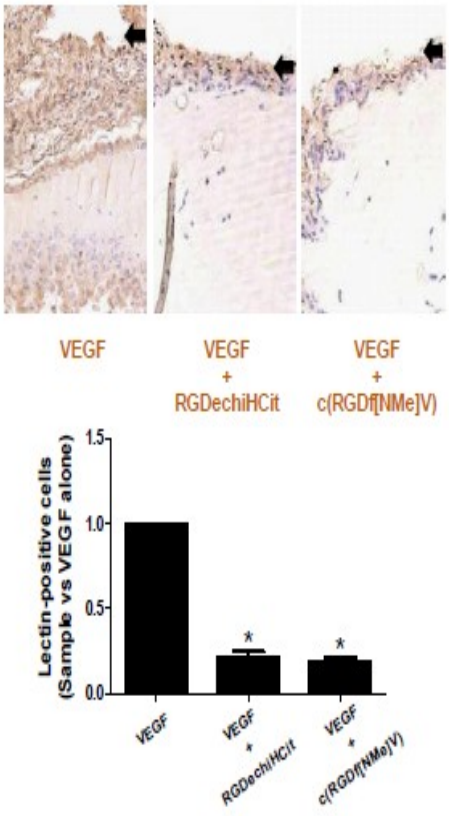

Figures legends

Figure 1
Reversed-phase high performance liquid chromatography (RP-HPLC) chromatograms and mass spectra at t=0 and t=24 h for RGDechiHCit (A and B) and c(RGDf[NMe]V) (C and D), respectively. In panel B the chromatographic peaks at tr=11.70 (★), 12.04 (■) and 10.93 min (●) are marked.

Figure 2
In vitro effects of c(RGDf[NMe]V) and RGDechiHCit on cell proliferation (Panel A) and DNA synthesis assessed by [^{3}H]thymidine incorporation **(Panel B)** in bovine aortic endothelial cells (EC). Given alone, c(RGDf[NMe]V) or RGDechiHCit did not affect EC proliferation. Neverteless, incubation with these $\alpha_V\beta_3$ integrin antagonists inhibited in a comparable way EC proliferation in response to the mitogenic stimulus, hFN. All experiments depicted in this figure were performed from three to six times in duplicate (*= $p<0.05$ vs Basal, #= $p<0.05$ vs hFN). **Panel C**. *In vitro* effects of c(RGDf[NMe]V) and RGDechiHCit on EC signal transduction. Extracellular signal regulated kinase (ERK)/mitogen-activated protein kinase activation: western blot of activated (phosphorylated: pERK) ERK2 after hFN-stimulation. Equal amounts of proteins were confirmed via blotting for total ERK. Densitometric analysis (bar graph) showed that hFN stimulation caused ERK activation (*= $p<0.05$ vs Basal) and that treatment with $\alpha_V\beta_3$ antagonists blunted such activation (#= $p<0.05$ vs hFN). Error bars show SEM. Representative blots are shown in the inset.

Figure 3
In vitro effects of c(RGDf[NME]V) and RGDechiHCit on vascular smooth muscle cell (VSMC) cell proliferation **(Panel A)** and DNA synthesis assayed by [^{3}H]thymidine incorporation **(Panel B)**. In this cellular setting, hFN induced a mitogenic stimulus, appreciable especially at 20h. c(RGDf[NMe]V) but not RGDechiHCit at that time-point induced an attenuation of such proliferative response. All experiments were performed from three to five times in triplicate (*= $p<0.05$ vs Basal; #= $p<0.05$ vs hFN). *In vitro* effects of c(RGDf[NMe]V) and RGDechiHCit on VSMC signal transduction were represented in **Panel C**. Extracellular signal regulated kinase (ERK)/mitogen-activated protein kinase activation: western blot of activated (phosphorylated: pERK) ERK2 after hFN-stimulation. Blots were then stripped and reprobed for either total ERK as a loading control. Densitometric analysis (bar graph) showed that hFN induced ERK phosphorylation (*= $p<0.05$ vs Basal) and that treatment with c(RGDf[NMe]V) but not RGDechiHCit decreased such activation (#= $p<0.05$ vs hFN). Error bars show SEM. Representative blots are presented in the inset.

Figure 4
VEGF production in bovine aortic endothelial cells (ECs) measured by Western blot (inset). Shown are VEGF levels after 6 hours of serum starvation. Equal amount of proteins were verified by blotting for actin. Quantification of western blot from all experiments demonstrated that hFN was able to increase VEGF production (*= $p<0.05$ vs Basal), while after c(RGDf[NMe]V) or RGDechiHCit treatment VEGF levels returned to basal conditions (#= $p<0.05$ vs hFN). All data derived from three different experiments performed in duplicate. The results were expressed as fold increased with respect to the basal condition in untreated samples. Error bars show SEM.

Figure 5
Representative phase contrast photomicrographs of bovine aortic endothelial cells (ECs) are shown plated on Matrigel. Both c(RGDf[NMe]V) and RGDechiHCit inhibited hFN-induced tube formation. Microscopy revealed numbers of network projections (branches) formed in each group after 12 h of incubation. Data from three experiments in triplicate are summarized in the graph (*=$p<0.05$ vs Basal; #= $p<0.05$ vs hFN). Error bars show SEM. The black bar corresponds to 100 μm.

Figure 6
Both c(RGDf[NMe]V) and RGDechiHCit slowed down the closure of full thickness punch biopsy wounds. Three to five rats were analyzed at each time point. Gross appearance (representative digital photographs) after 5 days of the wound treated with pluronic gel containing c(RGDf-[NMe]V), RGDechiHCit (10^{-6}M) or saline. Diagram of the kinetics of wound closure; *=$p<0.05$ vs Control; #=$p<0.05$ vs c(RGDf-[NMe]V, ANOVA). Error bars show SEM. Histological analysis revealed a retarded repair pattern in treated rats, which is consistent with inhibition of angiogenesis in the granulation tissue. Representative sections of excised wounds; 5 μm, ×20 objective (Hematoxylin & Eosin, Lectin immunohistochemical staining, Masson's trichrome). In control animals, epidermal cell growth achieved complete re-epitalization (green arrowheads) and there is a well defined and organized fibrous core of scar tissue. Both in c(RGDf[NMe]V) and RGDechiHCit treated rats there is a chronic inflammatory infiltrate (red arrows) and lectin staining shows (in brown) the presence of vessels in the granulation tissue.

Figure 7
Representative immunohistochemical sections (5 μm) of Matrigel plugs subcutaneously injected, at ×20 magnification. ECs were identified by lectin staining, that gave a brown reaction product, as described in Methods. Both c(RGDf[NMe]V) and RGDechiHCit treatment reduced the number of invading cells from the edge to the core of implanted Matrigel plug. Analysis was conducted in 20 randomly chosen cross-sections per each group. *=$p<0.05$ vs VEGF. Error bars show SEM.